Investigating nucleotide excision repair in prokaryotes and eukaryotes

PhD Thesis for the degree of PhD in Cell Biology

Faculty of Sciences

School of Biosciences

University of Kent

Luke Springall

2019

Declaration,

I confirm that no part of this thesis has been submitted in support of an application for any degree or qualification of the University of Kent, or any other University or higher education learning institution.

Luke Springall

23rd March 2020

Acknowledgments

I would like to take this opportunity to thank everyone who has supported me throughout the course of this PhD. First and foremost, I would like to thank Neil Kad for allowing me to pursue a PhD in his laboratory, but most importantly, for all the guidance, support and encouragement that is needed to begin a career in science.

Next, I would like to thank the Kad group, in particular Alessio, Jamie and Jingyu, for putting up with me every day, but mostly for constant insightful discussion and input that shaped this thesis into what it is today.

Finally, I would like to thank my parents, Julie and Kevin, without their complete support, financial and emotional, I wouldn't have been able to realise this PhD and I wouldn't be where I am today without them.

Abstract

Nucleotide excision repair is the primary mechanism for removal of UV induced photoproducts but also exhibits a wide substrate range for damage processing. This process is highly mechanistically conserved across all kingdoms of life and involves damage detection, damage removal, DNA repair and ligation. Here we examine prokaryotic and eukaryotic NER repair at the single molecule level. Canonically during prokaryotic NER UvrAB scans the DNA for lesions, UvrC incises the lesion both sides of the damage, and UvrD, DNA polymerase and DNA ligase repair and seal the DNA. The process of protein complex is not fully understood. Next, we explored the eukaryotic NER proteins, XPD and p44, which form part of the multi complex TFIIH after initial lesion detection by XPC and Rad23. We examine their interaction with double stranded DNA using single molecule fluorescence imaging for the first time.

Firstly, we examined the damage detection role of bacterial NER complexes on DNA tightropes with damage constructs. We found that UvrBC in the absence of UvrA was able to bind to damage at similar levels with UvrAB. UvrBC previously had no known damage detecting role unlike UvrAB, which has clear damage recognition function. This lesion detection is mediated primarily by the β-hairpin of UvrB in both complexes. We also show that UvrA exhibits tension dependence when locating damage, in agreement with recent structural studies. We also demonstrate, using live cell fluorescence imaging, that eGFP labelled UvrB and UvrC, likely in

complex, can bind directly to DNA damage *in vivo* independently from UvrA, demonstrating an *in vivo* damage sensing role. Additionally, we confirm this loading of UvrBC complexes to damaged DNA improves cell survival at low levels of UV damage. Next, we demonstrate that XPD and p44, subunits of the TFIIH complex can independently translocate along double stranded DNA tightropes, though both prefer single stranded regions, suggesting they are able to scan DNA searching for other TFIIH factors and may initiate TFIIH formation.

These data indicate UvrBC complexes form *in vivo* and directly contributes to DNA damage processing and repair. This process could take place when UvrA is overwhelmed by lesions but the damage is not sufficient to trigger the SOS-response. We also performed the first single molecule analysis of the interaction between the UvrC homologue, Cho, and double stranded DNA. Finally, we show XPD translocation along DNA appears to be ATP-mediated as increasing the concentration of ATP reduced the number of pauses observed in motility. Together these data show that single components of well-established pathways and newly discovered protein complexes still are still required to fully understand these vital processes.

Table of Contents

List of Abbreviations

ADP: Adenosine diphosphate

AFM: Atomic force microscopy

ANOVA: Analysis of variance

ATP: Adenosine triphosphate

DNA: Deoxyribonucleic acid

DTT: Dithiothreitol

EGFP: Enhanced green fluorescent protein

GGR: Global genome repair

Mfd: Transcription repair coupling factor

NER: Nucleotide excision repair

OAF: Oblique angle fluorescence

RNA: Ribonucleic acid

SEM: Squared error of the mean

TCR: Transcription coupled repair

TIRF: Total internal reflection fluorescence

UV: Ultraviolet

XPA: Xeroderma pigmentosum group A-complementing protein

XPB: Xeroderma pigmentosum group B

XPC: Xeroderma pigmentosum group C-complementing protein

XPD: Xeroderma pigmentosum group D

Chapter 1. Introduction

DNA is a helical molecule consisting of two complimentary strands running in opposite directions (Watson and Crick, 1953; Wing *et al.*, 1980). DNA is comprised of nucleotides. The general structure of nucleotide is a phosphate group, deoxyribose and a nitrogenous base, either a purine or a pyrimidine (Houten, 1990; Travers and Muskhelishvili, 2015). Nucleotides form polynucleotides through the sugar phosphate backbone this is created by covalent bonds from the deoxyribose (sugar) of one nucleotide and the phosphate of the next (Houten, 1990; Travers and Muskhelishvili, 2015). The two strands are connected between the nitrogenous bases. A purine forms hydrogen bonds with a pyrimidine in specific base pairs, adenine with thymine and guanine with cytosine (Chargraff *et al.*, 1951; Watson and Crick, 1953). DNA has three structures, A-DNA, B-DNA and Z-DNA. These structures vary in their helical properties. A/B-DNA is righthanded (Malinina *et al.*, 1999; Ng, Kopka and Dickerson, 2000) and Z-DNA is left handed (Herbert and Rich, 1999). A-DNA forms within stretches of purines and results in a stiff structure compared to B DNA (Ng, Kopka and Dickerson, 2000). Z-DNA forms by alternating pyrimidine purine steps and is narrower than the right handed structures (Ng, Kopka and Dickerson, 2000). B-DNA favoured by mixed base sequences and is the most common DNA structure, this form was first described by Watson and Crick (Watson and Crick, 1953; Malinina *et al.*, 1999). The double helix formed by the complementary strands of nucleotides in B-DNA is righthanded with 10.4 bases per turn

(Watson and Crick, 1953; Wang, 1979; Wing *et al.*, 1980). As they are not symmetrical they differ in size and grooves form between the stands. The major groove , is 22 Å in wide and the minor groove is 12 Å wide (Wing *et al.*, 1980; Drew *et al.*, 1981; Drew and Travers, 1984).

1.1 UV radiation

UV radiation comprises three parts, UV-A radiation from 390 to 320 nm UV-B from 320 to 286 nm and UV-C includes wavelengths shorter than 286 nm (Cutchis P., 1974; Pollard, 1974; Willson *et al.*, 1981; Gascón *et al.*, 1995). UV radiation from the sun contains all three wavelengths (Willson *et al.*, 1981; Davies, 1995; Sliney, 2007). UV radiation is 95% UVA, this wavelength damages DNA indirectly generating reactive oxygen species (Brem, Guven and Karran, 2017; Mullenders, 2018). UV-B/C radiation is absorbed by DNA and directly induces covalent links between adjacent pyrimidines (Kiefer, 2007; Chatterjee N, 2017) however UVB is also crucial for vitamin D synthesis (Wacker and Holick, 2013) and UVC is mostly absorbed by the ozone layer (De Gruijl and Van der Leun, 2000). UVB/C radiation results in two damage products, cyclobutene-pyrimidine dimers (CPDs) and 6-4 photoproducts, these lesions are devastating to organism survival and evolution has provided a number of repair mechanisms to tolerate this DNA damage (Setlow and Carrier, 1966; Sinha and Häder, 2002). CPDs account for 75% of the DNA lesions from UV radiation, they distort the DNA by as much as 9 degrees, these lesions can lead to mistakes in DNA transcription and arrest DNA replication (Kim, Patel and Choi, 1995; Sinha and Häder, 2002; Li *et al.*, 2006). CPD formation at dipyrimidine sites are not equally distributed between bases,

there are 55 times more CPDs between thymine-thymines than cytosine-cytosine sites (Douki and Cadet, 2001). *E. coli* exposed to a small dose, 22 J/m^2 of 254 nm UVC, kills 90% of cells (Starr, 1981; Miller and Kokjohn, 1990; Gascón *et al.*, 1995). Nucleotide excision repair (NER) is the primary mechanism of removing DNA lesions caused by UV radiation.

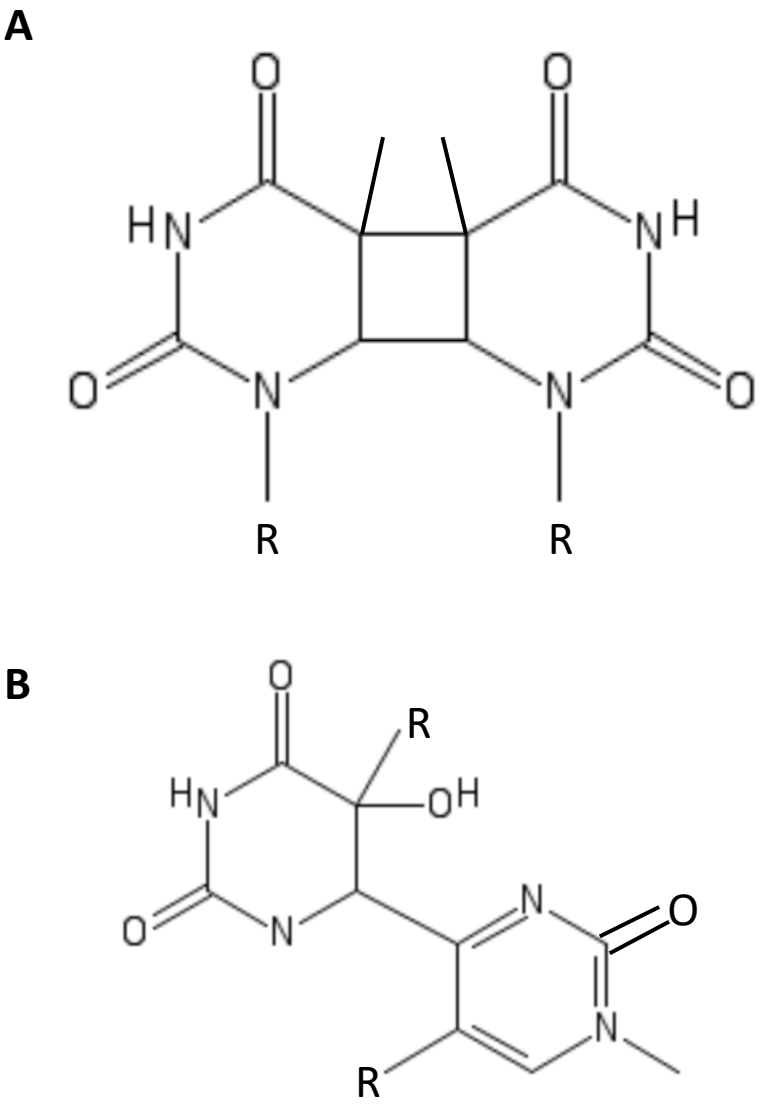

Figure 1.1 Chemical structures of DNA damage by UV radiation. **(A)** Cyclobutane pyrimidine dimer (CPD). **(B)** (6-4) pyrimidine photoproducts
Structures made using PubChemSketcher V2.4

1.2 DNA repair

Single stranded DNA damage is repaired by three pathways, base excision repair (BER), nucleotide excision repair (NER) and mismatch repair (MMR) (Chatterjee N, 2017).

BER repairs damage from oxidation and alkylation and the processing of single small base lesions (Almeida and Sobol, 2007). Initial lesion detection is directed by a glycosylase (Odell, Wallace and Pederson, 2013). The glycosylase family recognises a variety of single site damage markers and cleaves the bond between the base and the deoxyribose, leaving an AP site, a short patch (Dianov and Hübscher, 2013). This is AP site is the target for AP endonucleases which nicks the DNA backbone (Chatterjee N, 2017). DNA polymerase fills the single nucleotide gap and DNA ligase seals the DNA backbone (Almeida and Sobol, 2007).

BER repairs processed small, single base pair lesions, NER repairs bulkier adducts and helical distortions. NER recognizes a wide range of DNA substrates and primarily lesion caused by UV light. After initial lesion detection the DNA is nicked either side of the lesion by an endonuclease targeting the phosphodiester bonds, a single-stranded oligonucleotide is released leaving a single stranded patch (Houten, 1990; Compe and Egly, 2012). DNA polymerase and DNA ligase fill and seal the patch in a similar mechanism too BER (Orren and Sancar, 1990). This will be discussed in more detail later.

The final repair pathway for damage on single strands of DNA is MMR, this pathway deals with errors made during DNA replication. DNA polymerase catalyses the incorporation of complimentary DNA bases to the template strand. During this process non complimentary bases can be incorporated into the DNA resulting in a mismatch (Kunkel, 2009). MMR recognises this single stranded DNA 'damage' on the daughter strand (Arana and Kunkel, 2010). MutS homologs scan the DNA to find the DNA mismatch (Qiu *et al.*, 2015), MutL, in an ATP dependent manner traps MutS on the damaged region (Grilley *et al.*, 1989; Habraken *et al.*, 1998). This recruits a DNA helicase to unwind the DNA strands (Qiu *et al.*, 2015). MutH the endonuclease of this pathway joins the MutS/L complex translocated along and nicks the single strand of DNA around the lesion releasing neighbouring nucleotides from the DNA backbone. DNA polymerase and DNA ligase complete the process in a similar manner as the previous two pathways.

Double stranded DNA damaged is repaired by two pathways, homologous recombination (HR) and non-homologous end joining (NHEJ).

HR can repair double stranded DNA (DSB) breaks and interstrand crosslinks (Li and Heyer, 2008). After a DSB occurs, DNA around the 5' ends undergo a process called resection. This involves 5' DNA degradation to generate 3′ overhangs (Sung and Klein, 2006; Chen *et al.*, 2008; Nimonkar *et al.*, 2011). This 3' overhang invades a homologous sequence of undamaged DNA (Sung and Klein, 2006; Li and Heyer, 2008). DNA synthesis is primed of the invading 3' stand of DNA using the template DNA creating a D-loop (Sung and Klein, 2006; Li and Heyer,

2008). DNA polymerase extends the invading strand creating a holiday junction (Fekairi *et al.*, 2009).

Two pathways can progress from here, double-strand break repair of synthesis-dependent strand annealing (Sung and Klein, 2006).

In double stranded break repair DNA annealing or a second invasion event allows the other 3’ overhang to create a second holiday junction (Sugiyama, 2006 and Sugiyama, 1998). The two holiday junctions are resolved by endonuclease activity (Liu, 2004). During single strand break repair the holiday junction is resolved through branch migrations as the DNA slide, the invading strand is displaced after repair synthesis (Ira *et al.*, 2003). This newly synthesized 3' end of the invading anneals to the 3' overhang in the damaged DNA strand. (Allers & Lichten, 2001; Petalcorin, 2006).

The NHEJ repair pathway does not require homologous templates to repair DNA, unlike HR. This pathway again exploits DNA overhangs. Nucleases degrade these overhangs generated by the double stranded break in a process called resection and DNA polymerase resynthesises DNA from the processed DNA backbone (Chang *et al.*, 2017). This process can be repeat multiple times and a number of proteins are able to process the various DNA ends formed from a double stranded breaks. (Chang *et al.*, 2017). DNA ligase completes seals the DNA and completes this pathway (Wilson, Grawunder and Lieber, 1997).

1.3 SOS Response

Although the DNA repair mechanisms discussed earlier are extensive these pathways can be overwhelmed by large amounts of damage. When this happens the cell cycle is arrested and a global network of multiple DNA repair pathways is transiently activated to attempt DNA repair and cell survival, the SOS response (Baharoglu and Mazel, 2014).

The SOS response is induced by an accumulation of single stranded DNA during replication of DNA that is damaged (Sassanfar and Roberts, 1990). DNA polymerases are stalled near the replication fork as local DNA helicases attempt to unwind the DNA (Maslowska, Makiela-Dzbenska and Fijalkowska, 2019). Under these conditions the RecA protein, in an ATP dependent manner, binds to the these single stranded DNA regions and becomes activated (Walker, 1984; Houten, 1990). RecA activation stimulates self-cleavage of the repressor protein LexA (Little and Mount, 1982; Little, 1991). This LexA cleavage and degradation abolishes the repression of the SOS genes. This proteolysis affect at least forty genes in *E. coli* (Courcelle, 2001). In bacterial NER, which will be discussed further later, UvrA and UvrB are upregulated by the SOS response (Crowley & Hanawalt, 1998; Sancar, 1981) but the endonuclease, uvrC, is not (Yoakum and Grossman, 1981).

1.3 Nucleotide Excision Repair

Nucleotide excision repair is highly mechanistically conserved across all kingdoms of life. Damage detection, damage verification, DNA incision,

removal of the lesion containing DNA and DNA synthesis follows a similar pathway in all organisms.

Nucleotide excision repair in bacteria initiates via two different, but similar, pathways. Global genomic repair involves a complex of UvrA and UvrB scanning the genome searching of lesions. Next UvrC incises the damaged DNA (Verhoeven *et al.*, 2000).UvrD subsequently removes the lesion (Caron, Kushner and Grossman, 1985; Husain *et al.*, 1985) and DNA polymerase I and DNA ligase resynthesize and seal the DNA (Sancar and Rupp, 1983; Orren *et al.*, 1992). In addition to global NER, transcription-coupled repair occurs when damage stalls the translocating, transcribing, RNA polymerase (RNAP) (Mellon and Hanawalt, 1989). Mfd (transcription-coupling protein) displaces the damage-induced stalled RNAP (Selby and Sancar, 1993; Manelyte *et al.*, 2010) and recruits UvrA and UvrB to verify the damage (Assenmacher *et al.*, 2006; Deaconescu *et al.*, 2006, 2012; Ho, Van Oijen and Ghodke, 2018). Damage verification by UvrB and incision via UvrC and repair steps take place in the same way as global genomic repair.

1.5.1 Global Genome Repair (GGR)

The UvrA-C gene products were first identified in 1981 but it was n0t until 1983 that the mechanism by which they acted was first reconstituted *in vitro* and it was shown that the three proteins were required to cut the lesion either side of damaged DNA (Kacinski, Sancar and Rupp, 1981; Sancar, Clarke, *et al.*, 1981; Sancar, Kacinski, *et al.*, 1981; Sancar, Wharton, *et al.*, 1981; Sancar and Rupp, 1983). UvrA, UvrB and UvrC can

locate repair an incredibly chemically diverse range of damage substrates (Hanawalt and Haynes, 1965; Setlow and Carrier, 1966; Hanawalt *et al.*, 1979; Batty and Wood, 2000; Van Houten *et al.*, 2005). NER is mechanistically highly conserved, with damage detection, lesion incision, lesion removal and repair synthesis and ligation are performed by six proteins in prokaryotes and 30 proteins in eukaryotes. UvrA-D, DNA polymerase 1 and DNA ligase repair UV-induced lesions in bacteria (Figure 1.2)**Error! Reference source not found.**. UvrA performs a 3D search of DNA but in complex with UvrB, likely with a A_2B_2 stoichiometry, shifts to 1D sliding along DNA (Moolenaar, Schut and Goosen, 2005; Truglio, Croteau, *et al.*, 2006; Goosen and Moolenaar, 2008; Kad *et al.*, 2010). UvrA dissociates after the formation of a pre-incision complex where the lesion is passed to UvrB (Moolenaar, Höglund and Goosen, 2001; Wagner *et al.*, 2009). UvrC, a dual endonuclease, then binds to the DNA and performs single-stranded incisions on either side of the lesion on the same damaged strand (Verhoeven *et al.*, 2000). UvrD subsequently removes the damaged oligonucleotide and allows the UvrC to be recycled and nick the DNA elsewhere (Caron, Kushner and Grossman, 1985; Husain *et al.*, 1985). DNA polymerase I displaces the bound UvrB and resynthesizes the correct DNA followed by DNA ligase sealing the remaining nick (Sancar and Rupp, 1983; Orren *et al.*, 1992).

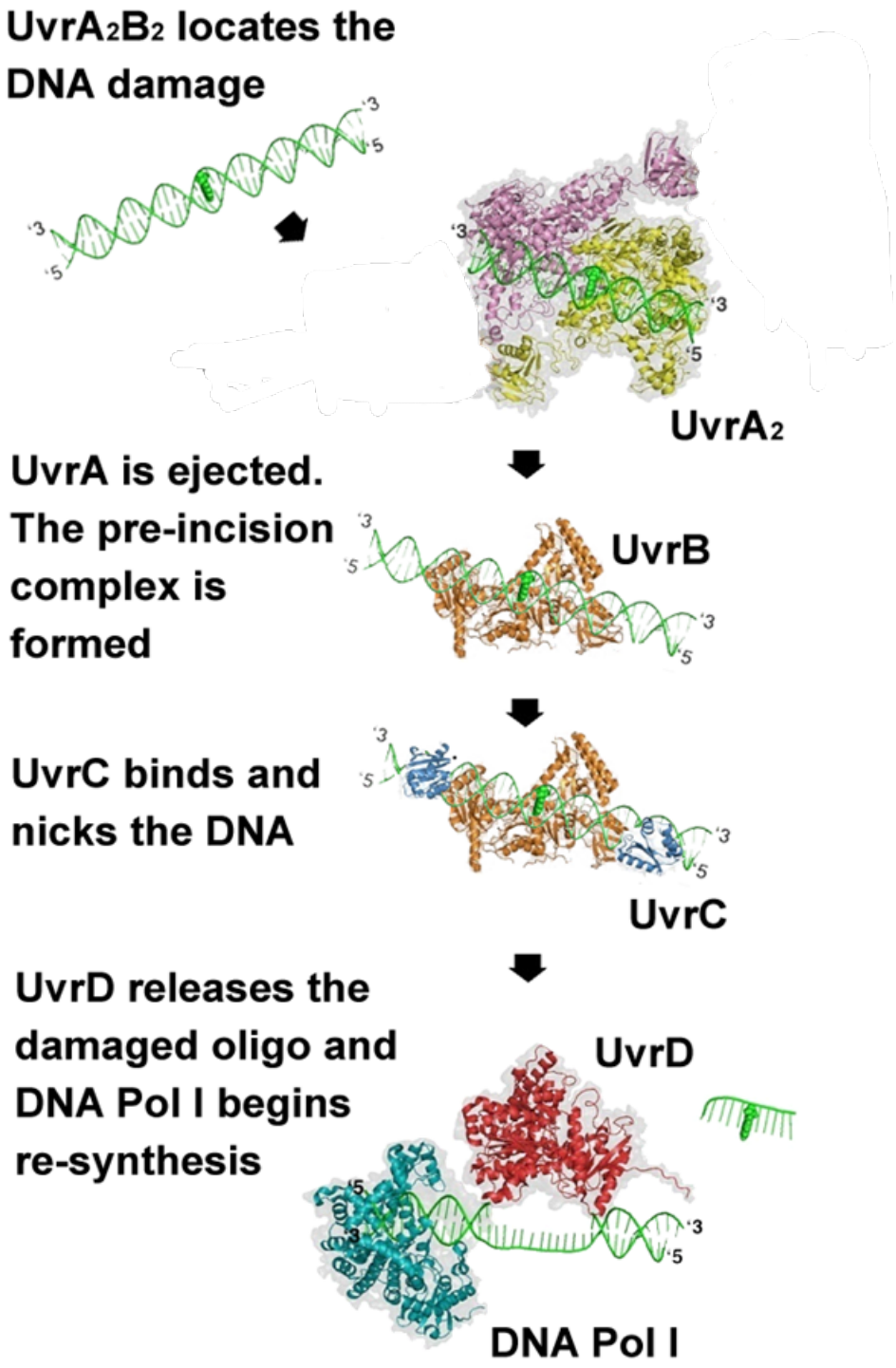

Figure 1.2. Structural model of bacterial nucleotide excision repair (taken from Kad and Van Houten 2012).

This shows DNA damage detection, damage verification, DNA incision, oligo release and DNA resynthis.

1.5.2 UvrA

A UvrA monomer contains two ATPase domains which belong to the ABC ATPase superfamily and work cooperatively together (Wagner, Moolenaar and Goosen, 2011), ATP binding domain 1 contains the insertion domain and UvrB binding domain, ATP binding domain 2 contains the zinc finger motif involved in DNA repair (Pakotiprapha *et al.*, 2008; Wagner, Moolenaar and Goosen, 2011). Inactivation of one ATP domain results in a loss of ATPase activity, ATP binding and hydrolysis is required for damage detection (Myles, Hearst and Sancar, 1991; Thiagalingam and Grossman, 1991; Thiagalingams and Grossman, 1993; Malta, Moolenaar and Goosen, 2007; Wagner, Moolenaar and Goosen, 2010). Each ATPase domain contains a Walker A motif (figure 1.3) ; mutations in these domains affects the loading of UvrB differently and are connected by a flexible linker (Pakotiprapha *et al.*, 2008; Timmins *et al.*, 2009; Stracy *et al.*, 2016). Recent single-molecule fluorescence studies combined with bulk assays have shown negative cooperativity between the ATPase sites, where the second site is only activated in the presence of damage (Barnett and Kad, 2018). UvrA binds to UvrB through the first nucleotide binding domain and domain 2 of UvrB, which will be discussed later (Claassen and Grossman, 1991; Pakotiprapha *et al.*, 2008). UvrA has two zinc fingers, the N-terminal finger is not essential for NER but has a role in processing Okazaki fragments via UvrD in a DNA pol 1 free replication pathway (Visse *et al.*, 1993; Moolenaar, Moorman and Goosen, 2000).

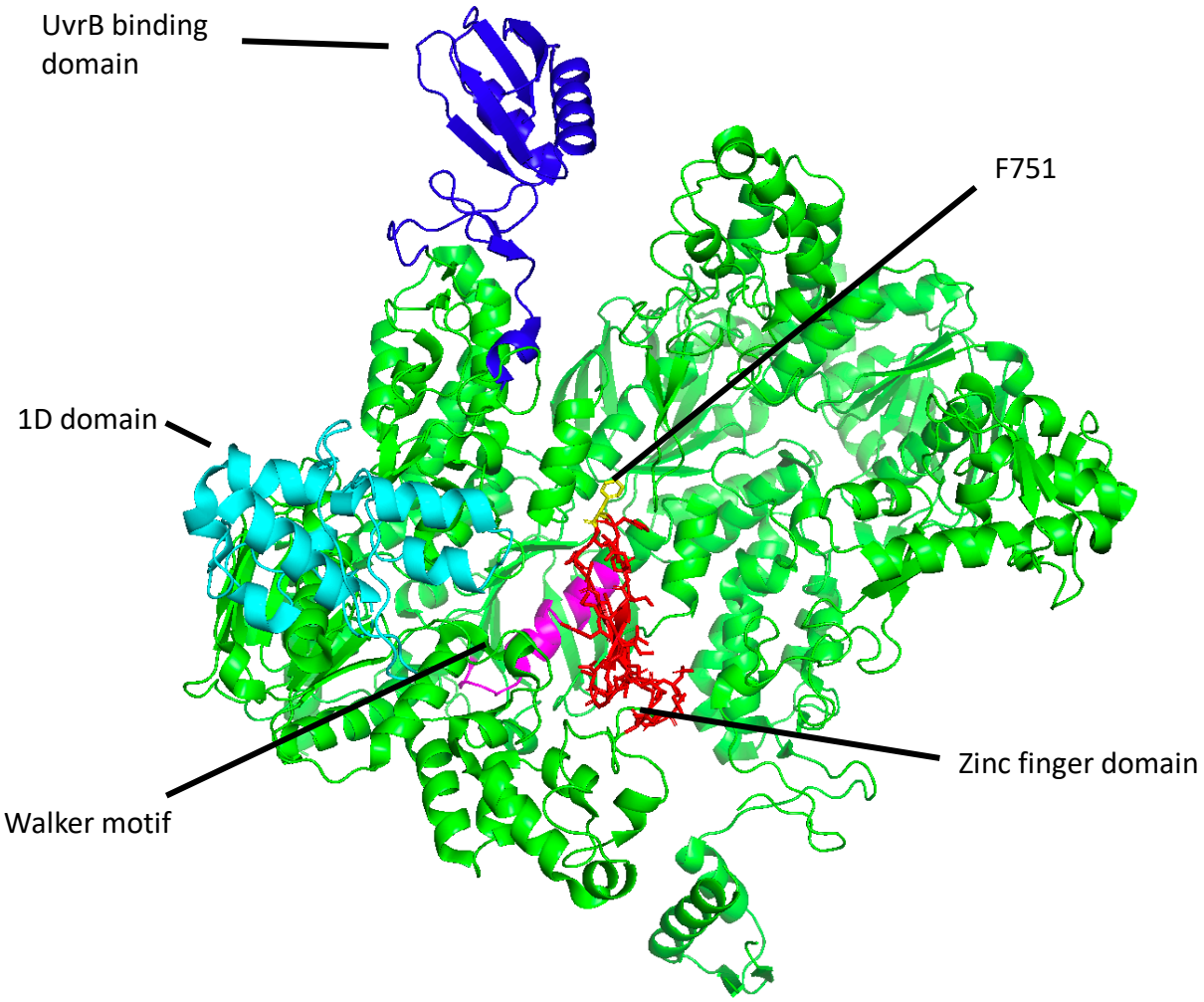

Figure 1.3. Crystal structure of *B. stearothermophilus* UvrA.
UvrB binding domain in blue, 1D domain in cyan, Walker motif in magenta, the zinc finger domain in red with the tip of the zinc finger F751 shown in yellow
PBD number: 2R6F

1.5.3 The C-terminal Zinc finger of UvrA

The C-terminal Zinc finger, in Figure 1.3, is located in ATP binding domain 2 and has a clear damage related function as well as a role in the overall stability of the UvrA structure (Visse *et al.*, 1993; Wang, Mueller and Grossman, 1994; Croteau *et al.*, 2006; Wagner, Moolenaar and Goosen, 2011). Replacing this zinc finger domain with 11 glycine residues (ZnG-UvrA) does not affect the mutant's ability to bind DNA, the mutant binds to DNA with tighter affinity than the wildtype, but rather affects damage

specific binding (Croteau *et al.*, 2006). This directly affects UvrB, ZnG-UvrA exhibits reduced UvrB loading to damage and fails to stimulate the ATPase of UvrB due to nonspecific DNA binding (Croteau *et al.*, 2006). The structural disorder displayed by the ZnG-UvrA is likely due to disrupted dimerization, the zinc finger and hydrolysis of ATP stabilize the UvrA into its DNA binding dimer conformation (Malta, Moolenaar and Goosen, 2007; Wagner *et al.*, 2009; Kad *et al.*, 2010; Wagner, Moolenaar and Goosen, 2010)

1.5.4 UvrA Dimer

The UvrA dimer has a groove which allows DNA to fit between the UvrA subunits, the dimer interacts with 30-33 bps of the DNA backbone, interpreting DNA lesions indirectly through conformational changes in the DNA structure allowing for a range of DNA lesions to be detected, a key characteristic of NER (Van Houten *et al.*, 1987; Pakotiprapha *et al.*, 2008; Timmins *et al.*, 2009; Jaciuk *et al.*, 2011). UvrA dimers bend the DNA to varying degrees, in some damage substrates by as much as 50% (Bellon, Coleman and Lippard, 1991; Van Houten and Snowden, 1993; Jaciuk *et al.*, 2011). The NER proteins range of damage substrates include processing the extremely dangerous DNA crosslinks (Bhagwat and Roberts, 1987). The area of DNA interaction in the UvrA dimer is highly conserved and positively charged allowing for structural disruption of DNA to be detected via electrostatic interaction as seen in XPA, which has a

similar DNA cleft (Camenisch *et al.*, 2006, 2007). The insertion domain of nucleotide binding domain 1 stabilizes the UvrA interaction with the DNA backbone through two highly conserved arginine residues, ATP hydrolysis leads to strand separation of the DNA and verification of damage by UvrB (Wagner, Moolenaar and Goosen, 2010, 2011).

1.5.5 UvrB

UvrB is stable as a monomer (Orren and Sancar, 1989) but is able to form dimers in solution through the C-terminal region (Moolenaar *et al.*, 1995) UvrB can interact with UvrA and UvrC (figure 1.4) simultaneously to form a motile complex on DNA (Springall *et al.*, 2017) and performs the last damage sensing check before incision takes place (Moolenaar, Moorman and Goosen, 2000; Verhoeven, van Kesteren, *et al.*, 2002). UvrB contains 5 domains (figure 1.4), 1a, 1b, 2, 3 and 4 with six helicase domains found in domains 1a and 3, UvrA interacts with both domain 2 and 4, UvrC binds to domain 4 only (Hsu *et al.*, 1995; Truglio, Karakas, *et al.*, 2006; Pakotiprapha *et al.*, 2008; Kisker, Kuper and Van Houten, 2013).

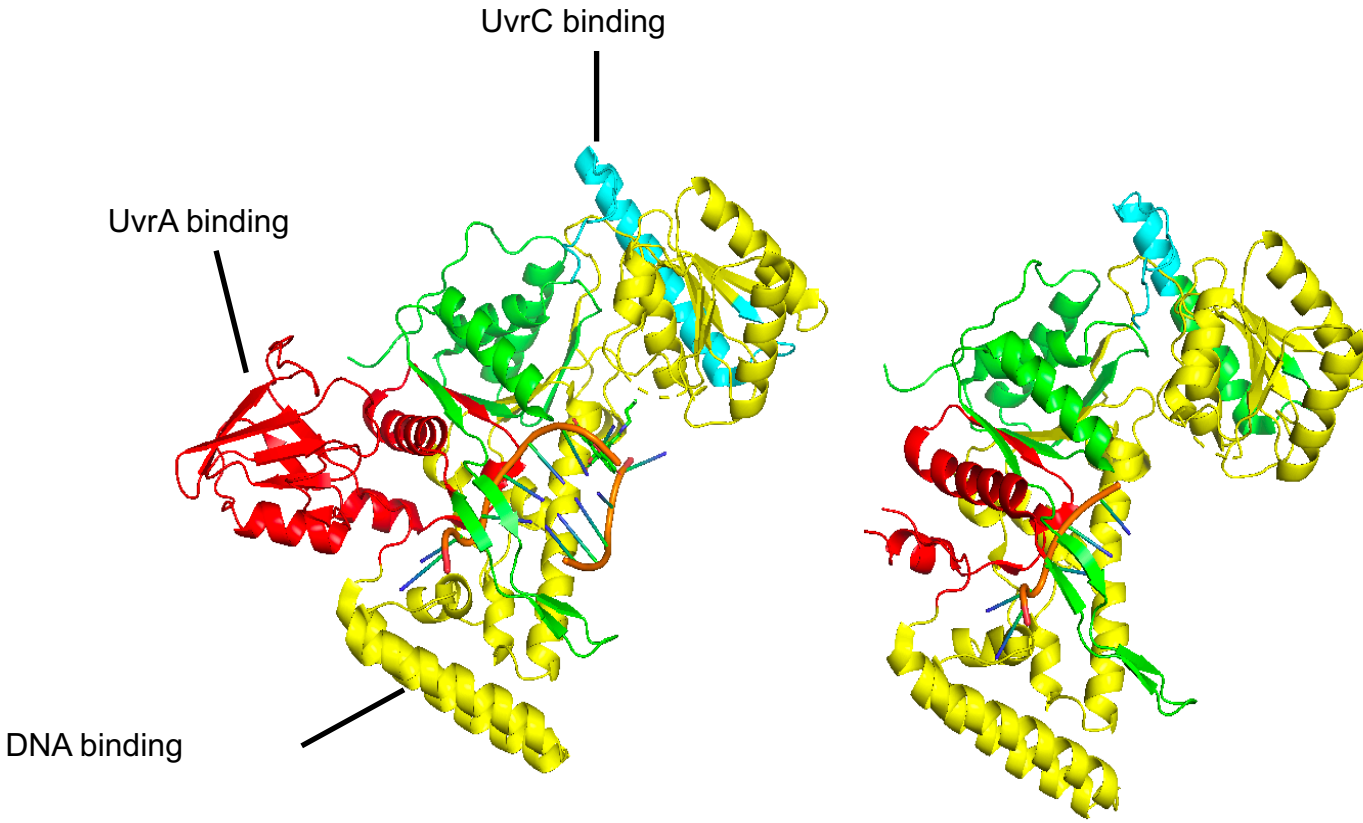

Figure 1.4. Crystal structure of *Bacillus caldotenax* UvrB in complex with DNA.

Two views are presented to clearly show the DNA.

UvrA binding domain is shown in red, the DNA binding domain is shown in yellow and the less well defined UvrC binding domain is shown in cyan.

The DNA backbone is shown in orange and bases are represented by blue and green.

Domains 1a and 1b are connected by a highly conserved β-hairpin, UvrB interacts with DNA by inserting this β-hairpin between the strands of DNA with a padlock mechanism (Truglio, Karakas, *et al.*, 2006) (Figure 1.5).

The β-hairpin contains several aromatic and hydrophobic amino acids.

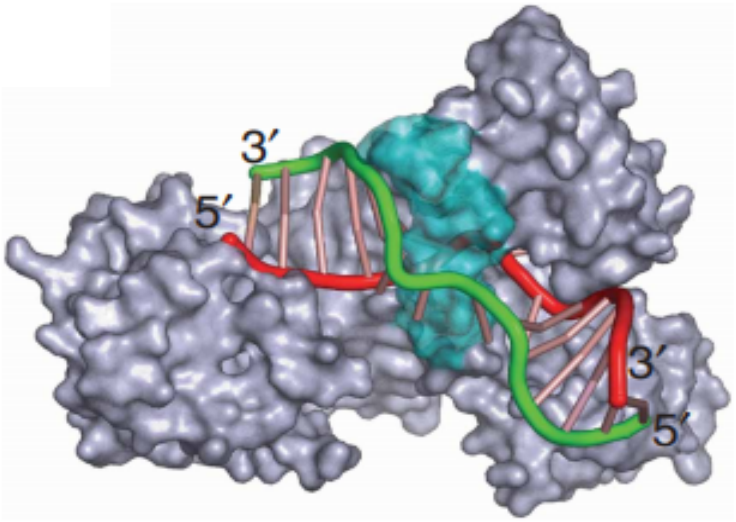

Figure 1.5. Model of UvrB 'padlock' interaction showing the β–hairpin directly interrogating the DNA, taken from Truglio *et al*., 2006. The inner strand of the DNA (red) threads and is clamped between the β–hairpin (cyan) and domain 1b of UvrB and the outer strand (green) travels around the β–hairpin.

Pheylalanine108 located at the tip of the hairpin helps to separate the DNA strands and tyrosine93 prevents UvrB from binding to undamaged DNA (Moolenaar, Höglund and Goosen, 2001; Skorvaga *et al.*, 2004; Truglio, Karakas, *et al.*, 2006). During translocation nucleotides are flipped behind the β–hairpin into a hydrophobic nucleotide binding pocket, Tyr96 at the base of the β–hairpin is essential for damage verification (Theis *et al.*, 1999; Skorvaga *et al.*, 2002, 2004; DellaVecchia *et al.*, 2004; Truglio, Karakas, *et al.*, 2006; Wang *et al.*, 2006) (figure 1.6).

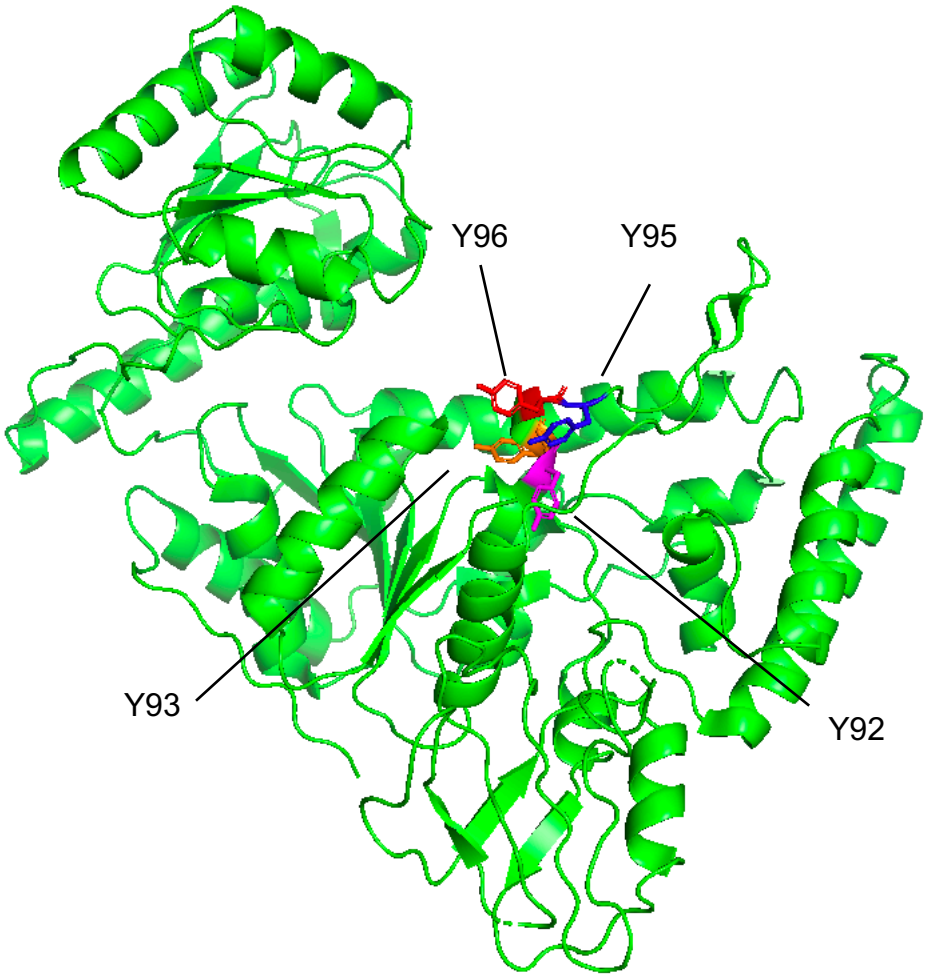

Figure 1.6. Crystal structure of *Bacillus caldotenax* UvrB. Key tyrosine residues in the β-hairpin are highlighted.
Tyrosine 96 is shown in blue, Tyrosine 95 is shown in red , Tyrosine 93 orange is shown in blue and Tyrosine 92 is shown in magenta.
PBD number: 1D9X

Current studies have not conclusively proven whether the damaged or undamaged strand is clamped between the β–hairpin and domain 1b but it is likely the undamaged strand ensuring the damaged strange is interrogated directly (Van Houten *et al.*, 1987; Orren *et al.*, 1992).

1.5.6 Stoichiometry of the UvrAB Complex

The oligomeric state of UvrAB is controversial, initial bulk studies without DNA and in solution suggest an A_2B_1 conformation but with another UvrB binding site available (Orren and Sancar, 1989). More recent light scattering experiments support this stoichometry even with an excess of UvrB which would reflect in vivo concentrations (Pakotiprapha *et al.*, 2009). Small-angle X-ray scattering combined with structural studies of the *Geobacillus stearothermophilus* UvrAB show an elongated heterotetramer in solution with a UvrB flanking a central UvrA dimer with two distinct conformations observed by the UvrA dimer. The first 'open tray' ready to bind DNA and closed groove when in contact with native DNA. When UvrA locates damage the DNA would force the former conformation creating a highly stable complex (Thiagalingams and Grossman, 1993; Pakotiprapha *et al.*, 2012). The presence of two UvrB subunits allows for damage detection in both strands of the DNA, likely in an orientation with damage sensing β–hairpins directed inwards towards each other allowing for easy handover of the damaged DNA from the

dissociating UvrA dimer to from a UvrB-DNA complex (Verhoeven, Wyman, *et al.*, 2002; Pakotiprapha *et al.*, 2012; Webster *et al.*, 2012). Scanning force microscopy has revealed two UvrB subunits allow for damage in both DNA strands simultaneously, increasing the efficiency of NER (Verhoeven, Wyman, *et al.*, 2002). Fluorescent studies using both quantum dots and fluorescent proteins further support the A_2B_2 structural data (Malta *et al.*, 2008; Kad *et al.*, 2010). With the *in vivo* excess of UvrB compared to UvrA pre-SOS response and with the support of the more sophisticated methods of detection, the most reasonable stoichiometry is A_2B_2 (for simplicity A_2B_2 will be called UvrAB). UvrAB as a damage sensing complex has many advantages over UvrA dimer alone, an increased number of damage-sensing domains can detect lesions and helical distortions of both stands DNA and biochemical studies have demonstrated a higher binding affinity with damage than UvrA alone (Reardon *et al.*, 1993; Jaciuk *et al.*, 2011; Wirth *et al.*, 2016). UvrAB scans DNA more efficiently than UvrA. UvrA has a DNA footprint of 33bp and a lifetime on DNA of 7 seconds, 50 UvrA dimers would search only 6% of genomic DNA in *E. coli* before the cell population divide every 20 minutes (Van Houten *et al.*, 1987; Sancar and Sancar, 1988; Kad *et al.*, 2010). The UvrAB complex has a smaller DNA footprint (19bp) but has an increased lifetime on DNA of 40 seconds (Van Houten *et al.*, 1987; Kad *et al.*, 2010). Single molecule fluorescence imaging has revealed that UvrAB slides along DNA one dimensionally rather than the UvrA dimer which employs 3D binding and releasing, as such a single UvrAB can scan 2500 base pairs in a single encounter, native pre-SOS levels of UvrAB (50-100)

are sufficient to scan the entire *E. coli* genome before cell division (Sancar and Sancar, 1988; Kad *et al.*, 2010). However, it should be noted, recent single molecule live cell fluorescence imaging suggests initial lesion detection is directed by UvrA, rather than the UvrAB complex, and UvrB is recruited later (Stracy *et al.*, 2016). When DNA is damaged severely cell division can be halted, during this SOS response the repressor, LexA, is inactivated which results in a tenfold increase in the cellular concentration of UvrA and UvrB allowing for quicker location of DNA lesions (Huisman, D'Ari and Gottesman, 1984; Sancar and Sancar, 1988).

1.5.7 UvrC

UvrC is a dual endonuclease which cuts the DNA either side of a lesion, *E. coli* UvrC has a low copy number ,10 (Yoakum and Grossman, 1981; Houten, 1990), and is not upregulated by the SOS response (Sancar, Kacinski, *et al.*, 1981; Sancar and Rupp, 1983). UvrC mediated incision is often considered the rate-limiting step of NER as it is the only protein capable of cutting the DNA both sides of the lesion and exists at a relatively low native concentration compared to UvrA and UvrB. Even with the low copy number of UvrC (Yoakum and Grossman, 1981) and incision of lesions being a potential bottleneck for NER, repair occurs quickly without a detectable accumulation of DNA strand breaks or the structural disruption (Gruskin and Lloyd, 1988). This was quantified further, at 100

J/m^2 of UVC, with no SOS upregulation, 10 $UvrA_2B_2$ complexes were found to be capable of processing 1000 photoproducts in 15 min (Chandrasekhar and Van Houten, 1994, 2000). *E. coli* genome is 4.6 × 10^6 bp long, 10–100 $UvrA_2B_2$ complexes result in a repair rate of 1 photoproduct per 1–2 kbp (Gruskin and Lloyd, 1988; Chandrasekhar and Van Houten, 1994, 2000). The single molecule florescence imaging studies described earlier have begun to explain how such a small number of proteins search through a vast sea of undamaged DNA locate and repair lesions, though the whole process is not fully understood (Kad *et al.*, 2010; Hughes *et al.*, 2013).

1.5.8 UvrBC

UvrB and UvrC can form complexes on processed DNA substrates (Zou *et al.*, 1997; Moolenaar, Uiterkamp, *et al.*, 1998; Wirth *et al.*, 2016), in solution (Seeberg, 1978; Hsu *et al.*, 1995) and using single molecule fluorescence imaging form a complex that can scan undamaged DNA (Hughes *et al.*, 2013). A full structure of UvrC and a UvrBC complex have not been determined, causing difficulties in confirming DNA binding domains and *in vivo* functions. As with UvrA and UvrB, a definitive UvrC stoichiometry has been indefinable, however, conclusive experiments show a single UvrC is sufficient for dual incision (Moolenaar *et al.*, 2000). However, there is evidence for dimeric conformations on certain DNA substrates, monomeric UvrC in solution and single UvrC molecules have been observed sliding along DNA strands (Schägger, Cramer and von Jagow, 1994; Singh *et al.*, 2002; Hughes *et al.*, 2013). The 3’ and 5’

incisions either side of the lesion are performed by the N and C terminals of UvrC respectively, independent inactivation of each domain revealed separate catalytic sites for each nick (Lin and Sancar, 1992; Verhoeven, van Kesteren, *et al.*, 2002). The N-terminal domain, 3' endonuclease, contains the UvrB binding domain, domain 4 of UvrB, interactions between these two domains result in the flexible UvrBC complex (Hsu *et al.*, 1995; Alexandrovich *et al.*, 1999; Sohi *et al.*, 2000). Deletion of domain 4 in UvrB abolishes 3' UvrC mediated incision, however, UvrB binding is not required for 5' cutting on a DNA substrate with a 3' nick (Moolenaar *et al.*, 1995; Wang *et al.*, 2006). The 3′-incision requires a stable UvrBC interaction unlike the 5′ cut. (Moolenaar *et al.*, 1995). It has been suggested UvrB could dissociate from the DNA before the 5' incision takes place rather than leaving via DNA pol I displacement before strand resynthesis, which was previously demonstrated (Orren *et al.*, 1992; Hsu *et al.*, 1995). The 3' incision precedes the 5' incision, however, a full 3' incision is not required for the second cut to take place, an artificial 3' nick can is sufficient for subsequent 5' endonuclease activity, removal of the 5' prime incision domain does not affect 3' prime cut (Moolenaar, Uiterkamp, *et al.*, 1998). Loss of the C-terminal domain abolishes 5' incision and ssDNA binding indicating a clear role in structure-specific DNA binding (Moolenaar, Uiterkamp, *et al.*, 1998; Singh *et al.*, 2002). The 5' endonuclease domain precedes two helix/hairpin/helix motifs (HhH), a flexible hinge connects these two areas and allows UvrC to exist in multiple conformations, this versatility contributes to the range of damage substrates NER can remove from DNA and helps UvrC to clamp on, and

stabilise, the DNA interaction (Aravind, Walker and Koonin, 1999; Shao and Grishin, 2000; Singh *et al.*, 2002; Verhoeven, van Kesteren, *et al.*, 2002; Karakas *et al.*, 2007). The HhH domain plays a key role in how UvrC binds to DNA, it allows UvrC to bind to regions of unpaired basses and could explain how UvrBC can bind to a bubble substrate in the absence of UvrA (Zou and Houten, 1999; Singh *et al.*, 2002). Early biochemical studies showed that UvrC has no effect on the DNA footprint of UvrB suggesting that the UvrBC interaction with DNA is mediated by UvrB, this was confirmed by single-molecule fluorescence imaging and AFM (Van Houten *et al.*, 1987; Hughes *et al.*, 2013; Wirth *et al.*, 2016). These experiments reveal UvrB and UvrC can form motile complexes on DNA, a number of mutations in UvrB affect the diffusion constant and lifetime of the complex on DNA confirming UvrB mediates the interaction between DNA in the UvrBC complex (Hughes *et al.*, 2013). UvrB in complex with both UvrA and UvrC increases the lifetime on DNA promoting more efficient one dimensional scanning of DNA, however, unlike UvrA UvrB does not affect the speed at which UvrC scans the genome, both UvrC and UvrBC scan the genome at the same speed, before cell division every 20 minutes at physiological salt concentrations (Kad *et al.*, 2010; Hughes *et al.*, 2013). Increasing the salt concentration increased the speed the proteins scan DNA indicating a hopping motion, due to the nature of this interaction with DNA UvrB could aid UvrC overcoming obstacles on DNA *in vivo*. (Tafvizi *et al.*, 2008; Hughes *et al.*, 2013). This function of this complex remains unclear, the complex was identified in bulk studies (Seeberg, 1978; Hsu *et al.*, 1995), but no clear

ability to repair DNA confirmed *in vitro* (Zou *et al.*, 1997; Moolenaar, Uiterkamp, *et al.*, 1998; Wirth *et al.*, 2016). The speed at which these proteins can scan, locate and remove damage is key to organism survival. The cellular environment *in vivo* is incredibly complex, UvrB has many binding partners that could affect NER activity.

1.5.9 UvrC Homologue, Cho

A second protein, homologous to the N-terminal domain of UvrC, is able to perform the 3' incision only (Lewis *et al.*, 1994; Moolenaar *et al.*, 2002). Cho is able to incise some bulky lesions more efficiently than UvrC alone and binds to a different UvrB domain than UvrC, permitting cooperation between the endonuclease proteins (Moolenaar *et al.*, 2002; Moolenaar, Schut and Goosen, 2005). Cho homologues are seen in bacteria closely related to *E. coli*, such as *Listerias* and *Clostridia*, though it is much more common for only UvrC to be present (Moolenaar *et al.*, 2002; Van Houten, Eisen and Hanawalt, 2002). Surprisingly, sequencing shows mycoplasmas only have Cho and are missing UvrC, presumably an unrealised protein performs the 5' incision as Cho does for the 3' (Van Houten, Eisen and Hanawalt, 2002). Interestingly, Cho is capable of making the 3' incision with UvrB in complex with DNA, UvrC must displace UvrB to perform the equivalent nick (Moolenaar, Schut and Goosen, 2005). Unlike UvrC, Cho is upregulated by the SOS response and has

been linked to interstand crosslink repair (Lewis *et al.*, 1994; Fernández De Henestrosa *et al.*, 2000; Courcelle *et al.*, 2001; Perera *et al.*, 2016).

1.5.10 UvrD and Post Incision Events

UvrD is the most abundant helicase found in *E.coli* and upregulated by the SOS–response, single molecule studies have shown that UvrD can unwind double stranded DNA from a single nick, the key regulator of mismatch repair, MutL, can enhance this process (Arthur and Eastlake, 1983; Dessinges *et al.*, 2004; Matson and Robertson, 2006; Ordabayev *et al.*, 2018). UvrD can also expose blocked DNA lesions by forcing stalled RNA polymerase back along DNA, this will be discussed more later (Epshtein *et al.*, 2014).

After the dual incision directed by UvrC, the 12 - 13 nucleotide patch is no longer hydrogen bonded, but remains in the post incision complex (Sibghat-Ullah, Sancar and Hearst, 1990; Orren *et al.*, 1992). UvrD subsequently removes the damaged oligonucleotide and allows the UvrC to be recycled and nick the DNA elsewhere (Caron, Kushner and Grossman, 1985; Husain *et al.*, 1985). DNA polymerase I with UvrD displaces the bound UvrB and resynthesizes the correct DNA followed by DNA ligase sealing the DNA (Orren *et al.*, 1992). In the absence of UvrD, UvrC dissociates from the DNA slowly, likewise, UvrB requires both UvrD and DNA polymerase to be efficiently recycled (Caron, Kushner and Grossman, 1985; Husain *et al.*, 1985; Orren *et al.*, 1992). UvrD in the

absence of other NER proteins exhibits a very slow helicase activity indicating direct protein interactions are needed for efficient lesion removal *in vivo* (Runyon and Lohman, 1993). Unique interactions between the NER proteins and UvrD were confirmed to remove damage as the homologous Rep helicase cannot be substituted for UvrD in NER (Husain *et al.*, 1985). UvrB is the likely candidate as it has been shown to remain bound to DNA after UvrD activity, waiting to be displaced by DNA pol 1 (Orren *et al.*, 1992). Immunoprecipitation and surface plasmon resonance spectroscopy have revealed direct interactions between UvrB and the C-terminal domain of UvrD, suggesting that UvrB in the preincsion complex recruits UvrD to initiate DNA unwinding (Ahn, 2000; Manelyte *et al.*, 2009).

The main role of DNA polymerase I is processing the lagging strands of the DNA fork in replication, in DNA polymerase I negative cells UvrB and UvrD direct DNA polymerase independent DNA replication (Olivera and Bonhoeffer, 1974; Joyce and Grindley, 1984; Moolenaar, Moorman and Goosen, 2000). DNA polymerase I deficient cells require UvrA/B/D to process Okazaki fragments by activating the helicase activity of UvrD (Moolenaar, Moorman and Goosen, 2000; Atkinson *et al.*, 2009). In this DNA Pol I independent pathway UvrC binding to UvrAB would be lethal on the template strand, producing double stranded breaks, conversely, incision on Okazaki fragments could help to remove RNA primers (Moolenaar, Moorman and Goosen, 2000). This could be a general role for the UvrBC complex. When UvrB and UvrC were discovered to form a motile complex on DNA it was suggested UvrC was chaperoned by UvrB

to limit unwanted nuclease activity (Hughes *et al.*, 2013). However bulk studies revealed the Uvr proteins have been shown to incise undamaged DNA with a nucleotide turnover analogous to base excision repair acting on spontaneous DNA lesions (Holmquist, 1998; Kunkel and Bebenek, 2000; Branum, Reardon and Sancar, 2001).

1.5.11 Transcription Coupled Repair

During transcription, Mfd recruits UvrA to, and displaces, stalled RNAP on DNA lesions (Selby and Sancar, 1993; Manelyte *et al.*, 2010). Interestingly both UvrA and XPC, the canonical initiators of GGR in both eukaryotes and prokaryotes, are non-essential to transcription coupled repair (TCR), indicating Mfd initiates bacterial lesion detection (Mu and Sancar, 1997; Manelyte *et al.*, 2010).

Mfd interacts with UvrA after large structural changes which result in conformational similarity to three N-terminal domains of UvrB, including the UvrA binding domain (Assenmacher *et al.*, 2006; Deaconescu *et al.*, 2006, 2012). This would allow a UvrA dimer to simultaneously bind to one UvrB and one Mfd and scan for DNA lesions, a similarly complex translocating ‘repairosome’ structure has been imaged between UvrA/B/C (Assenmacher *et al.*, 2006; Springall *et al.*, 2017). Single molecule studies have revealed that upon binding RNAP, RNAP and Mfd would rapidly dissociate from this complex leaving $UvrA_2$-UvrB-DNA complex (Fan *et al.*, 2016). After the recruitment of UvrA to the lesion via Mfd the

subsequent damage verification by UvrB and dual incision via UvrC mechanistically takes place in the same way as global genomic repair.

UvrD has been shown to expose DNA lesions covered by stalled RNAP in cooperation with NusA without terminating transcription (Epshtein *et al.*, 2014). As discussed earlier UvrD can interact with UvrB, UvrA can also directly bind to NusA (Cohen *et al.*, 2010). UvrD could directly bring UvrB to exposed lesions or help to initiate GGR repair via UvrAB complexes. A similar mechanism could involve NusA and UvrA, these processes provide direct links between RNAP and GGR and highlight the complexity of DNA repair.

1.4 Eukaryotic NER

Initial lesion detection is mediated by XPC, like UvrA this initiator of NER can deal with a range of chemically diverse DNA damage substrate and has been shown to bend the DNA, distorting the double helix backbone (Bunick *et al.*, 2006; Mocquet *et al.*, 2007; Sugasawa *et al.*, 2009; Clement *et al.*, 2010; Puumalainen *et al.*, 2016).

Rad23 can help to stabilize this XPC lesion complex (Araki *et al.*, 2001; Xie *et al.*, 2004). UV-DDB can aid in lesion detections, UV-DDB binding to lesions promotes ubiquitin of XPC (Keeney, Chang and Linn, 1993; Takao *et al.*, 1993; Fitch *et al.*, 2003; Xie *et al.*, 2004; Fei *et al.*, 2011). This XPC modification leads to other NER factor recruitment (Gillette *et al.*, 2006). Cockayne syndrome B protein (CSB) recruits ubiquitin ligase to sites of DNA damage and may play a role in XPC ubiquitylation (Weems *et al.*, 2017). CSB is very structurally similar to Mfd (Troelstra *et al.*, 1992; Selby and Sancar, 1993) and has been shown to enhance transcription elongation by RNAP (Selby and Sancar, 1997). It should be noted that, in *in vitro* assays, Rad23 and UV-DDB are not essential for lesion removal (Tapias *et al.*, 2004; Xie *et al.*, 2004).

XPC is able to recruit the TFIIH complex (Table 1) to verify and remove the damage by interacting with p62 and XPB directly (Araújo, Nigg and Wood, 2001; Bernardes de Jesus *et al.*, 2008). TFIIH is a highly conserved 10 subunit complex (figure 1.7) with two ATP dependent helicases, XPD and XPB which have 5’ – 3’ and 3’ – 5’ polarity respectively, they direct DNA repair (Compe and Egly, 2012; Gibbons *et*

al., 2012; Luo *et al.*, 2015; Greber *et al.*, 2017). XPB from within the TFIIH complex, together with RNA polymerase II, plays a vital role in transcription (Thomas and Chiang, 2006; Grünberg and Hahn, 2013; Luo *et al.*, 2015). The CAK complex regulates transcription through the CDK7 subunit (Busso *et al.*, 2000; Sandrock and Egly, 2001) and is not involved in DNA repair (Compe and Egly, 2012).

The ATPase activity of XPB is mediated by p52 and p8 and directs TFIIH to bind stably to damage, the helicase activity of XPD is facilitated by p44 and exposes the DNA lesion (Compe and Egly, 2012; Abdulrahman *et al.*, 2013; Luo *et al.*, 2015; Greber *et al.*, 2017). XPD will be discussed more later. Unlike bacterial NER, two proteins perform the dual incision of the DNA lesion and the initiation of repair and DNA synthesis does not require the 3' incision to take place (Staresincic *et al.*, 2009). XPF makes the 5' incision, DNA polymerase begins resynthesis using the undamaged DNA strand as a template, finally XPG makes the 3' incision (O'Donovan *et al.*, 1994; Staresincic *et al.*, 2009; Manandhar, Boulware and Wood, 2015).

Cryo-electron microscopy revealed that the second RecA domain of XPD and XPB interact with p44 and p52 respectively and p8 further stabilizes TFIIH via XPB (Kainov *et al.*, 2008; Greber *et al.*, 2017). The ATPase activity and helicase activity of XPB and XPD respectively, together, open the damaged DNA for lesion processing, the helicase action of XPB is not required for NER (Coin, Oksenych and Egly, 2007). The TFIIH complex is stabilized at damaged sites by the ATPase activity of XPB (Oksenych *et al.*, 2009). Similarly to how the helicase XPB activity is dispensable for NER, the ATPase activity of XPD is not needed for DNA transcription

(Tirode *et al.*, 1999; Coin, Oksenych and Egly, 2007). XPB from within the TFIIH allows promotor escape in transcription by separating the DNA strands (Moreland *et al.*, 1999; Tirode *et al.*, 1999; Luo *et al.*, 2015). CDK7 from within the CAK complex phosphorylates RNA polymerase II, initiating dissociation and allow for mRNA processing factors to bind (Moreland *et al.*, 1999; Tirode *et al.*, 1999; Larochelle *et al.*, 2012). Mutations in XPB result in rapid dissociation of CAK from the TFIIH complex stalling transcription, conversely, CAK accumulates at DNA damage in XPD mutated cells (Zhu *et al.*, 2012). CAK inhibits the helicase activity of XPD, CDK7 specifically has been shown to phosphorylate several NER regulators (Araújo *et al.*, 2000).

The accessory proteins that regulate enzyme activity of XPB and XPD are vital to the structural integrity of TFIIH. p44 and p34 interact to provide stability to the TFIIH complex mostly through the C-terminal zinc-binding domain of p34 (Radu *et al.*, 2017). The RING domain of p44 interacts with an N-terminal von Willebrand factor A fold in p34, the C4 domain of p34 stabilizes this interaction greatly (Riedinger *et al.*, 2010; Schmitt *et al.*, 2014; Radu *et al.*, 2017). There is evidence the p44/p34 interaction could begin the TFIIH formation, p44 has been to shown interact with p62 and p34 can bind to p52 providing a highly stable core, this would allow the other enzymes to bind after assembly (Tremeau-Bravard, Perez and Egly, 2001; Luo *et al.*, 2015). The C-terminal of p34 directly stabilizes p52 and p62 interactions providing further evidence for core stability roles (Radu *et al.*, 2017).

Mutations in the TFIIH complex can lead to xeroderma pigmentosum, Trichothiodystrophy and Cockayne syndrome, reviewed in (Cleaver *et al.*, 1999), the majority of these mutations affect the two motor domains of XPD disturbing DNA and ATP binding regions and therefore NER (Dubaele *et al.*, 2003). These diseases are devastating, extreme photosensitivity causes higher rates of skin cancers, premature aging and early death (Ahmad and Hanaoka, 2008).

Table 1. Composition of the TFIIH complex. Key roles of individual subunits are

TFIIH Subcomplex		**Function**
Core	XPB	3′ to 5′ ATP-dependent helicase.
	p62	Can bind p44. Structural roles
	p52	Regulates ATPase of XPB. Structurally important.
	p44	Regulates ATPase of XPD. Structurally important.
	p34	Evidence to show, with p44, could begin TFIIH formation.
	p8	Regulates ATPase of XPB.
XPD	XPD	5′ to 3′ ATP-dependent helicase. Very little helicase activity without p44. Forms a bridge between the CAK and the core.
CAK	CDK7	Negatively regulates XPD.
	Cyclin H	Regulates the CDK7 kinase activity
	Mat1	Structurally important for CAK

1.4.1 XPD

XPD is a 5’ – 3’ helicase containing two motor domains (HD1 and HD2) a 4Fe-S cluster, ARCH domain and C-terminal domain which allows for TFIIH incorporation via p44 displayed in figure 1.7 (Sung *et al.*, 1993; Lehmann, 2001; Abdulrahman *et al.*, 2013). XPD is vital in the overall structure of TFIIH linking the core subunits with the CAK complex (Keriel *et al.*, 2002; Dubaele *et al.*, 2003).

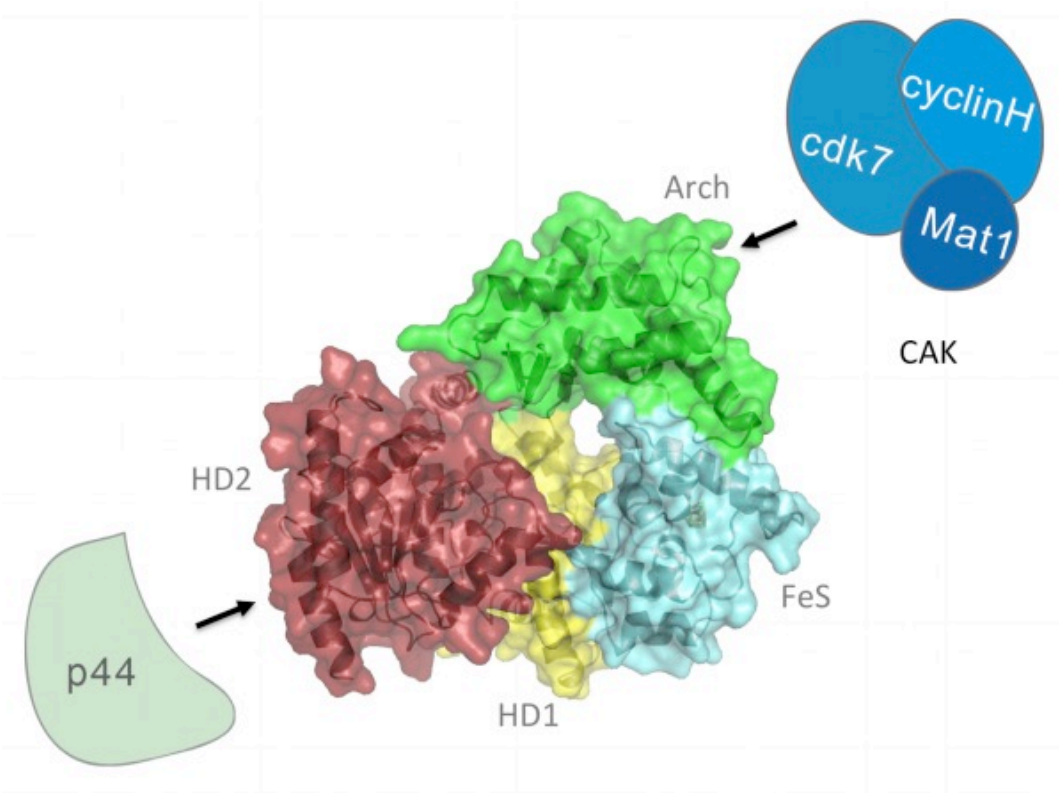

Figure 1.7. Model representation of XPD and its binding partners p44 and MAT1 within CAK taken from Kuper *et al*., 2014. The two motor domains, HD1 and HD2, are marked as yellow and red respetivley. The FeS domain is shown in cyan. The ARCH domain (green) binds to MAT1 in the CAK complex, p44 binds to the C-terminal domain of XPD.

The N-terminal domain of XPD binds MAT1, mutations in either the N or C-terminal destabilase binding interactions with the respective binding partners and affect transcription and DNA repair, reducing cell survival (Taylor *et al.*, 1997; Sandrock and Egly, 2001; Kim *et al.*, 2015).

Two RecA domains, HD1 and HD2, contain the helicase motifs, HD1 also contains the ARCH domain and FeS cluster (Kuper *et al.*, 2014; Greber *et al.*, 2017). In other SF2 helicases, the RecA like folds have been shown to couple ATP hydrolysis to DNA translocation, given the highly conserved nature of motor domains a similar process could take place in XPD (Dillingham, Wigley and Webb, 2000; Singleton and Wigley, 2002). Indeed it has been demonstrated that ATP binds and is hydrolyzed between the two motor domains, the simultaneous action of these domains working together drives DNA translocation (Liu *et al.*, 2008).

The 4Fe-4S cluster is critical in the stability of the protein, disruptions in this domain result in loss of helicase activity (Rudolf *et al.*, 2006; Pugh *et al.*, 2008). ATP can still be hydrolyzed if the FeS cluster is completely removed and protein structure remains, demonstrating a direct role in DNA strand displacement for helicase activity (Rudolf *et al.*, 2006). This domain also mediates ssDNA translocation and unwinding of DNA duplexes, likely, the FeS mediates the coupling of ATP hydrolysis to translocation (Pugh *et al.*, 2008). This highly conserved domain could play a role in damage verification, in MutY the redox properties of a similar cluster are modulated by DNA binding (Boon *et al.*, 2003). At the equivalent position in UvrB is a β–hairpin which interrogates the DNA for lesions, a similar change in oxidation state could be involved in DNA

damage verification of XPD (Rudolf *et al.*, 2006; Pugh *et al.*, 2008; Wolski *et al.*, 2008). Adjacent to the FeS cluster is a pocket (Wolski *et al.*, 2008) similar to the hole nucleotides are flipped into while the β–hairpin interrogates the DNA (Skorvaga *et al.*, 2002; Truglio, Karakas, *et al.*, 2006). Redox potential changes have been reported when XPD binds to DNA and increases after ATP hydrolysis further linking redox to enzymatic activity (Mui *et al.*, 2011). The ARCH domain anchors CAK via the MAT1 (figure 1.7) subunit and contributes to the overall stability of TFIIH, removing the ARCH domain completely abolishes XPD interaction with TFIIH core (Abdulrahman *et al.*, 2013). CAK complex binding to the ARCH domain inhibits the helicase activity of XPD (Araújo *et al.*, 2000; Kuper *et al.*, 2012; Abdulrahman *et al.*, 2013). CAK inhibition can be relieved by p44 and binding of NER factors once XPD is integrated into TFIIH, suggesting CAK negatively regulates lesion removal (Sandrock and Egly, 2001; Coin *et al.*, 2008). Disrupting the p44/XPD interaction destabilizes the anchoring of CAK to the ARCH domain and overall TFIIH. p44 has been shown to anchor the subunits via MAT1 suggesting this interaction mediates p44 relieving CAK inhibition (Sandrock and Egly, 2001; Kim *et al.*, 2015). Together the cluster and ARCH domains form a deep groove which interacts with ssDNA (Fan *et al.*, 2008; Liu *et al.*, 2008; Abdulrahman *et al.*, 2013). Single-stranded DNA can thread though this groove to reach the two motor domains (Greber *et al.*, 2017). Despite this deep grove, XPD can directly bypass proteins in complex with DNA, an undoubtable characteristic of the cellular environment *in vivo* suggesting large conformation changes are needed to translocate past obstacles

(Honda *et al.*, 2009). The C-terminal domain binds directly to the N-terminal domain of p44, this interaction directly regulates the DNA unwinding properties of XPD and will be discussed more later (Kuper *et al.*, 2014; Kim *et al.*, 2015).

Unlike the bacterial NER, proteins XPD reacts to different lesions in dissimilar ways. Bulky lesions on the translocating strand stall the protein whereas smaller lesions are recognised more efficiently on the opposite strand and form more stable complexes (Mathieu, Kaczmarek and Naegeli, 2010; Buechner *et al.*, 2014).

1.4.2 p44

The N-terminal domain of p44 interacts with XPD and the C-terminal domain binds three zinc atoms, one on the C4 zinc finger and two in a RING domain (Coin *et al.*, 1998; Fribourg *et al.*, 2000; Tremeau-Bravard, Perez and Egly, 2001; Kim *et al.*, 2015). This subunit of TFIIH has roles in both NER and transcription and directly activates the helicase activity of XPD , these are shown in figure 1.8 (Seroz *et al.*, 2000; Dubaele *et al.*, 2003; Kuper *et al.*, 2014).

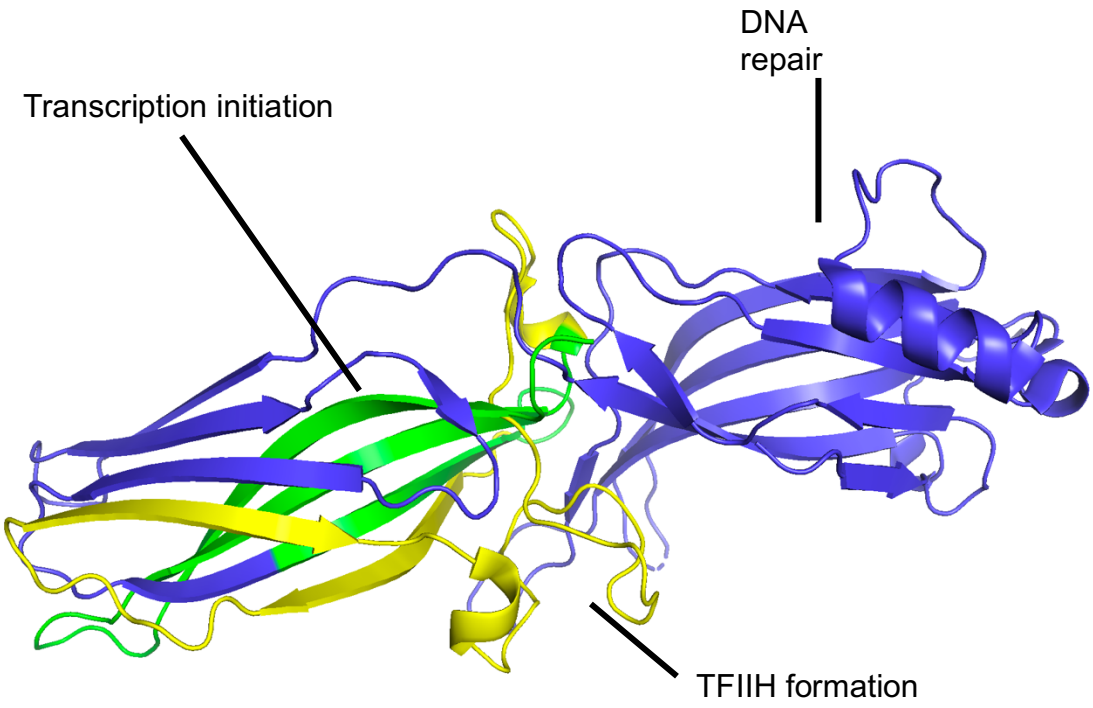

Figure 1.9. Crystal structure of *Bos taurus* p44.

The domain associated with DNA repair is show in blue, the domain associated with TFIIH formation is show in shown in yellow and he domain associated with transcription initiation is show in green.

PBD number: 3UGU

In yeast, p44 was determined to be essential for translation initiation and affected UV sensitivity (Yoon *et al.*, 1992). This was confirmed through mutations in the conserved N-terminal domain of p44 reducing TFIIH activity, directly through loss of interaction with XPD which disrupts helicase function, XPB-mediated phosphodiester bond formation and overall core TFIIH stability (Geourjon and Deléage, 1994; Coin *et al.*, 1998; Moreland *et al.*, 1999; Seroz *et al.*, 2000). A von Willebrand factor A fold in the N-terminal domain of p44 directly interacts with XPD to stimulate helicase actively, mutating nearby alpha helices does not affect XPD binding or function, indicating a small binding surface area (Kim *et*

al., 2015). In TFIIH p44 has been shown to bind near HD2 of XPD, delicately affecting the helicase motifs that couple ATPase and helicase activity (Fairman-Williams, Guenther and Jankowsky, 2010; Greber *et al.*, 2017).

The C-terminal zinc finger plays a significant role in the TFIIH structure, mutating key cysteine residues disrupts the overall complex by stopping p62 incorporation into the complex core, immunopurification showed p44 and p62 were still able to interact demonstrating the specific structural role of the zinc finger in TFIIH (Tremeau-Bravard, Perez and Egly, 2001). Mutations in the ring finger motif or complete removal of p44 does not have this effect on p62, and still allow p62 integration into the TFIIH core (Tirode *et al.*, 1999; Tremeau-Bravard, Perez and Egly, 2001).

The p44 RING domain interacts with the N-terminal zinc binding domain of p34 to provide stability to the TFIIH complex (Radu *et al.*, 2017). Mutating the cysteine-rich ring domain revealed that, unlike mutations in the N-terminal domain, this region does not affect phosphodiester bond formation but inhibits RNA poll II directed RNA synthesis and does not affect XPD helicase activity (Fribourg *et al.*, 2000; Tremeau-Bravard, Perez and Egly, 2001). Surprisingly, the binding between p34 and p44 is not mediated by the first zinc-binding site nor the local hydrophobic residues, but rather a cysteine residue which is structurally important for a specific protein fold (Kellenberger *et al.*, 2005). Hydrophobic residue contacts mediate the two proteins binding, unlike electrostatic interactions observed in other RING domains, as discussed earlier this unique

interaction between p34 and p44 greatly stabilizes the TFIIH complex (Schmitt *et al.*, 2014; Radu *et al.*, 2017).

1.5 Single Molecule Fluorescence Imaging

Single molecule biology has revolutionised biological science since the first experiments with ion channels (Neher and Sakmann, 1976). The beauty of single molecule experiments is in exploring the individual characteristics that would be lost in the noise and averaging of an ensemble approach (Zlatanova and van Holde, 2006; Leake, 2014). A population of cells or molecules will generally be heterogeneous. Significant subpopulations of data can be overlooked, using a single molecule approach we can develop a more precise understanding of complex processes (Leake, 2014; Shashkova and Leake, 2017). Fluorescence microscopy is a widely used single molecule technique to address a number of biological questions. Single molecule imaging allows for powerful investigation of protein kinetics, the first of these assays visualised single RNA polymerases sliding along single strands of immobilised DNA (Kabata *et al.*, 1993). Advances in fluorescent microscopy have revealed proteins employ 1D and 3D search mechanisms to scan the genome, these mechanisms can be manipulated by changing ionic buffer conditions (Berg, Winter and Von Hippel, 1981;

Tang, Iwahara and Clore, 2006; Bonnet *et al.*, 2008; Kad *et al.*, 2010; Gorman *et al.*, 2012; Hughes *et al.*, 2013).

Tightropes are a powerful tool in single molecule imaging. As the imaging is raised from the surface, actin (Desai, Geeves and Kad, 2015) or DNA (Kad *et al.*, 2010; Hughes *et al.*, 2013; Springall, Inchingolo and Kad, 2016), tightropes can be imaged without labelling the binding substrate and imaged with a high signal to noise ratio in the focal plane. Since, in the case of DNA tightropes, the DNA does not need to be directly visualised, several proteins can be imaged at once and allows a clearer observation of dynamic interactions. Recently UvrA UvrB and UvrC have been imaged translocating together along undamaged DNA, this precision was lost in the ensemble biochemical studies that dominate the field (Springall *et al.*, 2017).

Visualising protein motion *in vivo* can be used to determine if proteins are diffusing freely or in complex with genomic DNA. Proteins bound to DNA become visualised as punctate fluorescent spots, single diffusing proteins are difficult to differentiate as they blend into the background (Smith, Grossman and Walker, 2002; Kuhlman and Cox, 2012; Uphoff *et al.*, 2013; Etheridge *et al.*, 2014; Springall *et al.*, 2017). Specifically, 1D diffusion and 3D scanning of DNA can be differentiated in the cytoplasm in live cells (Elf, Li and Xie, 2007; Chen *et al.*, 2014; Stracy *et al.*, 2016). Single molecule fluoresce imaging and AFM have been used to directly examine the physical length of DNA samples, this can be used to identify a range of DNA lesions (Filippova *et al.*, 2003; Jiang *et al.*, 2007).

1.5.1 Magnetic Tweezers

Optical traps have revolutionised biophysics providing single molecule data for the force producing actions on, and manipulation of, biological systems and can be fully incorporated into existing optical set ups (Ashkin *et al.*, 1986; Wuite *et al.*, 2000). This tool has been invaluable in studies of DNA-protein interactions in particular, permitting force interactions between single DNA strands and proteins to be investigated with unrivalled precision (Davenport *et al.*, 2000; Strick, Croquette and Bensimon, 2000). The measurements are so precise DNA cleavage by a restriction enzyme on a tightened DNA strand can me recorded by the recoil of the beads back to the fixed position, providing unique kinetic rates of enzymes (Seidel *et al.*, 2004; van den Broek, Noom and Wuite, 2005). Optical traps can be used to trap microstructures, these can be used to apply physical pressure on biological complexes to measure force-tension relationships at the single molecule level (Phillips *et al.*, 2012; Maragò *et al.*, 2013; Simons *et al.*, 2015).

1.6 Thesis Aims

The primary aim of this project was to examine the function of the UvrBC complex.

UvrBC has recently been shown to form complexes on certain, processed, substrates, and can form a motile complex on double stranded DNA. Using single molecule fluorescence imaging of all known bacterial NER protein complexes on defined lesions incorporated into double stranded DNA tightropes we have examined the role of UvrBC and the other NER complexes at the single molecule level. We also investigate the role tension dependence in damage detection exhibited by UvrA.

Next, we examined the *in vivo* role of the UvrBC complex by using live cell fluorescence imaging of eGFP tagged UvrB and UvrC in UvrA knockout cells. Using this knockout line, we removed lesion detection initiated by UvrA or UvrAB complexes and could explore the function of UvrBC clearly. To ascertain if UvrB and UvrC could detect damage *in vivo* we imaged the intracellular movement of fluorescent proteins in response to UV damage. Using cell survival assays we further explored if this complex could improve cell survival relative to the UvrA knockout line. We also performed the first single molecule analysis of the interaction between the UvrC homologue, Cho, and double stranded DNA.

Moreover, this work aims to understand the interaction of XPD and p44 with double stranded DNA at the single molecule level. Previous work has focused primarily on XPD interaction with single stranded DNA and in compklex with p44. Here we directly interrogate the relationship between XPD and double stranded DNA without the helicases binding partner. ATP

hydrolysis has been heavily linked to single stranded DNA translocation but the link with double stranded DNA remains unclear. Using oblique-angle fluorescence imaging of Qdot labelled XPD, under a range of nucleotide conditions and ATP concentrations, we have explored the link between ATP hydrolysis and double stranded DNA translocation.

We next aimed to understand the interaction of p44 with double stranded DNA. Previous studies have usually considered p44 in complex and interacting with XPD. Here, for the first time we examine p44 alone and its ability to translocate on DNA independently from other TFIIH subunits.

Chapter 2: Materials and Methods

2.1 Flow cell

Single molecule biology requires the development of chambers to control the conditions of experiments. These chambers act at as an artificial cell. Small tubing and pumps to control flow of buffers can be delicately used at velocities that does not break molecular polymers, like DNA (Brewer and Bianco, 2008).

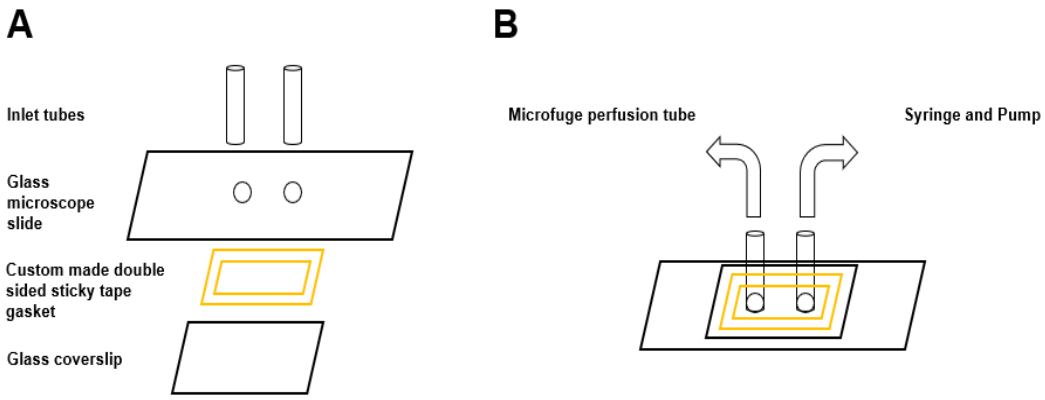

Figure 2.1. Flow cell construction. **A** Schematic design of flowcell. **B** Constructed flowcell.

2.1.1 Flow cell construction

Figure 2.1 depicts a schematic of a flow cell. Flowcells were constructed by drilling two holes 15 mm apart through a standard glass microscope slide (Fisher finest) using a Dremel electric hand drill with a diamond coated dental drill tip. Two pieces of polythene tubing (0.75 mm (inner) x 1.22 mm (outer) were then attached and glued in place by UV glue (NOA68 Thorlabs) ensuring no access for air. Excess tubing protruding from the bottom of the glass slide is removed with a scalpel blade to ensure later coverslip adhesion is stable. A custom-made gasket seals the coverslip with the glass slide. The flow cell needs to be air-tight to prevent any sudden change in the volume or pressure within the flow cell will destroy the tightropes. This also prevents oxygenation of the sample which results in unwanted photodamage. The gasket controls the final volume of the flow cell we generally use a rectangle of dimensions 15 mm x 10 mm. The constructed flowcell is then PEGylated using mPEG (**2.5**) solution overnight. The flow cell is washed with water and then blocked using ABT buffer (**2.4)** and left to incubate overnight. ABT buffer and mPEG solutions are used to reduce the number of Qdot-protein conjugates sticking to the surface therefore reducing the background noise.

2.1.2 Cleaning Methods

Glass cover slides (Agar scientific) and drilled microscope slides were cleaned in ethanol via sonication for 30 minutes, followed by 30 minutes

sonication in KOH twice. Slides and coverslips were then sonicated in acetone for 10 minutes, and rinsed clean with acetone. The glass was salinized with a 2% solution of 3-aminopropyl-triethoxysilane (Sigma) in acetone for 2 minutes. The slides and coverslips were then rinsed in pure water, and dried using N_2 gas and finally cured at 100^{o}c in an oven for 30 minutes.

2.1.3 Silica Beads and Poly-L-Lysine

Silica monosphere beads (5 μM diameter) are used in the flowcells as a platform to suspend DNA between. The beads are prepared for the DNA via a wash with poly-L-lysine. DNA binds to the beads via electrostatic interaction with the coating. The beads are elevated from the surface preventing surface bound protein interaction and the use of OAF imaging reduces background illumination highlighting fluorescence in the focal plane (Kad *et al.*, 2010; Springall, Inchingolo and Kad, 2016). Silica beads (Polysciences Inc.) are vortexed to resuspend the beads in their water solution. 100μL of beads are resuspended in 350 μg/mL of poly-L-lysine. The mixture is then let to settle for at least 30 minutes and stored at 4 °C.

2.2 Buffers

2.2 ABC

All experimental procedures with prokaryotic proteins (UvrA-C, mutant constructs and Cho) were performed at room temperature in ABC buffer (50 mM Tris–HCl (pH 7.5), 50 mM KCl, 1 mM adenosine triphosphate (ATP) and 10 mM $MgCl_2$, 10 mM Dithiothreitol (DTT)).

2.3 XPD

All experimental procedures with eukaryotic proteins (XPD and p44) were performed at room temperature in XPD buffer (20 mM Tris (pH 8), 10 mM KCl, 5 mM $MgCl_2$ and 1 mM EDTA). 2 mM of ATP or ADP was added as indicated.

2.4 ABT Buffer

1x ABC Buffer, 1 mg/ml BSA, 0.001% Tween 20

2.5 mPEG Solution

25 mg/ml mPEG5000 in 250 mM NaHCO3, pH 8.15-8.3. This can be stored for 3 months at -20°C.

2.3 DNA tightropes

λ DNA (lambda bacteriophage DNA, New England Biolabs) 500 µg/mL, 48500 base pairs long is used for DNA tightropes, the DNA contains 12 base overhangs which allow it to ligate to other linear strands and can be exploited to create tightrope constructs.

2.3.1 Concatemerized DNA

The over hangs of λ DNA can be exploited to create longer tightropes to increase the number of protein interaction with DNA. A solution containing 2 µL of 10x Ligase buffer**,** 7 µL of water**,** 10 µL of DNA**,** 1 µL of T4 DNA Ligase is Left at room temperature overnight, then store at 4 °C for use. T4 DNA ligase was removed from DNA tightropes by washing with 25 flowcell volumes of 1M NaCl.

DNA ligase buffer contains 50 mM Tris-HCL, 10 mM $MgCl_2$ 1 mM ATP 10 mM DTP.

2.3.2 Damaged Tightropes

The DNA damage construct is based on earlier studies (Kuhn and Frank-Kamenetskii, 2008; Kochaniak *et al.*, 2009; Tafvizi *et al.*, 2011). λ-DNA is nicked by Nt.BstNBI (New England Biolabs). Lambda DNA digested by Nt.BstNBI creates several nicks, only one pair of which is close enough together to generate an oligonucleotide fragment capable of spontaneous release at 65°C (region 33776 – 33807 on lambda). Nicking was performed for 2 hours at 65°C before a ten-fold excess of the replacement oligonucleotide (PHO-TTCAGAGZCTGAC-BIOT (where Z is fluorescein-dT, PHO is phosphorylated and BIO represents the biotin used for Qdot conjugation)) was added (replacing the lost oligo). Overnight ligation was performed at room temperature, supplemented with 1mM ATP then stored at 4ºC. T4 DNA ligase was removed from DNA tightropes by washing with at least 25 flowcell volumes of 1M NaCl.

2.3.3 Single Stranded Tightropes

Single stranded patches were created through the ligation of the DNA oligonucleotide (5'GGGCGGCGACCT**GCGTGATCTTTGCCTTGCGACAGACTTCCTTGGCT**GGGCGGGCTGGC3') to one cos end of lambda DNA. To the other cos end we ligated the shorter oligonucleotide (5'AGGTCGCCGCCCGCCAGCCCGCCC(TEG-bio)3'). Upon tandem ligation of these constructs a 35 base single stranded region (marked in bold) was created. The addition of streptavidin coated Qdots (10 nM for 20 minutes) to the tightropes permitted visual localization of the single stranded region. A tenfold excess of each oligonucleotide to lambda DNA was heated separately to 62 ºC for five minutes. The reaction was ligated overnight at room temperature and then for 24 hours 4 ºC with T4 DNA ligase. The ligation reactions were mixed and heated to 62 ºC for five minutes and allowed to ligate further overnight at room temperature with T4 DNA ligase. T4 DNA ligase was removed from DNA tightropes by washing with 25 flowcell volumes of 1M NaCl.

2.3.4 Tightrope Construction

Normal DNA tightropes and DNA constructs are constructed in the same way. Tightropes that contain an element that is visualised whilst imaging require an extra step. After the glass has been treated the tightropes are constructed as described (Kad *et al.*, 2010; Springall, Inchingolo and Kad, 2016).

10 µL of poly-L-lysine coated beads are added to 500µL of water, centrifuged at 14,000 rpm for 2 minutes, and water is replaced. This step is repeated twice to remove excess poly-L-lysine which would result in clumped DNA when imaging. The bead solution is sonicated at 80% amplitude for 1 second bursts (up50 Huntersonic processor), four times to separate the beads resulting in an even distribution of the beads in the flowcell. The solution is immediately introduced in the flow chamber, the beads are allowed to settle randomly on the glass surface. Introducing water to the flowcell ensures the beads are adhered to the surface and further reduce excess poly-L-lysine. Imaging buffer can be introduced to the flowcell and connected to two perfusion tubes (Figure 2.1). One attached to a syringe and linked with a pump to control the flow of liquid and the other to a microfuge tube to which the environment of the flow cell can be controlled and protein/imaging buffer can be added. Removal of air from the system is essential as air bubble will disrupt formed tightropes. 1µL of DNA to 99 µL of imaging buffer (2.2,2.3) (final DNA concentration 20 nM), and introduced in the flow cell via the microfuge tube. The pump controls bi-directional flow, at a rate of 300 µL per minute, alternating every 100 µL (per the length of perfusion tubes) for at least 20 minutes unless otherwise stated. The alternating direction of flow allows DNA to unravel and attach at either ends to the silica bead (figure 2.2). Tightropes with constructs require an extra step for visualising while imaging. The constructs (2.3.2, 2.3.3) contain a biotin, incubating the DNA with 10 nM streptavidin Qdots for 20 minutes before elongation into DNA tightropes allows visualization of damage while imaging. Streptavidin

Qdots do not bind to DNA tightropes without biotin (data not shown). Biotin-streptavidin binding interactions are an extremely stable interaction, providing a reliable fluorescent marker during imaging (Sano, Vajda and Cantor, 1998; Stayton *et al.*, 1999; Chivers *et al.*, 2011).

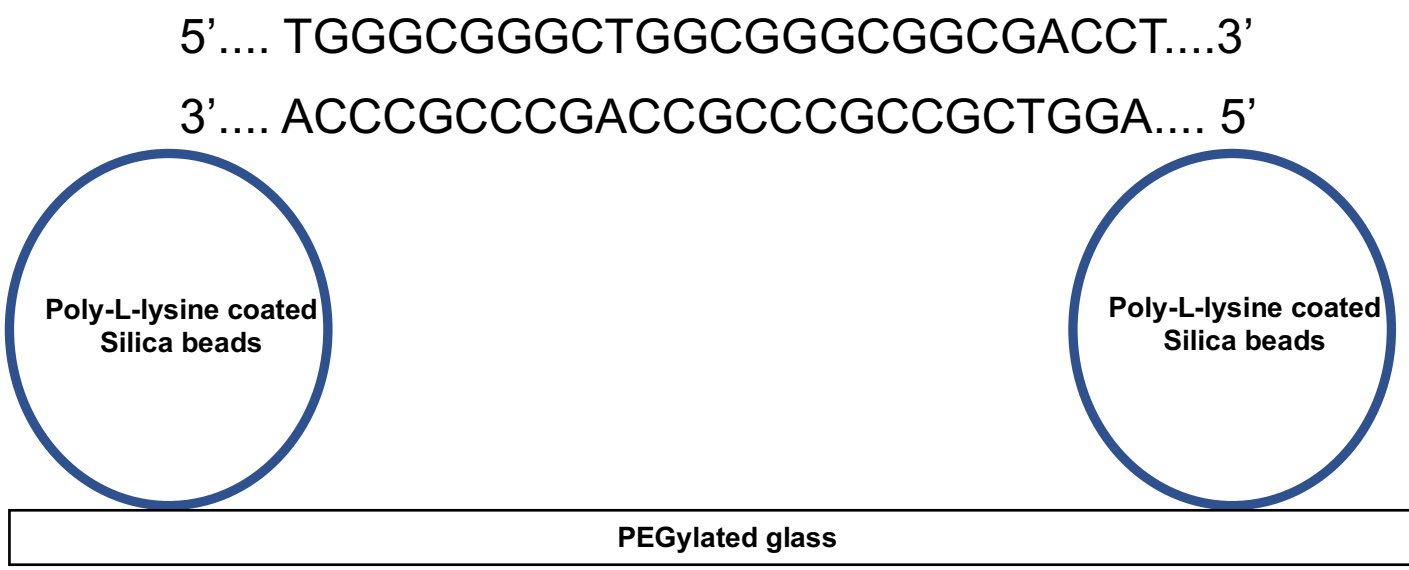

Figure 2.2. Schematic of a DNA tightrope.
As flow is introduced into the chamber the DNA unravels and attached to the glass beads via electrostatic interactions with Poly-L-lysine

2.3.5 Fluorescence Imaging

1 nM of YOYO-1 dye in 1X imaging buffer 100 mM DTT) can be introduced into the flowcell to allow imaging of the DNA. YOYO-1 iodide is a high affinity bi-intercalator, that has over a three thousand-fold increase in fluorescence when bound to double stranded DNA.(Thompson, Larson

and Webb, 2002; Murade *et al.*, 2009) Though YOYO-1 does not affect protein binding as it binds between base pairs it can disrupt the structure of DNA increasing elongation and unwinding and was not while collecting data (Lerman, 1961; Doyle, Ladoux and Viovy, 2000; Sischka *et al.*, 2005). YOYO-1 could be removed by from DNA tightropes and the flowcell by washing with 25 flowcell volumes of high salt ABC buffer (Kad *et al.*, 2010; Springall, Inchingolo and Kad, 2016).

2.4 Proteins Used

Prokaryotic proteins were a generous gift from our collaborator Professor Ben Van Houten from the Department of Pharmacology and Chemical biology at the University of Pittsburgh.

Eukaryotic proteins were a generous gift from our collaborator Professor Caroline Kisker at the Rudolf Virchow Centre for Experimental Biomedicine in the University of Würzburg.

Protein activity was tested by electrophoretic mobility shift assays, incision assays, ATPase assays were appropriate.

2.4.1 UvrA

Wild type *Bacillus caldotenax* UvrA was purified as described previously (Kad *et al.*, 2010). UvrA used contains C-terminally engineered biotin ligase recognition sequence (GLNDIFEAQKIEWHEGGG) which, via BirA biotin ligase, was used to attach biotin for later streptavidin Qdot conjugation (Chapman-Smith and Cronan, 1999; Kad *et al.*, 2010). ZnG-

UvrA construct was purified as descried previously (Croteau *et al.*, 2006). ZnG-UvrA has eleven highly conserved residues in the C-terminal zinc finger substituted with glycine, the resulting mutant can bind to DNA but has lost its damage-specific DNA binding (Croteau *et al.*, 2006).

2.4.2 UvrB

Wild type *Bacillus caldotenax* UvrB was purified as described previously (Skorvaga *et al.*, 2004; Croteau *et al.*, 2006). UvrBΔβhairpin construct was purified as described previously (Skorvaga *et al.*, 2002). UvrB has an N-terminal hemagglutinin (HA) epitope tag (YPYDVPDYA), exploited during fluorescence imaging (Wang *et al.*, 2008). UvrBΔβhairpin construct is able to bind to UvrA and form a UvrAB complex and lacks the key damage sensing domain of the UvrB β hairpin (Skorvaga *et al.*, 2002).

2.4.3 UvrC

Wild type *Bacillus caldotenax* UvrC was purified as described previously (Hughes *et al.*, 2013). UvrC used contains N-terminally engineered biotin ligase recognition sequence which, via BirA biotin ligase, was used to attach biotin for later streptavidin Qdot conjugation (Chapman-Smith and Cronan, 1999; Hughes *et al.*, 2013).

2.4.4 Cho

Escherichia coli Cho was purified as described previously (Moolenaar *et al.*, 2002). Cho used contains N-terminally engineered biotin ligase recognition sequence which, via BirA biotin ligase, was used to attach biotin for later streptavidin Qdot conjugation (Chapman-Smith and Cronan, 1999).

2.4.5 XPD and p44

Chaetomium thermophilum XPD, mutant constructs and p44 were N-terminally His-tagged (Kuper *et al.*, 2014).

2.5 Quantum dots

Qdots are a very stable bright fluorescent probes, well suited for *in vitro* assays (Gao *et al.*, 2005; Walling, Novak and Shepard, 2009). These fluorophores were used as they were found to have no effect on protein activity. UvrA and UvrB displayed wild type DNA binding and lesion detection (Wang *et al.*, 2008; Kad *et al.*, 2010). UvrC-avi constructs showed comparable incision to wild type (Hughes *et al.*, 2013). Cho-avi constructs showed comparable incision to wild type (Moolenaar *et al.*, 2002). His tagged XPD and p44 showed normal ATPase activity (described in Chapter 5).

2.6 Protein Labelling Methods

To ensure proteins were labelled with a single Qdot a 4:1 excess of Qdots was used (Wang *et al.*, 2008).

2.6.1 Biotinylated Proteins

Biotinylated avi-tagged Uvr proteins (UvrA, UvrC and Cho) were incubated separately with streptavidin-conjugated Qdots in ABC buffer for 30 minutes prior to dilution to 1 nM immediately before imaging. Unless otherwise stated UvrAB/UvrBC complexes were imaged with UvrB labelled only to ensure the full complex was present (Kacinski and Rupp, 1981; Kad *et al.*, 2010; Hughes *et al.*, 2013).

2.6.2 HA Tagged Proteins

UvrB was labelled via an antibody sandwich described previously (Wang *et al.*, 2008). N-terminal hemagglutinin tagged (HA) UvrB was added to 1 μM mouse monoclonal HA antibody. Quantum dots that were covalently coupled to goat antimouse antibodies were then conjugated to the antibody sandwich in a 1:1:4 ratio and diluted to 1 nM before imaging (Wang *et al.*, 2008; Kad *et al.*, 2010). Proteins in complex with UvrB or UvrBΔβhairpin construct were labelled via UvrB as UvrB is unable to bind DNA alone, this ensured the full complex was present while imaging (Kacinski and Rupp, 1981; Kad *et al.*, 2010; Hughes *et al.*, 2013).

2.6.3 His Tagged Proteins

XPD and mutant variant were was purified as described previously (Kuper *et al.*, 2014). Briefly, XPD-Qdot conjugates were prepared by incubating His tagged XPD (100 nM) Anti-His monoclonal mouse antibody for 20 minutes in XPD buffer. To ensure proteins were labelled with a single Qdot a 4:1 excess of Qdots was used, (Wang *et al.*, 2008). Anti-mouse IgG-conjugated Qdots were incubated for 30 minutes and dilution to 1 nM for imaging

2.7 Green Fluorescent Protein

The eGFP variant of GFP has a maximum excitation of 488 nm and max emission of 509nm (Cormack, Valdivia and Falkow, 1996; Cinelli et al., 2000; Gambotto et al., 2000). C-terminally eGFP tagged UvrA, UvrB and UvrC were used.

2.8 Single Molecule Fluorescence Imaging

Imaging was performed using a custom-built fluorescence microscope capable of oblique-angle fluorescence (OAF) excitation and multichannel emission. The same optical platform was used for imaging single molecules on DNA tightropes and single molecules in cells except for the cameras used (discussed below). We performed oblique angle fluorescence (OAF) microscopy using our custom built microscope (Kad *et al.*, 2010; Hughes *et al.*, 2013; Springall, Inchingolo and Kad, 2016). OAF imaging is a variation of TIRF imaging. With a TIRF system, the

beam, in a flowcell, would internally reflect at the interface between the glass and water.

2.8.1 Optical set up

This custom-built microscope is built on Olympus IX50 frame with a custom excitation path consisting of a 488 nm JDSU DPSS laser source beam expanded 17.5x. This beam is focused using a 250 mm plano-concave lens to the back focal plane of an Olympus 1.45NA 100x objective lens. This generates a defined beam at the sample plane and the lateral position of the focal point at the back aperture defines the exit angle of the excitation beam; this was adjusted to a sub critical angle. Steering the beam at a sub critical angle helps to reduce excess background sample illumination and emphasises fluorescence in the focal plane. Because the Qdots used in this study can all be excited by this laser a long pass 500 nm dichroic was the only filter needed in the nosepiece; this is also ideal for imaging eGFP live cell experiments. To obtain triple color images we used an Optosplit III (Cairn Research, UK) optimized for 565 nm, 605 nm or 655 nm Qdots (see below) to separate the image into three channels which were projected and recorded using a DU897 EMCCD camera (Andor, Belfast, UK) at 10 fps for up to 120s. Live cell imaging was performed using the Hamamatsu Orca Flash4.0 V2 at the same frame rate on the same system for a maximum period of 20s with the exception of photobleaching acquisitions which continued until all fluorescence reached background levels, no longer than 5 minutes. The camera pixel sizes were equivalent to 75 nm (Andor) and 63.2 nm (Hamamatsu) respectively in the sample plane corresponding to a

magnification of 213x and 103x respectively (the difference is due to a change in the relay optics contained within the Optosplit III).

All images are processed using ImageJ and custom macros.

2.9 Live cell imaging

Cell survival assays and live cell imaging were performed with *E. coli* (K-12 strain BW25113) KEIO cells and C-terminally eGFP tagged *E. coli* Uvr proteins were obtained as ASKA clones from the National Bioresource Project (NIG, Japan) (Kitagawa *et al.*, 2005; Baba *et al.*, 2006; Yamamoto *et al.*, 2009). Uvr Protein-eGFP expression was regulated by the T5-lac promoter on the pCA24N plasmid with the $lacI^q$ for strict suppression (Kitagawa *et al.*, 2005). Protein expression was not induced at any point. 3% agarose/1× LB pads were created by warming a 3% agarose/1× LB at at 65 °C for 15 minutes. A rectangular gasket was placed on a clean glass slide (figure 2.3**)**. 50µl of the warm agarose solution was dropped in the middle of the gasket. The solution was covered with a clean cover slip and left to set. Once cooled, a flat agarose pad could be exposed by removing the coverslip.

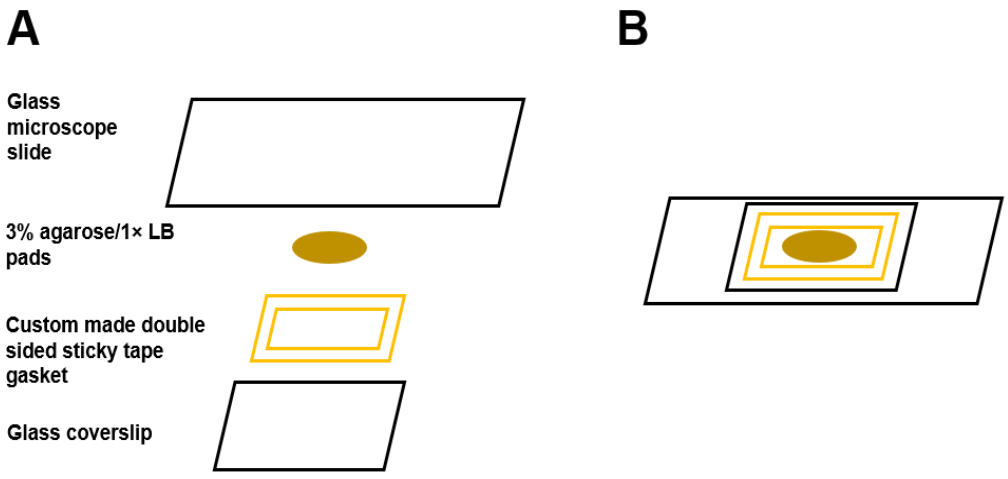

Figure 2.3. Agarose pad flow cell construction. **A** Schematic design flowcell for live cell imaging. **B** Constructed flowcell with agarose pad.

Lysogeny broth (LB) was inoculated with cells from a 15% glycerol stock and grown overnight at 37°C, then diluted into fresh LB and grown to OD_{600} 0.6. One millilitre of cells were centrifuged, resuspended in fresh LB, diluted 1/20 in LB before 5 µl was deposited on 3% agarose/1× LB pads. A coverslip could be carefully placed to secure the agarose pad for imaging. Non-damaged cells were imaged immediately after immobilization. Damaged cells were exposed to 5 or 25 J/m^2 UV (254 nm) and incubated at 37°C for 30 min to allow for an adequate SOS response prior to imaging (Crowley and Hanawalt, 1998; Smith, Grossman and Walker, 2002). Cells could then be excited at 488 nm and imaged in the set up described earlier (Cormack, Valdivia and Falkow, 1996; Cinelli et al., 2000; Gambotto et al., 2000).

2.9.1 Complementation Assay

To investigate whether our C-terminally eGFP tagged Uvr proteins could restore cell surivial we used complementation of eGFP proteins respective knockout cells as described (Barnett and Kad, 2018),

Lysogeny broth (LB) containing the appropriate antibiotic was inoculated from a 15% glycerol cell stock and grown overnight at 37°C; subsequently this was diluted into fresh LB and grown to OD_{600}0.6. Aliquots of undiluted and three serial ten-fold dilutions of cells were either spotted or spread on LB-agar plates. Plates were then exposed to the stated doses of 254 nm UV to induce DNA damage and incubated overnight (Barnett and Kad, 2018). To generate a UvrA-null control cell line ($UvrA^-$) that contained an equivalent protein load and antibiotic resistance to those with Uvr

proteins, we transformed UvrA KEIO cells with a plasmid containing the protein Yihf-eGFP, a protein unrelated to NER.

2.9.2 UV Damage

Cells were damaged with a 254 nm lamp (ENF-240C/FE; Spectronics, Westbury, NY, USA).

2.10 Data Analysis

The reslice function of ImageJ (NIH, USA) was used to create kymograph streaks of protein moving on DNA (Kad *et al.*, 2010; Hughes *et al.*, 2013; Desai, Geeves and Kad, 2015; Barnett and Kad, 2018). A protein was classified as moving if its kymograph showed movement of 3 pixels over 3 frames from the previous position.

Any complexes that were excessively bright indicating the presence of multiple Qdots were ignored during analysis as these could be proteins with more than one Qdot or unwanted aggregates.

2.10.1 Streak Analysis

The lifetime of attachment of proteins can be gathered from the length of the streak from a kymograph. Only streaks that started and ended in the movie were analyzed. Streaks that started and ended in the movie were analyzed only, as streaks that did not start or end during the movie would give inaccurate lifetime values, though this may result in underestimated

lifetime values. Multiple binding events could be observed in video, therefore to avoid interference from adjacent proteins during data analysis only DNA decorated with fewer than 6 proteins were analyzed

2.10.2 Lifetime Calculations

These streak data were plotted as cumulative frequency (CF) histograms and fitted to:

Equation 1: $CF = N(1-e^{(-k.t)})/(1-e^{(-k.t_{max})})$

where *N* is the number of observed points, *t* is the bin, t_{max} the maximum bin size and *k* the reciprocal of the dwell time (Hughes *et al.*, 2013).

2.10.3 Diffusion Constant and Coefficient

To quantify the movement of the protein over time each streak within a kymograph was fit to a Gaussian in each time frame. Gaussian fits produce five values; baseline, maximum height, mean peak position, standard deviation and r^2 providing super-positioning of the fluorophore for motion analysis. This custom built macro used the Gaussian distribution approximation of the point spread function for single fluorophores to provide positional accuracy beyond the limit of diffraction, which was determined as 8.7 nm (Thompson, Larson and Webb, 2002; Hughes *et al.*, 2013).

To quantify the motion of individual molecules their mean squared displacements (MSD) were determined using:

Equation 2: $$MSD(n\Delta t) = \frac{1}{N-n}\sum_{i=1}^{N-n}\left[(x_{i+n}-x_i)^2+(y_{i+n}-y_i)^2\right]$$

N is the total number of frames in the kymograph, *n* the frame, x_i and y_i the position of the protein, Δt is the time window.

MSDs were linear fit to determine diffusion constants. Increasing amounts of the data (minimum 10% of time record) were used until the r^2 fell below a value of 0.7. The linear slope is twice the value of the molecule's diffusion constant. To obtain information on how the protein diffuses their diffusive exponents were determined. The log of the MSD versus log of time provides another expected linear relationship, however this time the slope gives the diffusive exponent (α). An α of less than 1 indicated sub diffusion, a value of 1 is characteristic of pure one dimensional diffusion and more than 1 indicates directed motion (Dunn *et al.*, 2011).

2.10.4 Statistics

Unless otherwise stated, '*n*' refers to the number of flow chambers or agarose pads used per experiment. Significance was determined using the Student's *t*-test and consequent *P*-values are reported if two values are compared.

If multiple means are compared analysis of variance (ANOVA) was performed with a post hoc test, including a Bonferroni correction to consider multiple comparisons, shdsjd subsequent *p*-values are reported.

Chapter 3: DNA damage binding preferences of NER complexes

3.1 Introduction

Recent studies have shown that UvrB and UvrC form a complex on duplex DNA without the involvement of UvrA, suggesting that UvrC activates UvrB's ability to associate with DNA (Hughes *et al.*, 2013). A combination of single molecule fluorescence imaging and atomic force microscopy confirmed that UvrB and UvrC in the absence of UvrA were found to form stable, translocating, complexes on DNA with the DNA interaction mediated by UvrB (Hughes *et al.*, 2013; Wirth *et al.*, 2016). Given the 10-fold excess of UvrB to UvrC the UvrBC complex is the likely *in vivo* form of the dual endonuclease (Berg, Winter and Von Hippel, 1981; Hughes *et al.*, 2013). Unlike UvrAB, the role of UvrBC is unknown, previous studies have suggested this complex can repair specifically presented lesions, but not those within unmodified duplex DNA as expected *in vivo* (Caron and Grossman, 1988; Zou *et al.*, 1997; Wirth *et al.*, 2016). To understand the roles of UvrA, UvrB and the UvrBC complex in damage processing we have used a single molecule approach to assess colocalization with DNA damage. Two key mutants were used to assess the damage sensing ability of the NER complexes, ZnG-UvrA and UvrBΔβhairpin. An eleven amino acid deletion in the C-terminal zinc finger of UvrA (ZnG-UvrA) produces a mutant that retains the ability to bind DNA

and UvrB, but damage specific binding is lost (Croteau *et al.*, 2006, 2008; Wagner, Moolenaar and Goosen, 2011). The UvrBΔβhairpin construct is able to bind to UvrA, form a UvrAB complex and translocate on DNA but lacks the key damage sensing domain of UvrB the β–hairpin (Machius *et al.*, 1999; Theis *et al.*, 1999; Skorvaga *et al.*, 2002). Using defined lesions on DNA tightropes we were able to define which complexes colocalise with damage. Interestingly, we found reducing the tension of DNA tightropes by slowing the speed at which the tightropes were constructed increased UvrAs ability to bind damage to levels comparable with UvrAB. UvrAB and UvrBC complexes were found to have the same affinity for DNA damage, this preference was abolished when removing the β–hairpin of UvrB (Theis *et al.*, 1999; Skorvaga *et al.*, 2004; Truglio *et al.*, 2005). Finally, we performed the first single molecule analysis on the UvrC homologue, Cho, examining the proteins interaction with double stranded DNA tightropes. We found that when increasing the salt concentration Cho became more motile but showed a decrease in diffusion constant, NERs new endonuclease showed no preference for damaged DNA.

3.2 Material and methods

3.2.1 Standard conditions

Unless otherwise stated all experimental procedures in this section were performed at room temperature in ABC buffer (50 mM Tris–HCl (pH 7.5), 50 mM KCl, 1 mM adenosine triphosphate (ATP) and 10 mM $MgCl_2$, 10 mM Dithiothreitol (DTT)).

3.2.2 Damaged DNA tightropes

The DNA damage construct is based on earlier studies (Kuhn and Frank-Kamenetskii, 2008; Kochaniak *et al.*, 2009; Tafvizi *et al.*, 2011). The construct is described in Chapter 2.3.1 and DNA tightropes are constructed as described in Chapter 2.3.4 and described previously (Kad *et al.*, 2010; Springall, Inchingolo and Kad, 2016; Kong *et al.*, 2017; Springall *et al.*, 2017)**.** Briefly, λ-DNA is nicked by Nt.BstNBI producing a single-stranded fragment. This single stranded DNA patch spontaneously melts at room temperature and is then replaced with a lesion containing oligonucleotide (Figure 3.1A). Figure 3.1 B shows a DNA tightrope with damage visualised by a Qdot.

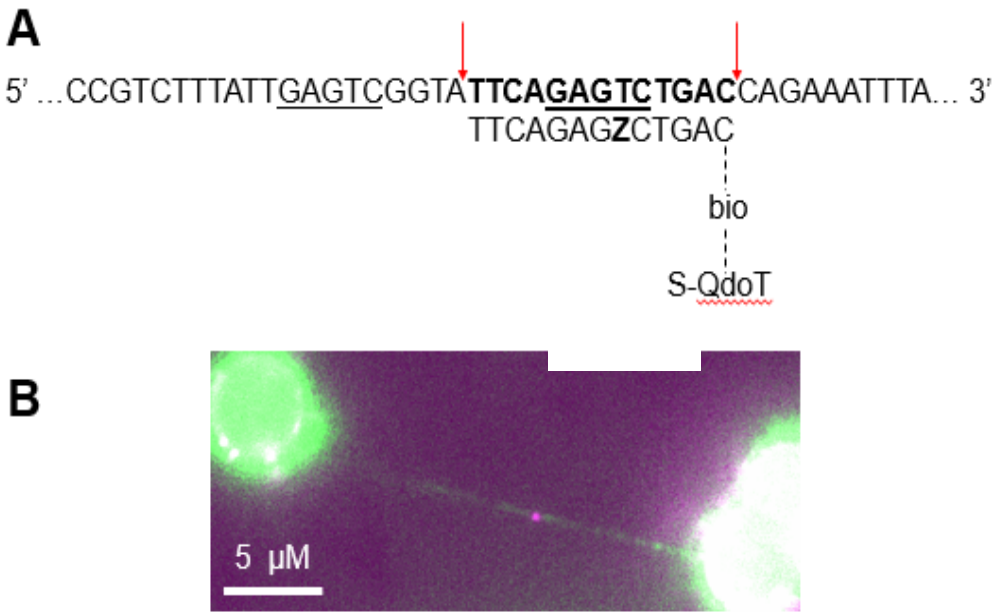

Figure 3.1. DNA damage tightrope construct and visualisation. **(A)** Schematic for damage construct. Upper sequence of λ-DNA shows key bases. Underlined bases show Nt.BstNBI binding sequence, red arrows indicate Nt.BstNBI single stranded incision sites. Bold sequence indicates the oligonucleotide released. The lower sequence refers to the oligonucleotide which replaces the lost oligo. **Z** represents fluorescein, recognised as damage by NER. Bio represents the biotin conjugated via TEG which can be visualised via streptavidin conjugated Qdots (S-Qdot). **(B)** DNA tightrope stained with YOYO-1 (green) damage is visualised with a 565 streptavidin-conjugated Qdot (magenta).

3.2.3 Single Molecule Fluorescence Imaging

All protein used in this chapter was a generous gift from our collaborator Professor Ben Van Houten from the Department of Pharmacology and Chemical biology at the University of Pittsburgh.

Protein used and labelling strategies are discussed in Chapter **2.4.**

Proteins in complex with UvrB or UvrBΔβhairpin construct were labelled via UvrB as UvrB is unable to bind DNA alone (data not shown), this ensured the full complex was present while imaging (Kacinski and Rupp, 1981; Kad *et al.*, 2010; Hughes *et al.*, 2013). 1 nM of respective proteins were used. To ensure proteins were labelled with a single Qdot a 4:1 excess of Qdots was used (Wang *et al.*, 2008).

3.2.4 Calculations

$$\mathrm{MSD}(n\Delta t) = \frac{1}{N-n}\sum_{i=1}^{N-n}\left[(x_{i+n}-x_i)^2+(y_{i+n}-y_i)^2\right]$$

Equation 1 from Chapter 2.12.3
N is the total number of fames in the kymograph from the image taken, *n* the is the frame, x_i and y_i the position of the protein, in one dimension along the tightrope and Δt the time window.

This equation is described in detail in Chapter 2.12.3. Briefly, MSDs were fitted to a straight line when the r^2 value of the fit dropped <0.7, no more data was used. The slope of this linear plot provides the diffusion constant. By replotting the MSD on log-log axis we were able to determine the mechanisms of motion, the slope of this plot defined 'α', the diffusive

exponent and describes how the protein diffuses (Berg, Winter and Von Hippel, 1981; Hughes *et al.*, 2013; Springall, Inchingolo and Kad, 2016). Unless otherwise stated, '*n*' refers to the number of flow chambers or agarose pads used per experiment. Significance was determined using the Student's *t*-test and consequent *P*-values are reported if two values are compared.

If multiple means are compared analysis of variance (ANOVA) was performed with a post hoc test, including a Bonferroni correction to consider multiple comparisons, shdsjd subsequent *p*-values are reported.

3.3 Results

To study how the NER proteins interact with damaged λ-DNA we removed a single stranded patch using the nicking enzyme Nt.BstNBI and inserted an oligonucleotide with fluorescein which is recognised as damage by NER proteins (DellaVecchia *et al.*, 2004). The DNA containing lesions could be made into tightropes as described in Chapter 2.3.1. The damaged oligonucleotide contained a biotin, incubating the DNA with 10 nM streptavidin Qdots for 20 minutes before elongation into DNA tightropes allowed visualization of damage while imaging as seen in Figure 3.2 (3.2.2). Streptavidin Qdots do not bind to DNA tightropes without biotin. To test this, we used a large excess of Streptavidin Qdots (10nm) on undamaged DNA tightropes and imaged for 15+ minutes to ensure binding did not occur. Protein conjugated Qdots bind almost

instantly to DNA tightropes when they are introduced to the flowcell, and we were confident that when the damage construct was introduced, we were marking the defined lesion. Biotin-streptavidin binding interactions are an extremely stable interaction, the strongest non-covalent biological interaction known, providing a reliable fluorescent marker during imaging (Sano, Vajda and Cantor, 1998; Stayton *et al.*, 1999; Chivers *et al.*, 2011).

3.3.1 Random Binding

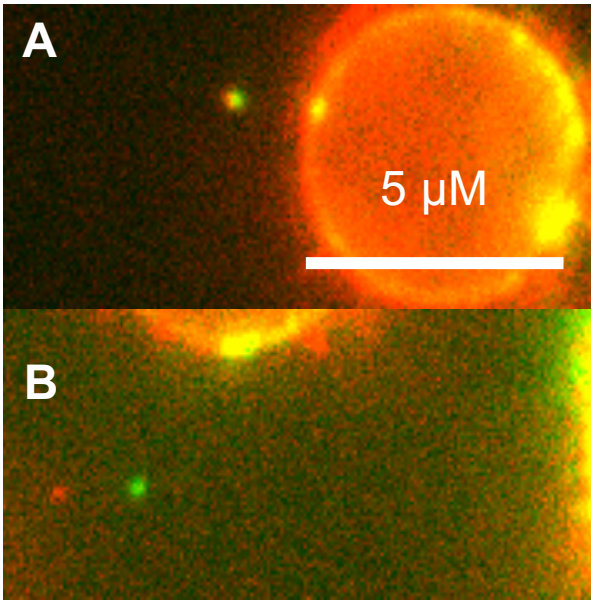

Figure 3.2. Examples of protein complex colocalization and non-colocalization with damaged DNA on tightropes. **(A)** UvrAB(green) complex colocalising with damaged DNA (red). **(B)** UvrBΔhC complexes (green) unable to recognise and colocalise DNA damage (red).

First, we established the background level of colocalization of proteins, the false positive threshold, as there would be a level of binding to the damage marker that was random and non-specific. We used four proteins that do not bind to specific sequences of double stranded DNA and recorded the level of colocalization to a defined point on the tightrope. We first observed UvrA binding to the midpoint of undamaged double-stranded DNA tightropes using the following criteria for damage localization. We recorded fluorophore colocalization, protein binding to damage, if the fluorophores were within 3 pixels of the center of each other. If colocalization was recorded on a tightrope, other proteins that were on the tightrope were not recorded in the statistics as non-binding since they did not have the opportunity to bind to the damage already occupied on the tightrope, see figure 3.2. We used UvrA which was labelled via biotin and streptavidin Qdots, analysis of 196 undamaged DNA tightropes revealed the threshold as 10.1% (±1.1% SEM; n = 2) as seen in Figure 3.3. We also checked that this was not protein or labelling specific by performing similar controls with UvrB.C and UvrC. Of 106 UvrB.C complexes, which used the antibody sandwich labelling method, 11.32% (±1.4% SEM) colocalized with the middle of the tightrope. UvrC uses a biotin streptavidin labelling method, the same as UvrA, and 9.68% (±6.4% SEM) of 71 molecules were observed in the middle of the tightrope, consistent with Qdot-UvrA. Finally, we used p44, a protein involved in eukaryotic NER and a different labelling method (described in 2.6.3). As with the other proteins 12.5% (±1.25% n = 2) of 80 molecules were bound to the middle of the tightrope. These statistics establish the

false positive threshold of damage binding, values above 10.1% are considered specific and directed by damage recognition, colocalization probabilities not significantly above this value are considered non-specific.

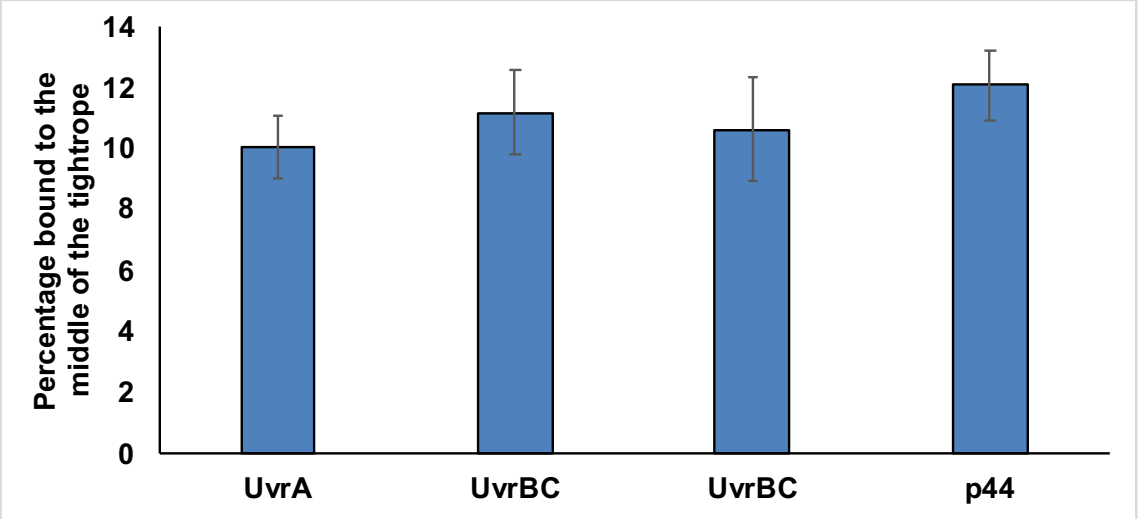

Figure 3.3. Probability of finding a NER proteins colocalized with the middle of undamaged DNA tightrope.

Values for mean probability percentage (±SEM, where, *n* refers to repeated experiments) bound to damaged DNA were 10.06% (±1% *n* = 3), 11.19% (±1.4% *n* = 3), 10.62% (±1.59% *n* = 3), 12.1% (±1.14% *n* = 3), UvrA, UvrB.C, UvrC, p44, respectively.

3.3.2 UvrAB preferentially binds to DNA damage

It has been previously demonstrated though fluorescent imaging the stoichiometry of the UvrAB complex is A_2B_2 (Malta, Moolenaar and Goosen, 2007; Kad *et al.*, 2010). As the primary lesion detector of NER we first examined this complex's interaction with damaged tightropes. As shown in figure 3.4, of 95 molecules observed 46% (±6% *n* = 4) were colocalised with damage. To confirm this observation, we also studied a mutant UvrB with the ß-hairpin removed, this has been shown to be essential for identifying DNA damage (Theis *et al.*, 1999; Skorvaga *et al.*, 2002; Truglio *et al.*, 2004). Of 92 UvrABΔh complexes only 18% (±2% SEM; *n*= 4) were colocalized with damage. This value is significantly lower (*P* = 0.003) than UvrA.B (46%), confirming protein binding to the damage marker is representative of damage recognition by the protein complex. UvrAB preferentially binding to the damage also demonstrated that the biotin and streptavidin Qdot method to visualise damage did not impair DNA binding, the biotin may actually be recognised as a lesion in this method (Haines *et al.*, 2014). The C-terminal zinc finger of UvrA has been shown to activate the damage detecting ATPase activity of UvrB (Croteau *et al.*, 2006, 2008). By removing this domain, we were able to examine this process. Only 12.5% (±1% *n* = 3) of 120 ZnG-UvrA.B complexes colocalised with the damage marker, confirming this zinc finger has a clear damage detection role in the UvrAB complex. A final confirmation with both damage detection domains removed acted as a final control for

random binding. 12% (±0.8% *n* = 3) of 135 ZnG-UvrA.BΔh complexes were bound to damage. These complexes are not statistically different to the random binding threshold (P > 0.05) and statistically different from UvrA.B (P < 0.05). UvrA.B is statistically difference different (*P* < 0.05) to all the mutants complexes further confirming damage detection using our assay. As seen in figure 3.4 all the mutant UvrA.B complexes are not statistically different to each other or the random binding threshold (*P* > 0.4).

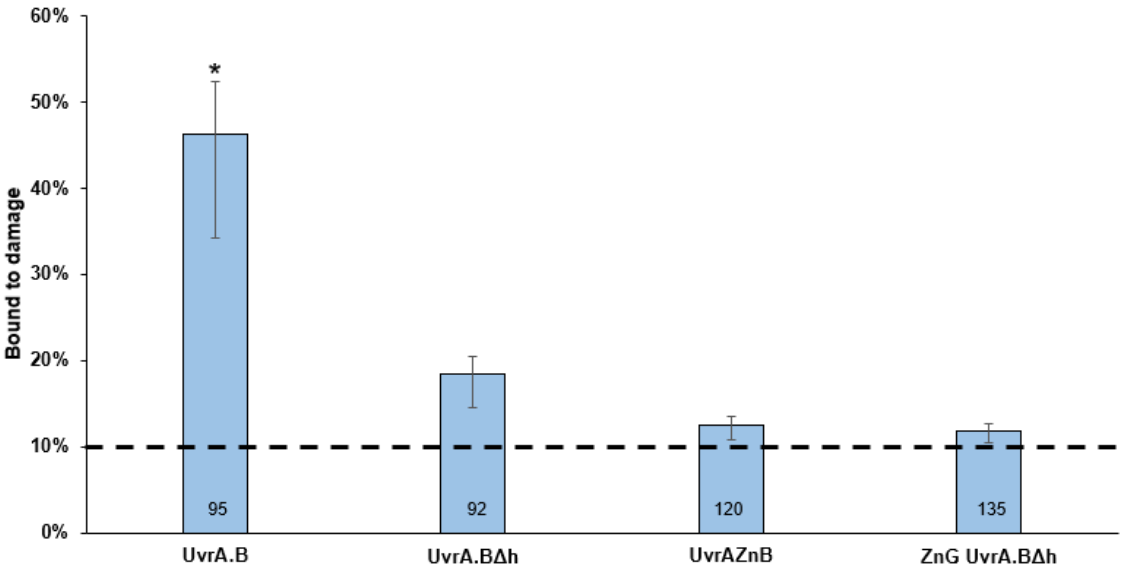

Figure 3.4 Probability of finding a UvrA, UvrB, UvrAB and respective mutant complexes colocalized with a damage marker.

Values for mean probability percentage (±SEM, where, *n* refers to repeated experiments) bound to damaged DNA were 46% (±6% *n* = 4), 18% (±2% *n* = 4), 12.5% (±1% *n* = 3), 12% (±0.8% *n* = 3), UvrA.B, UvrA.BΔh, ZnG-UvrA.B, ZnG-UvrA.BΔh, respectively. The dashed line represents the probability (10.1%) of random association to damage based upon UvrA-Qdot binding to the mid-point of a DNA tightrope.

*Indicates statistically significantly difference ($P = 0.0036$) relative to the 10.1% random association value. UvrA.BΔh, ZnG-UvrA.B, ZnG-UvrA.BΔh and the random association probability are not statistically different to each other ($P > 0.4$)).

3.3.3 Tension dependence of UvrA

The results from the UvrAB interaction with damaged tightropes gave us confidence this assay was reliable for examining NER proteins interacting with lesions. We next investigated the canonical initiator of NER. Of 189 UvrA molecules examined, 29% (± 3% SEM; n=5) were colocalized with DNA damage (figure 3.5), which is significantly lower than UvrAB (P = 0.0013) but significantly higher than random binding (P<0.05). The results from the UvrAB interaction with damaged tightropes gave us confidence this assay was reliable for examining NER proteins interacting with lesions. We next investigated the canonical initiator of NER. Of 189 UvrA molecules examined, 29% (± 3% SEM; n=5) were colocalized with DNA damage (figure **X)**, which is significantly lower than UvrAB ($P < 0.05$) but significantly higher than random binding (P<0.05). This data agrees with earlier studies that found UvrA had a lower affinity for damage than UvrAB complexes. (Reardon *et al.*, 1993; Jaciuk *et al.*, 2011; Wirth *et al.*, 2016). However, UvrA has been shown to bend DNA when searching for lesions, therefore, we investigated how tension affected damage detection (Bellon, Coleman and Lippard, 1991; Van Houten and Snowden, 1993; Jaciuk *et al.*, 2011). DNA melting and bending by UvrA enhances damage verification by UvrB (Croteau *et al.*, 2008; Wang *et al.*, 2009; Gantchev and Hunting, 2010). To investigate this reduced rate of binding to damage and whether tension affected damage recognition we lowered the tension on the DNA by reducing the flowrate at which tightropes were suspended. At 10% of the normal flow rate, 30 vs 300 µl/min, we were still able to

reliably produce tightropes, however when stained with YOYO-1 the tightropes were noticeably relaxed. Using this flow rate 62.7% (± 4.1% SEM; n=3) of 284 tightropes visualised were seen to move over 3 pixels orthogonally to the tightrope compared to 6.0% (± 0.1% SEM; n=3) of 599 tightropes prepared at the normal flow rate. As seen in figure **X** the different flow rate 10% of the original produced significantly different DNA tightropes. 30 µl/min was chosen as this produced a large number of usable visibly slack tightropes. Other flow rates were trialled between the two values but, due the nature of the relationship between drag and extension resistance, did not produce relaxed tightrope until a severely lowered rate of flow was used (Graneli *et al.*, 2006; Kad *et al.*, 2010; Rubenstein, Yin and Frame, 2012).

As shown in figure **X** 53% (± 9% SEM; n=5) of 79 UvrA molecules interacting with DNA tightropes under these conditions colocalised with damaged DNA. This shows a significantly increased ability of UvrA to detect damage compared with UvrA ($P<0.05$) at low tension suggesting UvrA is sensitive to the 3D structure of DNA.

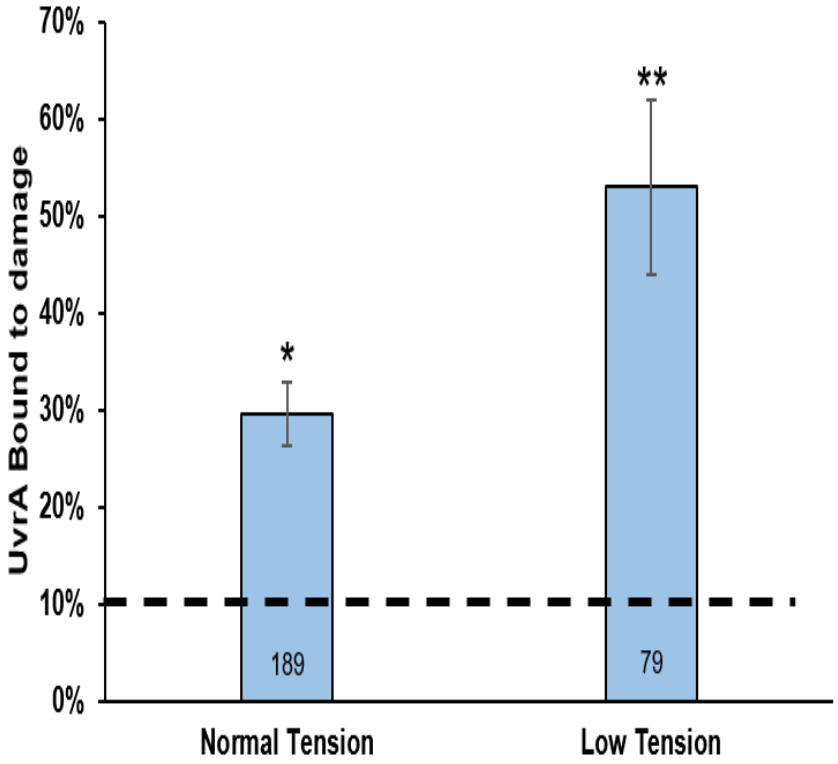

Figure 3.6. Tension of DNA tightrope affects the probability of finding a UvrA with a damage marker.

Values for mean probability percentage (±SEM, where, *n* refers to repeated experiments) bound to damaged DNA were 29.63 (±3.29% *n* = 5), 53% (±9% *n* = 5), for normal and low tension respectively.

The dashed line represents the probability (10.1%) of random association to damage based upon UvrA-Qdot binding to the mid-point of a DNA tightrope.

*Indicates statistically significantly difference (*P* = 0.01) relative to the 10.1% random association value.

**Indicates statistically significantly difference (*P* = 0.0054) relative to the 10.1% random association value.

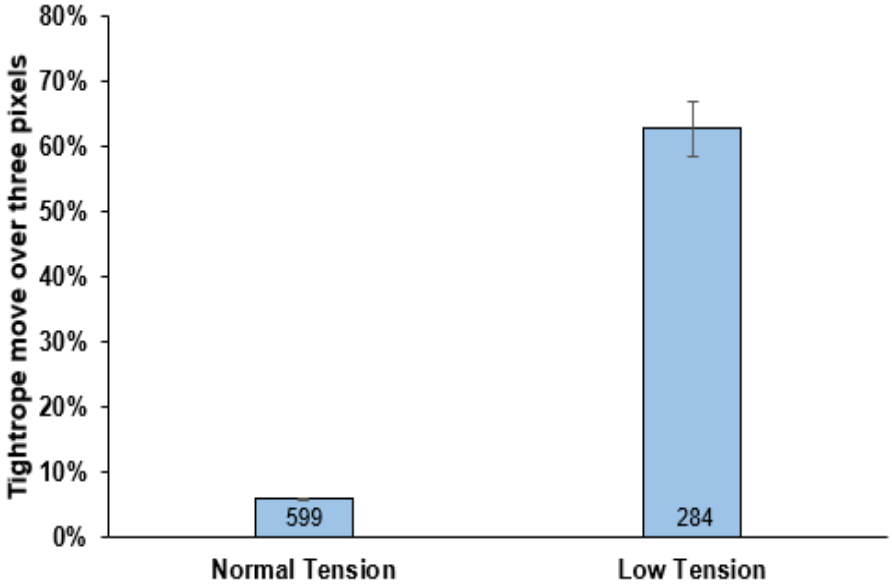

Figure 3.7 The effect of flow on whether the tightrope is visibly flexible and moves while imaging .

Values for mean probability percentage (±SEM, where, *n* refers to repeated experiments) tightropes showed movement over three pixels were 6% (±0.1% *n* = 3), 62.7% (±3.10% *n* = 3), for normal and low tension respectively.

*Indicates statistically significantly difference ($P < 0.01$) between the tension conditions.

3.3.4 UvrBC shows preference for damaged DNA

UvrBC has been shown to form a motile complex on double stranded DNA. Various UvrB mutant constructs affected this interaction revealing this interaction is likely mediated by UvrB (Hughes *et al.*, 2013). The initial role of UvrBC in NER is uncertain. UvrBC previously has be shown to bind constructs (discussed in 1.2.8) in the absence of UvrA but only with artificial DNA structures (Zou *et al.*, 1997; Moolenaar, Uiterkamp, *et al.*, 1998; Zou and Houten, 1999; Wirth *et al.*, 2016). We investigated the ability of this complex to locate damaged DNA using the tightrope assay. 52% (± 5% SEM; n=4) of 86 UvrBC interactions examined were found to colocalize with damage (Figure 3.8). This surprising result suggests that UvrBC is capable of locating damage. To confirm this result, we also studied the UvrBΔh mutant in complex with UvrC as this domain is key in the UvrAB complex (Theis *et al.*, 1999; Skorvaga *et al.*, 2002; Truglio *et al.*, 2004). Of 121 complexes studied we found 15% (± 5% SEM; n=5) to be colocalized with damage. This value is significantly ($P<0.001$) lower than that of UvrB.C suggesting UvrBC interacts with damaged DNA and uses the β-hairpin to distinguish damage, potentially in a similar way to UvrAB. Astonishingly, the damage colocalization probability for UvrA.B and UvrB.C complexes were not found to be statistically different ($P=0.4$), suggesting a previously unrealized damage recognition role for the UvrBC complex in NER. These results emphasize the importance of UvrB, specifically, the β-hairpin in NER. Like UvrBC, UvrC has been shown to diffuse along DNA but not recognize damage (Hughes *et al.*, 2013).

Consistent with earlier studies 18% (± 6% SEM; n=4) of 93 molecules were bound to damage, demonstrating a lack of damage specify, this is not statistically different to random binding (*P* = 0.83). There is no statistical difference between UvrC, UvrA.B/UvrB.C mutants (*P* = 0.35).

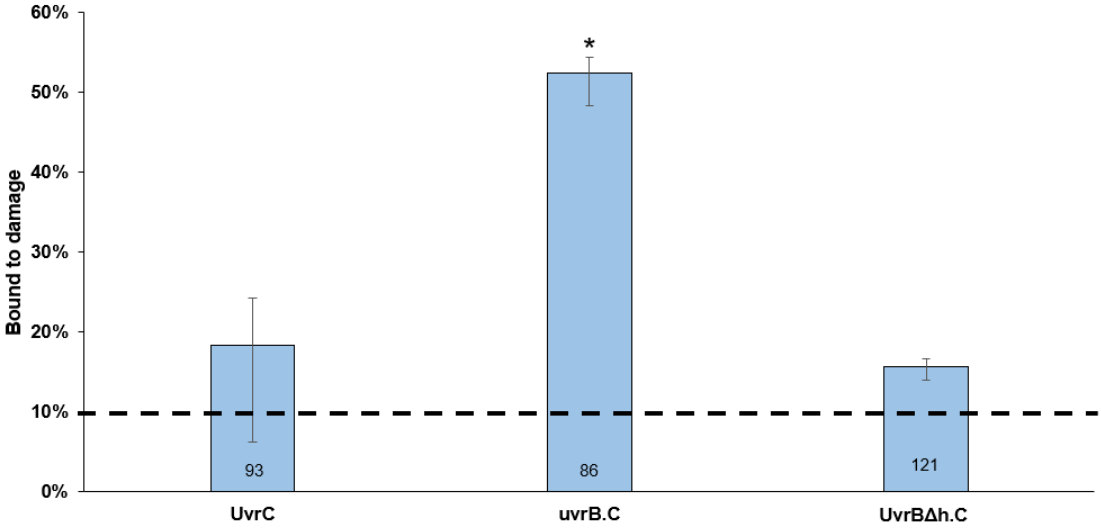

Figure 3.8. Probability of finding a UvrC, UvrB, UvrBC and respective mutant complexes colocalized with a damage marker.

Values for mean probability percentage (±SEM, where, *n* refers to repeated experiments) bound to damaged DNA were 18% (±6% *n*= 3), 52% (±5% *n* = 4) and 15% (±5% *n* = 5) for UvrC, UvrB.C and UvrBΔh.C, respectively.

The dashed line represents the probability (10.1%) of random association to damage based upon UvrA-Qdot binding to the mid-point of a DNA tightrope.

*Indicates statistically significantly difference (*P* = 0.002) relative to the 10.1% random association value.

UvrC and UvrBΔh.C and the random association probability are not statistically different to each other (*P* > 0.35)).

3.3.5 Cho interaction with DNA tightropes

The SOS-inducible gene *ydjQ*, renamed Cho, was discovered to be an N-terminal domain homologue of UvrC able to perform 3' incision in NER (Lewis *et al.*, 1994; Moolenaar *et al.*, 2002). This second endonuclease is upregulated by the SOS response, unlike UvrC, and able to incise certain bulky lesions more efficiently than UvrC (Lewis *et al.*, 1994; Fernández De Henestrosa *et al.*, 2000; Courcelle *et al.*, 2001; Moolenaar *et al.*, 2002; Moolenaar, Schut and Goosen, 2005).

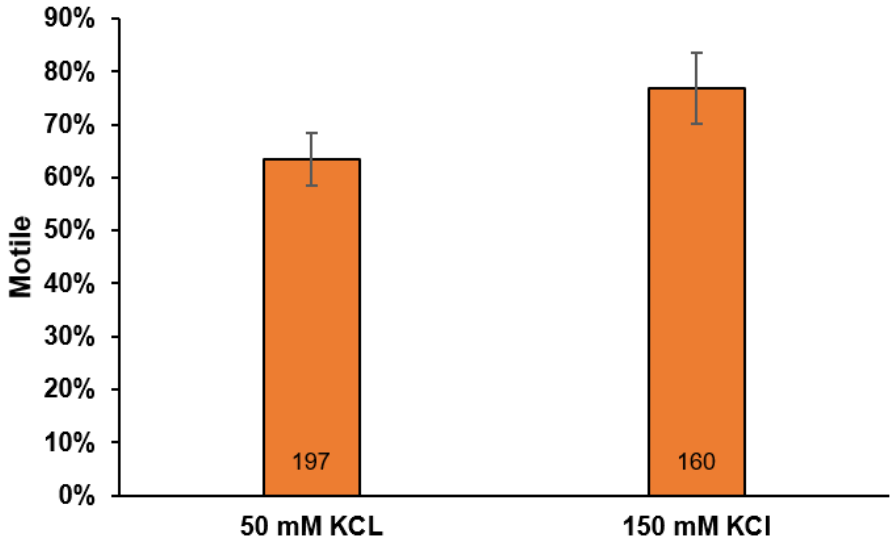

Figure 3.9. Motile properties of Cho on double stranded DNA tightropes. Percentage of moving Cho at low and high salt concentration. Values for mean percentage (±SEM, where *n* refers to repeated experiments) motile were 63.45% (±5.0, *n* = 6), 76.88% (±6.7, *n* = 5) for 50 and 150 mM KCl respectively.

At standard salt conditions of ABC buffer (50 mM KCl) 63.45% (±5.0, n = 6) of 197 molecules were found to be motile. Increasing the ionic strength to 150 mM KCl did not statistically increase the percentage motile (P=0.1356), 76.88% (±6.7, n = 5) of 160 were translocating along DNA (Figure 3.9).

The diffusion constant of Cho decreased significantly (P = 0.0129) from 9.30 (±0.6) $\times 10^{-3}\ \mu m^2\ s^{-1}$ at 50 mM KCl to 5.59 (±0.96) $\times 10^{-3}\ \mu m^2\ s^{-1}$ at 150 mM KCl (Table 3.1), three and two times slower than UvrC at the same conditions (Hughes *et al.*, 2013).

Like UvrC, in both salt conditions diffusive exponents were lower than 1 indicative of sub-diffusion by DNA interrogation (Saxton, 2001; Dunn *et al.*, 2011; Hughes *et al.*, 2013). We were unable to assess the lifetime of Cho on DNA due to the low number of proteins observed binding and releasing. The majority of Cho proteins observed on DNA bound before imaging had begun and very few left the tightropes, even when imaged for several minutes. The small number of clear bind and realease interactions imaged made statistics and lifetime estimates weak due to low n values.

Table 3.1. Motile properties of Cho–Qdot on DNA

Cho	50 mM KCl	150 mM KCl
d ($x10^{-3}$ um^2 $s^{-1)}$ (±SE)	9.30 (±0.6) n= 82	5.59 (±0.96) n= 70
Diffusive exponent (±SE)	0.94 (±0.04) n = 82	0.84 (±0.02) n= 70

ATP had no effect on the interaction between Cho and DNA, data for motile properties include ATP and non-ATP conditions combined. After

showing Cho can diffuse freely on DNA, we decided to investigate whether Cho was capable of detecting lesions. Since UvrC was unable to recognise lesions and Cho is essentially a truncated UvrC, we were unsurprised that only 8.9% (±0.59% *n* = 3) of Cho complexes observed were found bound to DNA (figure 3.10). There is no statistical difference between Cho and the random binding threshold (P>0.75).

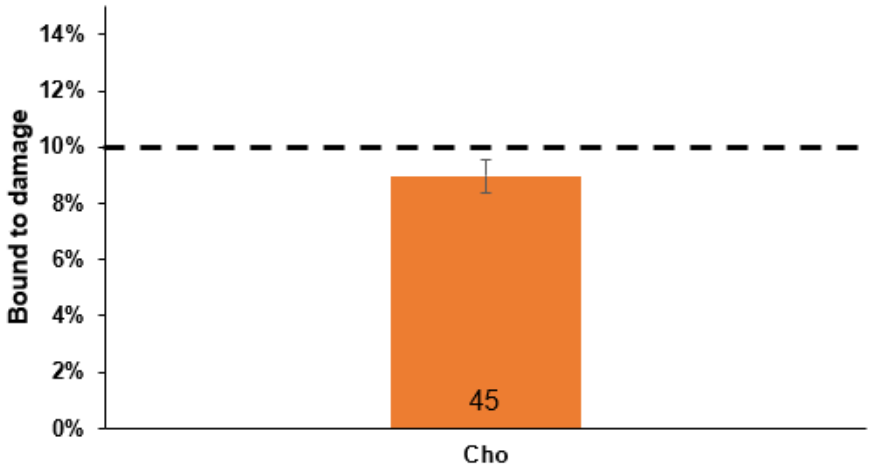

Figure 3.10. Probability of finding Cho colocalized with a damage marker on a DNA tightrope.
Values for mean probability percentage (±SEM, where, *n* refers to repeated experiments) bound to damaged DNA were 8.9% (±0.59% *n* = 3), The dashed line represents the probability (10.1%) of random association to damage based upon UvrA-Qdot binding to the mid-point of a DNA tightrope.

3.4 Discussion

NER is a multi-enzyme process that requires damage location, incision, removal and DNA resynthesis to seal the DNA backbone. UvrA and UvrC can scan DNA alone or in complex with UvrB (Kad *et al.*, 2010; Hughes *et al.*, 2013). How damage is located remains unclear and a primary function for motile UvrBC remains unknown. Here we developed an assay to examine which NER proteins can detect DNA damage at the single molecule level and found UvrBC can bind to DNA damage *in* vitro with the same levels as UvrAB.

3.4.1 UvrAB is the key NER damage detector

This single molecule data was in agreement with earlier studies that found UvrA had a lower affinity for damage than UvrAB complexes. (Reardon *et al.*, 1993; Jaciuk *et al.*, 2011; Wirth *et al.*, 2016). UvrA did show a significantly higher preference for damage than random binding alone. This confirms recent single molecule studies with *E .coli* UvrA, this data revealed UvrA has a 3-fold increase in lifetime on UV irradiated DNA tightropes compared to non-damaged tightropes (Barnett and Kad, 2018). These data and other studies show UvrA binds to damaged DNA with higher stability than non-damaged structures, characterized by the longer lifetime in single molecule data (Thiagalingams and Grossman, 1993; Pakotiprapha *et al.*, 2012).

We found that reducing the tension on the DNA tightropes increased UvrA's binding to damaged DNA levels that were statistically similar to UvrAB and UvrBC.

UvrA could twist and shorten the DNA upon binding damage, indeed it has been shown that UvrA can bend DNA structures by as much as 50% unwinding the DNA disrupting base stacking (Bellon, Coleman and Lippard, 1991; Van Houten and Snowden, 1993; Jaciuk *et al.*, 2011). Bending the DNA opens the DNA helix allowing subsequent lesion verification by UvrB, direct interrogation through the β–hairpin and related base flipping into the damage verification domain of UvrB (Croteau *et al.*, 2008; Wang *et al.*, 2009; Gantchev and Hunting, 2010). Tension did not affect UvrAB colocalizing with damage, when UvrA is in complex with UvrB this shortening might not occur, or this shortening and manipulation of DNA is performed by UvrAB. UvrAB could overcome this in an ATP dependent manner, such a process would explain why ZnG-UvrA and UvrB complex is unable to bind damage. UvrA has been shown to mediate DNA wrapping around UvrB during damage recognition and the C-terminal zinc finger directly stimulates the ATPase activity of UvrB (Verhoeven *et al.*, 2001; Croteau *et al.*, 2006, 2008; Wang *et al.*, 2009). UvrA has been shown to exist in two forms, 'open tray' and 'closed groove' (Pakotiprapha *et al.*, 2012). It is possible that UvrA attempts structural transition but under tension of a DNA tightrope is incapable of completing the reorganisation and leaves the DNA, resulting in lower damage affinity than UvrAB. Given the *in vivo* excess of UvrB, UvrA is likely in complex with UvrB in an A_2B_2 stoichiometry. This heterotetramer

can detect damage in both stands of DNA and recognise a wide range of DNA substrates (Van Houten *et al.*, 1987; Reardon *et al.*, 1993; Timmins *et al.*, 2009; Jaciuk *et al.*, 2011; Wirth *et al.*, 2016). UvrA alone likely only scans for damage when UvrB becomes overwhelmed by large amounts of damage, similar catalytic activity has been demonstrated conclusively *in vitro* and with *in vivo* live cell imaging (Orren and Sancar, 1989; Stracy *et al.*, 2016).

Unfortunately, we were unable to observe the ZnG-UvrA mutant alone without UvrB due to a lack of tag necessary for fluorescent labelling, undoubtedly this construct would not be able to recognise lesions on DNA, and like the other mutants, show no increased preference for DNA lesions. Predictably, the double mutant constructs, ZnG-UvrA and the UvrBΔh, together were unable to preferentially colocalize with damage.

3.4.2 UvrBC complexes can recognise DNA damage

UvrBC was previously shown to scan DNA in a process mediated by UvrB but the function remained uncertain (Hughes *et al.*, 2013). UvrBC previously has been shown to bind constructs in the absence of UvrA but only with a processed DNA flap or bubble substrates (Zou *et al.*, 1997; Moolenaar, Uiterkamp, *et al.*, 1998; Zou and Houten, 1999; Wirth *et al.*, 2016). Bulk assays used previously such as EMSAs require strong interactions for the protein DNA complexes to be detected (Hellman and Fried, 2007). If the damage-UvrBC interaction is weak these assays would not have identified a damage recognition role. The interaction between

UvrBC and damage could be weak for a number of reasons, UvrC may fail to properly activate the ATPase activity of UvrB or not sufficiently wrap DNA around UvrB, unlike UvrA (Verhoeven *et al.*, 2001; Croteau *et al.*, 2006, 2008; Wang *et al.*, 2009). We imaged protein interactions with damaged DNA tightropes as snapshots, this could explain why we were able to observe these weaker interactions when earlier biochemical studies did not. Pervious single molecule tightrope experiments showed UvrBC is unable to bind single stranded patches on DNA or double stranded junctions, confirming UvrBC is able to locate DNA damage via the β–hairpin domain (Springall *et al.*, 2017). UvrBC could also have another role *in vivo*, after UvrA dissociation from a UvrAB binding to damage, UvrBC could search DNA and locate this pre-incision complex. Dimerization of two UvrB proteins would allow for the two β-hairpins to verify damage and the chaperoned UvrC allow for quick DNA incision (Verhoeven *et al.*, 2001; Hughes *et al.*, 2013). UvrB and UvrD direct DNA polymerase independent DNA replication in DNA pol I negative cells by activating the helicase activity of UvrD (Olivera and Bonhoeffer, 1974; Joyce and Grindley, 1984; Moolenaar, Moorman and Goosen, 2000; Atkinson *et al.*, 2009). UvrBC could have a role helping to clear Okazaki fragments, by incision of RNA primers, in conjunction with the helicase activity of UvrD (Moolenaar, Moorman and Goosen, 2000). Additionally UvrD can expose DNA lesions covered by stalled RNAP (Epshtein *et al.*, 2014). As discussed earlier, UvrD can directly interact with UvrB, UvrBC could be involved in TCR repair via this UvrB-UvrD interaction *in vivo*.

3.4.3 Cho readily diffuses along double stranded DNA

Here we show Cho is able scan DNA independently from other NER factors. Changing the salt condition to physiological state did not affect the number of proteins that were motile on DNA, but did half the diffusion constant suggesting sliding rather than hopping on DNA (Berg, Winter and Von Hippel, 1981; von Hippel and Berg, 1986). Interestingly, 6 times as many Cho were diffusing on DNA but 3 times slower than UvrC at 50 mM KCl (Hughes *et al.*, 2013). We were unable to accurately report lifetime values on DNA due to low observations of binding and releasing from DNA. It is possible Cho has an extremely long lifetime on DNA that we were not able to report accurately. Another possibility is that the protein releases slowly from DNA by itself. There is a precedent for this in NER, UvrB requires both UvrD and DNA polymerase to be efficiently recycled (Caron, Kushner and Grossman, 1985; Husain *et al.*, 1985; Orren *et al.*, 1992) and UvrD recycles UvrC (Caron, Kushner and Grossman, 1985; Husain *et al.*, 1985). Cho is not required for general NER to remove lesions, the high motility and apparently long lifetime on DNA could relate to this as particular lesions or high levels of damage prove difficult for complete NER and often induce the SOS response. Cho is upregulated in this process and its high motile properties could relate to this need for quick lesion incision to aid the rate limiting step, UvrC incision due to the proteins low copy number (Yoakum and Grossman, 1981; Houten, 1990). Unsurprisingly Cho, like UvrC, was unable to recognise DNA damage and likely binds to preincsion complexes. Cho likely searches the DNA for

UvrBC complexes unable to complete 3' incision on bulky lesions, as demonstrated (Moolenaar *et al.*, 2002). UvrB and Cho could form a motile complex and search for preincsion complexes to allow dimerization of UvrB on damage, suggested for UvrBC complexes (Verhoeven *et al.*, 2001; Hughes *et al.*, 2013). Finally UvrC and Cho bind to different domains of UvrB and a Cho:UvrB:UvrC complex is possible on lesions that UvrC incise poorly (Moolenaar *et al.*, 2002; Van Houten, Eisen and Hanawalt, 2002).

3.5 Conclusions

In this chapter we confirm UvrAB is the crucial damage detecting complex in NER. We confirm a wealth of biochemical and structural studies that show the C-terminal zinc finger of UvrA and the β–hairpin of UvrB play vital roles in the damage processing pathway of bacterial NER. We demonstrate a tension dependence in the ability of UvrA to recognize damage efficiently likely by distorting the DNA when recognizing lesions to aid in damage verification by UvrB. Using single molecule fluorescence imaging we show, for the first time, that UvrBC can recognise and bind lesions incorporated into double stranded DNA and like UvrAB, this is mediated by the β–hairpin domain of UvrB. These data suggest, through the UvrBC complex, a more complex DNA repair, independent of UvrA, than the canonical linear pathway of bacterial NER. Finally, we show Cho is a highly diffusive protein capable of independent double stranded DNA translocation.

Chapter 4: UV damage response *in vivo* by UvrBC

4.1 Introduction

In the previous chapter we show for the first time UvrBC can locate lesions on unprocessed DNA tightropes in the absence of UvrA. Before these experiments, UvrBC complexes only displayed interaction with lesions on processed DNA substrates *in vitro* (Zou *et al.*, 1997; Moolenaar, Uiterkamp, *et al.*, 1998; Wirth *et al.*, 2016). In this chapter we explore the role of UvrBC complexes *in vivo*. We used live cell imaging to examine if fluorescently tagged UvrB and UvrC could respond to UV damage *in vivo* independently from UvrA. Qdots are more stable and brighter than other fluorescence probes, perfect for *in vitro* assays in the previous chapter, but these properties can limit their use *in vivo* as differentiating between individual fluorophores can be difficult (Gao *et al.*, 2005; Walling, Novak and Shepard, 2009). Interestingly the smaller Qdots that might be more suitable for imaging in cells appear to be more toxic (Fang *et al.*, 2012). Furthermore cells do not easily permit Qdot uptake, the cell membrane has to be disturbed and results in disrupted growth phases (Derfus, Chan and Bhatia, 2004; Fang *et al.*, 2012; Kim, Kwak and An, 2016). In some cultured cell lines the addition of UV increases Qdot toxicity (Derfus, Chan and Bhatia, 2004). To study the *in vivo* roles of UvrBC we decided to use fluorescent proteins rather than quantum dots. The green fluorescent protein was first purified from the jellyfish Aequorea

Victoria (Shimomura, Johnson and Saida, 1962). Reduced photobleaching and increased protein stability have vastly improved GFP since it was first isolated, the fluorescent molecule can now be expressed in complex organisms including mice and cats (Prasher et al., 1992; Ikawa et al., 1995; Tsien, 1998; Wongsrikeao et al., 2011). In this chapter we use the eGFP variant of GFP which has a maximum excitation of 488nm, ideal for our optical setup described in Chapter 2.8.1 (Cormack, Valdivia and Falkow, 1996; Cinelli et al., 2000; Gambotto et al., 2000).

UvrA has been shown to promote the disassembly of Mfd-RNAP complexes using single molecule *in vitro* assays (Fan *et al.*, 2016) and this was recently confirmed using live cell fluorescence imaging (Ho, Van Oijen and Ghodke, 2018). These *in vivo* imagine experiments confirmed a wealth of biochemical and structural data by visualising a direct interaction between Mfd and RNAP in live *E. coli* (Ho, Van Oijen and Ghodke, 2018). Other recent single molecule live cell fluorescence imaging studies have explored the *in vivo* activity of the UvrA and UvrB in relationship to damage detection (Stracy *et al.*, 2016). These data suggest initial lesion detection is directed by UvrA rather than the UvrAB complex as a number of *in vitro* studies had indicated previously (Orren and Sancar, 1989; Reardon *et al.*, 1993; Thiagalingams and Grossman, 1993; Verhoeven, Wyman, *et al.*, 2002; Pakotiprapha *et al.*, 2009, 2012; Kad *et al.*, 2010; Jaciuk *et al.*, 2011; Webster *et al.*, 2012; Wirth *et al.*, 2016). The live cell imaging showed two distinct UvrA ATP binding and hydrolysis events. Distal site activation with UvrB independent lesion detection, and proximal

activation to recruit UvrB from the cellular environment (Stracy *et al.*, 2016).

We first verified that fluorescently tagged Uvr proteins were able to restore cell viability in their respective null cells, confirming that the tag had no effect on protein function. Next, we established UvrB and UvrC were able to bind to genomic DNA in response to DNA damage with a full NER background ($UvrA^{+}$), confirming we were able to visualise damage responses *in vivo*. To investigate the *in vivo* function of UvrBC we used a Keio cell line with UvrA knocked out ($UvrA^{-}$) and ectopically expressed C-terminally eGFP tagged UvrB and UvrC.. To examine if the UvrBC complex can recognise DNA lesions we had to remove damage detection by UvrA. Using the $UvrA^{-}$ and fluorescently tagged UvrB and UvrC we were able to explore lesion recognition without interference from UvrA and canonical pathway of NER. Using the eGFP tagged proteins we could examine the change in protein motion in response to UV damage. Diffusing, non-DNA bound, molecules blend into the background whereas genome-associated molecules appear as fluorescence spots (Smith, Grossman and Walker, 2002; Elf, Li and Xie, 2007; Kuhlman and Cox, 2012; Uphoff *et al.*, 2013; Chen *et al.*, 2014; Etheridge *et al.*, 2014; Stracy *et al.*, 2016).Using live cell imaging we find UvrB and UvrC form stable complexes on DNA in response to UV damage independent of UvrA, demonstrating a UvrBC lesion detection role *in vivo*. Next, we quantify the number of ectopically expressed UvrC-eGFP present in our live cell and cell survival assays. Finally, astonishingly, we show that the ectopically

expressed UvrC increases cell survival compared to the UvrA$^-$ strain providing a damage repair role for UvrBC *in vivo*.

These data suggest an in vivo lesion repair role for UvrBC in a previously unrealised pathway pre-SOS response.

4.2 Material and methods

4.2.1 Cell line

UvrA$^-$ experiments in this chapter were performed with *E. coli* (K-12 strain BW25113) KEIO cells. C-terminally eGFP tagged *E. coli* Uvr proteins were obtained as ASKA clones from the National Bioresource Project (NIG, Japan) (Kitagawa *et al.*, 2005; Baba *et al.*, 2006; Yamamoto *et al.*, 2009).

In all live cell imaging and survival experiments Uvr proteins were transformed into the null cell line stated and glycerol stocks used as starters for subsequent investigations. Uvr Protein-eGFP expression was regulated by the T5-lac promoter on the pCA24N plasmid with the lacI^q for strict suppression (Kitagawa *et al.*, 2005). Protein expression was not induced in any experiment in this chapter.

4.2.2 Fluorescence imaging of UvrB-eGFP and UvrC-eGFP in *E. coli*

3% agarose/1× LB pads were created by warming a 3% agarose/1× LB at at 65 °C for 15 minutes. Damaged cells were exposed to 5 or 25 J/m^2 UV (254 nm) and incubated at 37°C for 30 min to allow for an adequate SOS response prior to imaging (Crowley and Hanawalt, 1998; Smith, Grossman and Walker, 2002).

4.2.3 Cell survival assay

Cells from glycerol cell stocks were grown overnight at 37°C and subsequently diluted into fresh LB and grown to OD_{600}0.6, described in more detail in Chapter 2.9.1. Aliquots of undiluted and three serial ten-fold dilutions of cells were either spotted or spread on LB-agar plates. Plates were then exposed to the stated doses of 254 nm UV to induce DNA damage and incubated overnight. We transformed UvrA KEIO cells with a plasmid containing the protein Yihf-eGFP, a protein unrelated to NER to generate a UvrA-null control cell line ($UvrA^{-}$) that contained an equivalent protein load and antibiotic resistance to those with Uvr proteins.

4.2.4 Determining the number of UvrC-eGFP present

Cells were grown to OD_{600}0.6 and their peak fluorescence intensity at 509 nm measured the relative quantities of eGFP, after excitation at 488 nm with a Cary Spectrophotometer (Varian) (Cormack, Valdivia and Falkow, 1996; Cinelli et al., 2000; Gambotto et al., 2000).

4.2.5 Statistics

Unless otherwise stated, '*n*' refers to the number of flow chambers or agarose pads used per experiment. Significance was determined using the Student's *t*-test and consequent *P*-values are reported if two values are compared.

If multiple means are compared analysis of variance (ANOVA) was performed with a post hoc test, including a Bonferroni correction to consider multiple comparisons, shdsjd subsequent *p*-values are reported.

4.3 Results

4.3.1 UV Survival of Uvr$^-$ cells complemented with Uvr proteins

Qdots are not ideal for *in vivo* imaging, the cell membrane has to be made permeable and subsequent fluorophore uptake results in abnormal growth phases (Derfus, Chan and Bhatia, 2004; Fang *et al.*, 2012; Kim, Kwak and An, 2016). Fluorescent proteins are robust fluorophores ideal for *in vivo* imaging (Contag *et al.*, 1998; Gogoi *et al.*, 2006; Mullineaux *et al.*, 2006; Wessels *et al.*, 2007)**.** In these *in vivo* experiments we use eGFP, which has a maximum excitation of 488nm, ideal for our optical setup (Cormack, Valdivia and Falkow, 1996; Cinelli et al., 2000; Gambotto et al., 2000). We first performed controls to ensure that cells containing the ectopically expressed proteins were viable, and that the fluorescent labelling had no effect on protein activity (Barnett and Kad, 2018). We complemented UvrA$^-$, UvrB$^-$ and UvrC$^-$ cells with their respective eGFP-fusion proteins and exposed them to various UV doses. Cell growth for all null cells was severely decreased following exposure to a relatively small doses, 5 J/m^2 and 10 J/m^2 of 254 nm, UV radiation (figure 4.1). Complementation of the knockout cell line with their respective Uvr-eGFP gene constructs, providing full NER machinery, were viable up to 25 J/m^2 (figure 4.1).

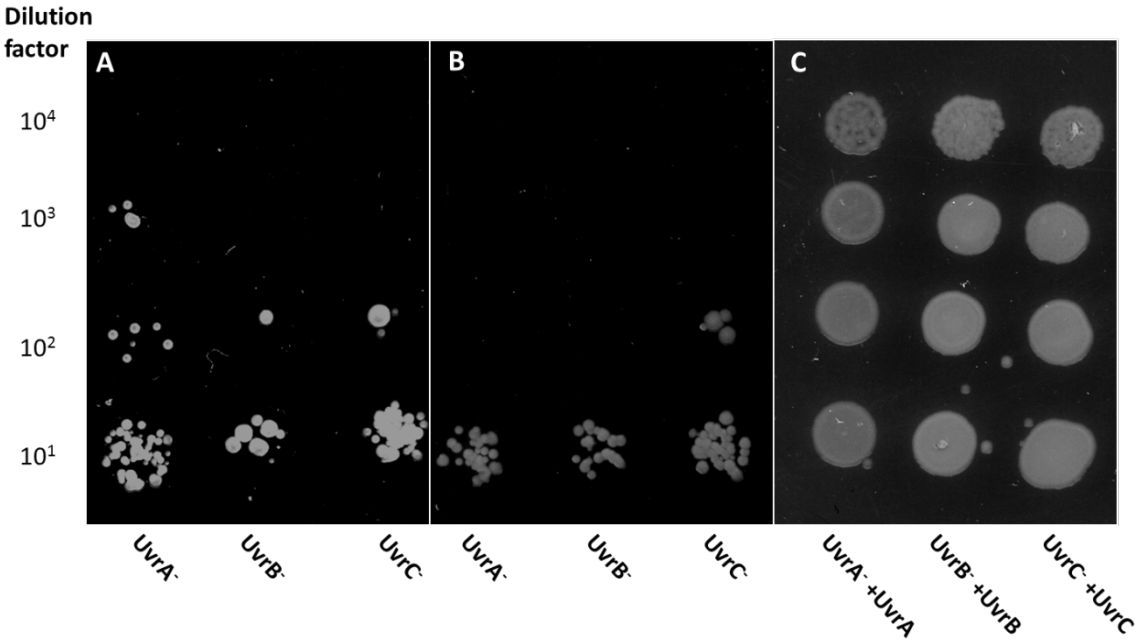

Figure 4.1. Survival of Uvr⁻ cells exposed to various does of UV damage. (A) Colony growth for null cells exposed to 5 J/m^2, **(B)** or 10 J/m^2. **(C)** Survival of null cells ectopically complemented with respective eGFP labelled Uvr proteins before exposure to 25 J/m^2 254 nm UV.

4.3.2 *In vivo* fluorescence imaging of UvrB/C-eGFP in UvrA$^+$ cells

Uvr Protein-eGFP expression was regulated by the T5-lac promoter on the pCA24N plasmid with the lacI^q for strict suppression (Kitagawa *et al.*, 2005). In this study we did not induce protein expression, all Uvr-eGFP present were ectopically expressed. As discussed in the previous section C-terminally tagged-eGFP had no effect on *in vivo* NER function, fluorescently tagged UvrB and UvrC could be used to examine the role of UvrBC. The intracellular dynamics of protein motion provides an excellent indicator for whether the proteins are freely diffusing through solution or interacting with DNA (figure 4.2). Diffusing molecules blend into the

background whereas genome-associated molecules appear as fluorescence spots (Smith, Grossman and Walker, 2002; Elf, Li and Xie, 2007; Kuhlman and Cox, 2012; Uphoff *et al.*, 2013; Chen *et al.*, 2014; Etheridge *et al.*, 2014; Stracy *et al.*, 2016). Using this approach, fluorescent molecules were examined on a cell-by-cell basis and were categorized as not binding the genome if a homogenous distribution of fluorescence was observed. By contrast, the appearance of spots that persist for the duration of our movies (10 s) in a cell indicated that the Uvr-eGFP proteins were binding to the genome.

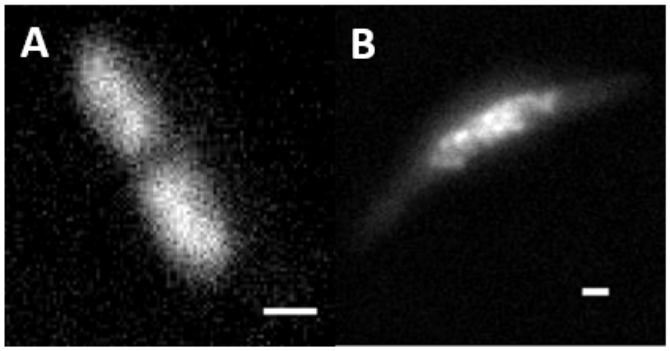

Figure 4.2. Genomic association of C-terminally eGFP-UvrC in live cell fluorescence imaging assay. **(A)** An example image of cells with homogenously diffusing proteins, **(B)** or static molecules indicating proteins bound to damaged DNA after 5 J/m^2 of UV exposure. Scale bars represent 1 μm.

Although the number of spots per cell varied, we classified a cell with one or more distinct spots as static. In figure 4.1 we show that complementing a Keio cell line with the respective eGFP tagged NER protein restores cell

viability, demonstrating that the fluorophore has no effect on the function of the protein. We first used UvrB and UvrC eGFP tagged proteins in cells with a full NER background ($UvrA^+$). In the absence of UV-induced damage 26.21% (±4.4% SEM; *n* = 5) of 206 UvrB-eGFP containing cells were static. The remaining cells appeared with a homogeneous background of fluorescence, consistent with proteins diffusing in the cellular cytoplasm. 5 J/m^2 of UV increased the static population to 45.45% (±6.0% SEM; *n* = 4) of 142 cells observed, significantly higher (*P* = 0.02) than undamaged cells. Further increasing the UV exposure to (figure 4.3) 25 J/m^2 showed an increase in the static population (69.02% ± 2.0% SEM; *n*= 4) of 184 observed cells, significantly higher (*P* < 0.05) than undamaged cells and 5 J/m^2.

UvrC-eGFP behaved quite differently from UvrB-eGFP without UV (figure 4.4). 37.38% (±6.3% SEM; *n* = 5) of 107 cells possessed static UvrC-eGFP. Similarly, to UvrB-eGFP behaviour with a full NER background, upon exposure to 5 J/m^2 UV the static population was significantly higher (*P* < 0.01) than undamaged cell, 67.94% (±2.8% SEM; *n* = 5) of 156 cells had static molecules indicative of genome association. Further exposure to UV damage (25 J/m^2) resulted in an even higher damage response 82.68% (±2.8% SEM; *n* = 5) of 179 cells observed. These data are statistically greater than the unexposed cells and to 5 J/m^2 (*P* < 0.05), in the same way as UvrB-$UvrA^+$ cells.

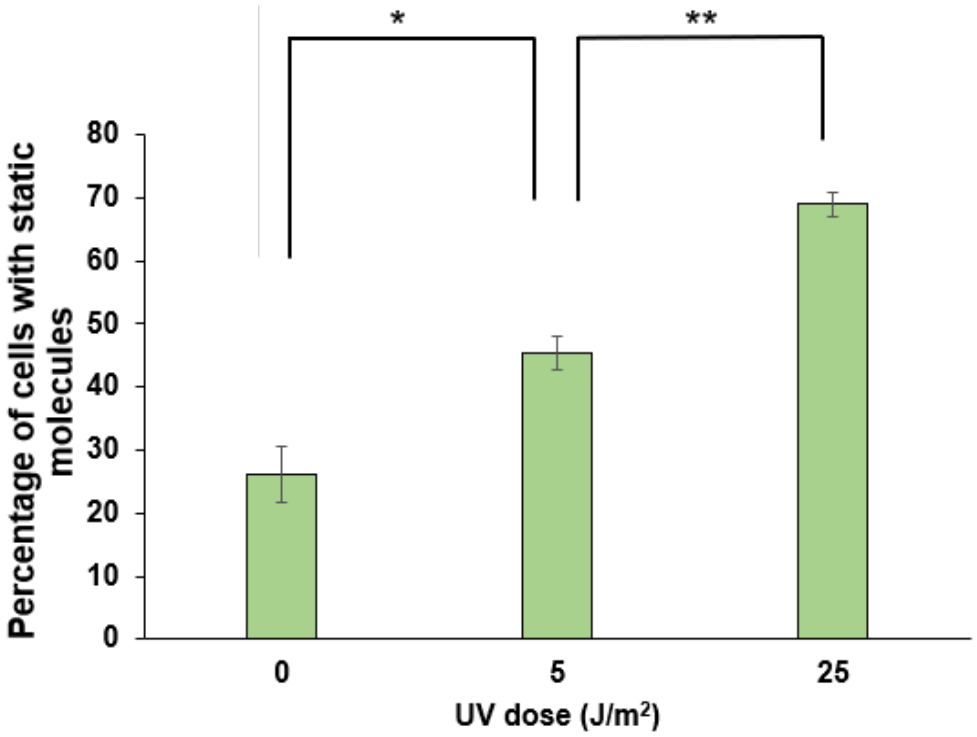

Figure 4.3. Genomic association of UvrB with a full NER background (UvrA+) examined fluorescence imaging.

The percentage of cells with pCa24N UvrB-eGFP plasmid with a static population of molecules 26.21% (±4.4% SEM; *n* = 5), 45.45% (±6.0% SEM; *n* = 4) and 69.02% (± 2.0% SEM; *n*= 4), at 0, 5 and 25 J/m^2 of UV (254 nm) exposure, respectively.

Statistics reported are mean ± SEM, where, *n* refers to repeated experiments.

*P < 0.05

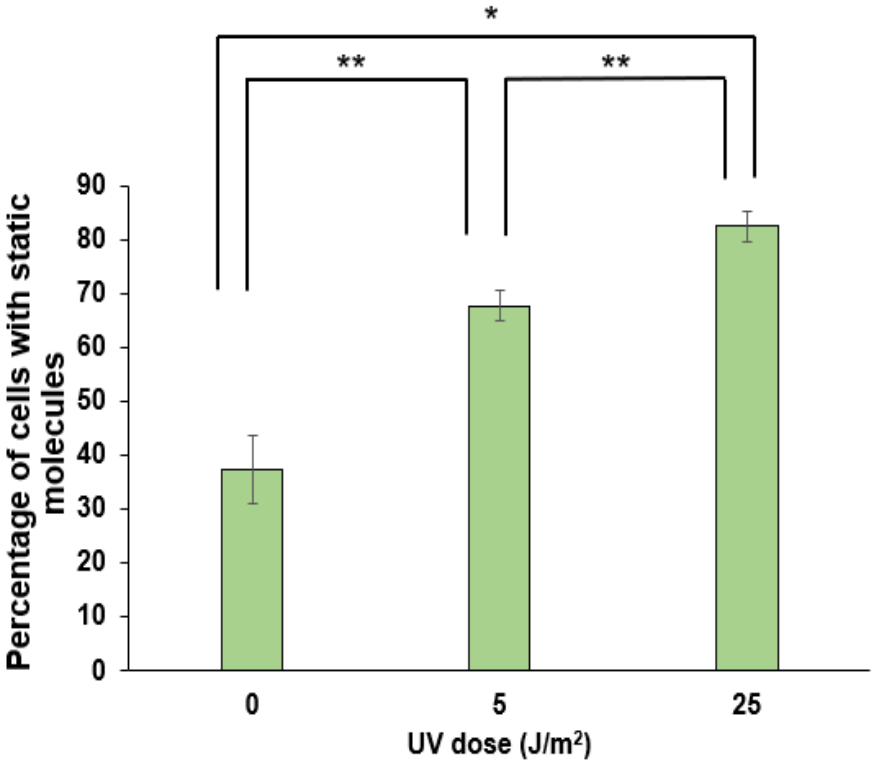

Figure 4.4. Genomic association of UvrC with a full NER background (UvrA+) examined by fluorescence imaging.

The percentage of cells with pCA24N UvrC-eGFP plasmid with a static population of molecules 37.38% (±6.3% SEM; *n* = 5), 67.94% (±2.8% SEM; *n* = 5) and 82.68% (± 2.8% SEM; *n*= 5), at 0, 5 and 25 J/m^2 of UV (254 nm) exposure, respectively.

Statistics reported are mean ± SEM, where, *n* refers to repeated experiments. *P < 0.1.

4.3.3 *In vivo* fluorescence imaging of UvrB/C-eGFP in UvrA$^-$ cells

In these live cell imaging and survival experiments that will be discussed Uvr proteins were transformed into the null cell line stated. Our observation that UvrBC complexes can recognise damage on DNA tightropes, in the previous chapter, may suggest a role in repair *in vivo*. In 4.3.2 we show that fluorescently labelling UvrB and UvrC with eGFP in cells, with a full NER background, show a response to UV damage. We therefore sought to determine if UvrB and UvrC respond to the presence of damage *in vivo* in the absence of UvrA. In the same way as the previous section we studied eGFP tagged UvrB and UvrC *in vivo* by ectopically expressing these protein fusions in UvrA$^-$. In the absence of UV-induced damage UvrA$^-$ complemented with UvrB-eGFP bound sparsely to the genome. 4% (±2.1% SEM; n = 4) of 100 UvrB-eGFP containing UvrA$^-$ cells were static, significantly lower (P < 0.01) than UvrB-eGFP UvrA$^+$ cells, this result was expected due to the abundance of the UvrAB complex under normal circumstances, UvrB has a greatly reduced number of partners to facilitate binding to DNA. Low UV exposure (5 J/m^2) increased the static population to 22% (±6.7% SEM; n = 4) of 121 cells observed, significantly higher (P = 0.08) than unexposed cells (figure 4.5). Further increasing the UV exposure to 25 J/m^2 showed no statistically significant (P = 0.9) change in the static population (19% ± 4.1% SEM; n= 4) of 124 observed cells, suggesting the damage response is saturated at low levels of exposure due to the lack of UvrA. As with the

previous experiment UvrC-eGFP behaved quite differently from UvrB-eGFP in UvrA^{-} cells, without UV. This is likely because UvrC can scan DNA alone, UvrB requires a partner to bind to DNA (Kacinski and Rupp, 1981; Kad *et al.*, 2010; Hughes *et al.*, 2013). 43% (±6.8% SEM; *n* = 3) of 86 cells showed static UvrC-eGFP molecules without UV, not statistically different from UvrA^{+} cells ($P > 0.001$). As with UvrB in the UvrA^{-}, upon exposure to 5 J/m^2 UV the static population rose to 65% (±7.7% SEM; *n* = 9) of 65 cells. However, unlike UvrB complementation, further exposure to UV damage (25 J/m^2) resulted in an even higher damage response 73% (±5.6% SEM; *n* = 8) of 102 cells observed (figure 4.6), statistically greater than the unexposed cells ($P = 0.025$). These results (figure 4.5 and figure 4.6) indicate that UvrB and UvrC respond to DNA damage independently of UvrA *in vivo*. These results confirm and further strengthen our *in vitro* observations in the previous chapter (2) with purified proteins using our damaged DNA tightrope assay.

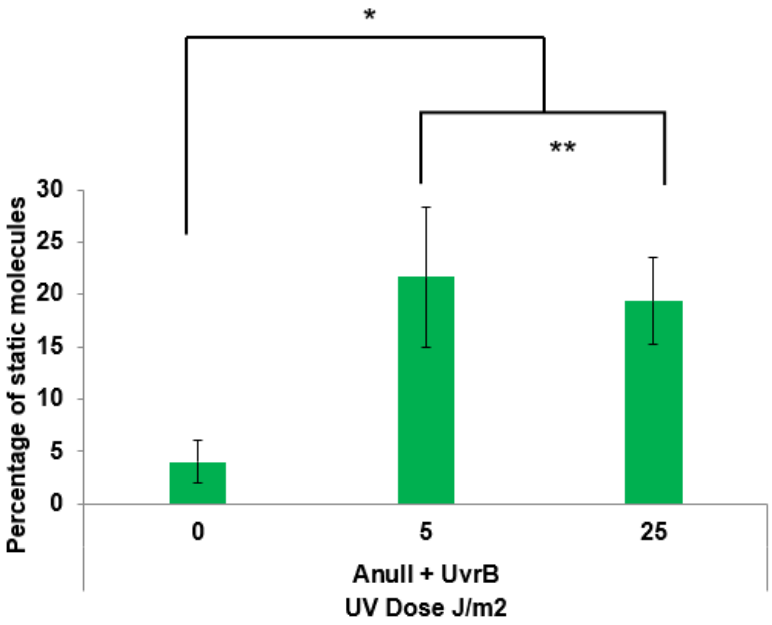

Figure 4.5. Genomic association of UvrB in UvrA^{-} is revealed by live cell fluorescence imaging.

The percentage of UvrA null cells complemented with UvrB with a static population of molecules were 4% (± 2.1% n=4), 21% (± 6.9% n=4), 19% (± 4.1% n=4), at 0, 5 and 25 J/m^2 of UVC exposure respectively.

Statistics reported are mean ± SEM, where n refers to repeated experiments. *P < 0.05, **P > 0.1

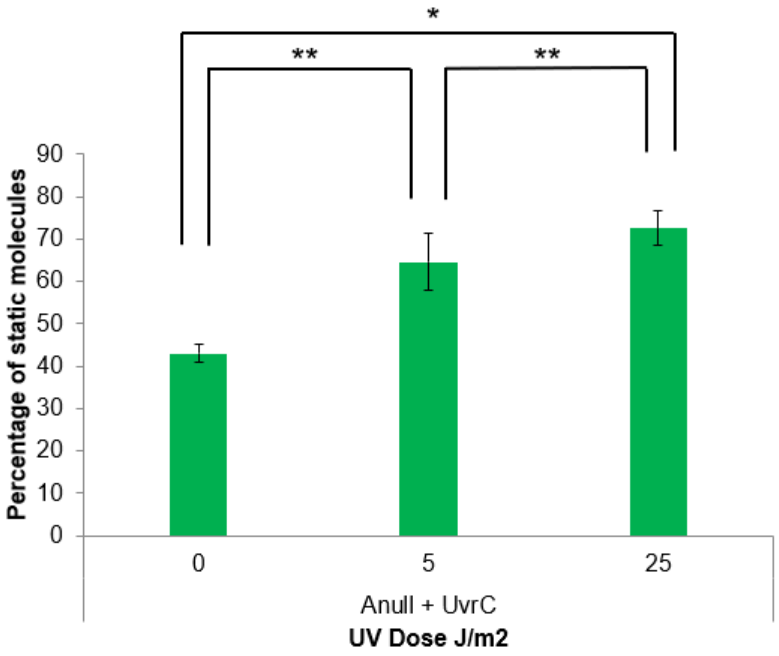

Figure 4.6. Genomic association of UvrC in UvrA$^-$ is revealed by live cell fluorescence imaging.

The percentage of UvrA-null cells complemented with UvrC with a static population of molecules were 43% (± 7.6% n=3), 65% (± 7.7% n=9), 72% (± 5.6% n=8), at 0, 5 and 25 J/m^2 of UVC exposure respectively. Statistics reported are mean ± SEM, where n refers to repeated experiments. *P < 0.05, **P > 0.1

4.3.4 Direct assessment of the number of UvrC proteins

To quantify the amount of protein present we performed a direct measure of the number of UvrC molecules present in a population of cells. UvrC-eGFP was used as a control as these cells appeared to fluoresce the least and would be easier to quantify. UvrA$^-$ cells ectopically expressing UvrC-eGFP were plated onto agarose pads in the same way as prepared for live cell imaging (Section 4.2.2/4.2.3). The cells were identified and focused using brightfield, recording was initiated prior to activation of the illumination laser at 488 nm, the maximum excitation for eGFP (Cormack, Valdivia and Falkow, 1996; Cinelli et al., 2000; Gambotto et al., 2000). Photobleaching would begin as soon as the sample was illuminated, recording before illumination meant we could accurately capture and record as many fluorophores as possible.

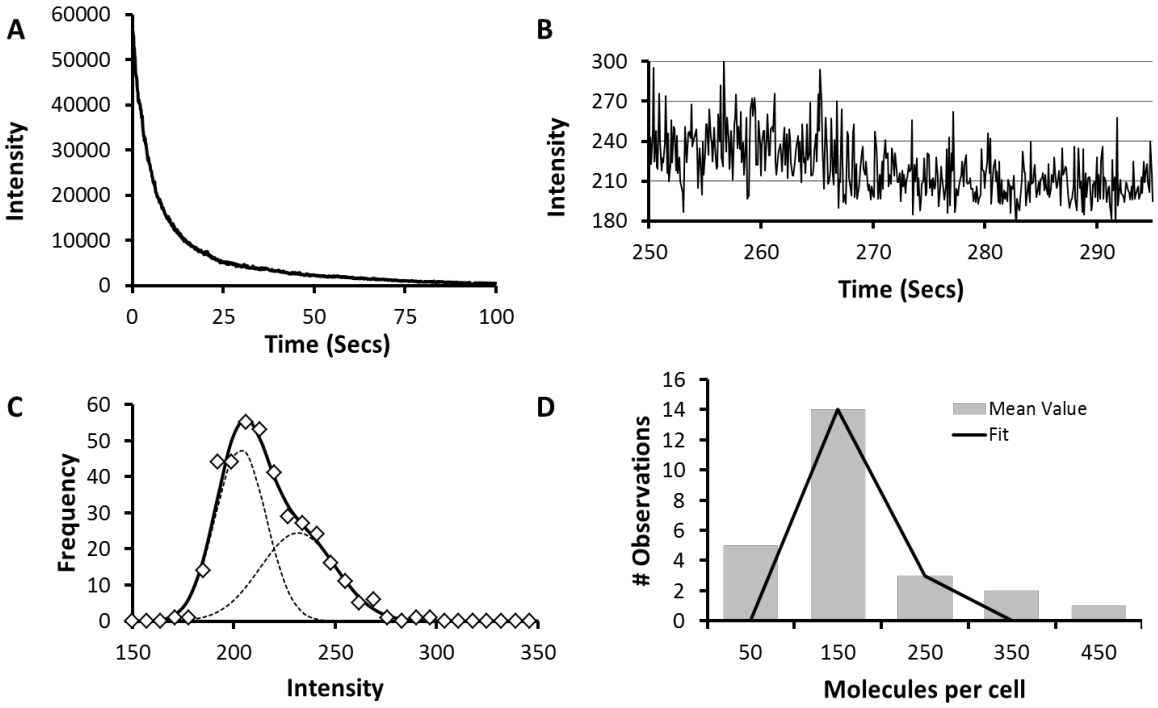

Figure 4.7. Quantifying UvrC-eGFP *in vivo*. **(A)** Representative single exponential photobleaching decay curve for a single cell. **(B)** Close-up of the last step to background from a photobleaching decay curve. **(C)** Data from (B) re-plotted as a histogram, showing the two components, noise and last step fitted to two Gaussians (dashed lines). **(D)** Histogram of the number of molecules per cell fitted to a Gaussian distribution to yield an average of 183 ±

The total intensity of fluorescence for each cell followed a single exponential decay as the ectopically expressed UvrC-eGFP would be photobleached (figure 4.7A)**.** Towards the end of the decay there would be a few molecules of UvrC-eGFP remaining. This region was used to quantify the stepwise photobleaching of the remaining individual fluorophores (figure 4.7B)**.** The data from the last step to background

resulted in a biphasic distribution that was fitted to the sum of two Gaussians consisting of background noise and fluorescence from a single UvrC-eGFP. The mean shift of the signal relative to noise was plotted for 16 molecules as a second histogram and fitted to a single Gaussian distribution (figure 4.7C). The mean of this distribution provided the average fluorescence intensity of a single UvrC-eGFP (30 ± 2.7, SEM, n = 16). Using the full single exponential decay from photobleaching we could calculate the number of molecules per cell using the average fluorescence intensity of UvrC-eGFP (30). We fit the full photobleach decay to a single exponential and divided the amplitude by the average fluorescence intensity. A histogram of 42 measurements was fit to a single Gaussian with a mean of 183 ± 5 (SEM) molecules of UvrC-eGFP per cell expressed ectopically (figure 4.7D). We next performed absorption spectrometry to establish the relative protein levels for all other Uvr-eGFP proteins expressed, using UvrC-eGFP as the control. Cells were grown to OD_{600} 0.6 and lysed. Emission spectra are shown in the figure 4.8 for each sample with excitation at 490 nm measuring their peak fluorescence intensity was measured at 509 nm (figure 4.8) determine the relative quantities of eGFP. As seen in figure 4.8 UvrC-eGFP ectopically expressed in UvrA- cells had an intensity at 509 nm of 11.30. To remove the background auto-fluorescence, cells complemented with a non-GFP labelled UvrA were measured under identical conditions and the spectrum subtracted from the Uvr-eGFP tagged protein spectra. Using UvrC-eGFP as a control the absorption of UvrA-eGFP was 4.5-fold higher, therefore

equivalent to 822 molecules and UvrB was 7.5 times higher equivalent to 1373 molecules.

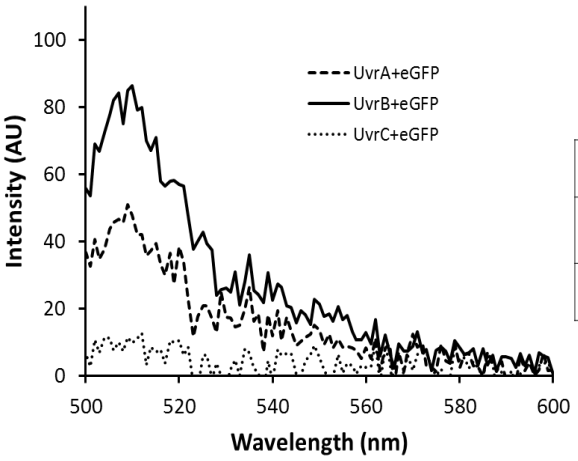

	UvrA-eGFP	UvrB-eGFP	UvrC-eGFP
Intensity at 509nm	50.77	84.74	11.30
Relative to UvrC-GFP levels	4.49	7.50	1
Molecules per cell	822	1373	183*

*Measured in figure S3

Figure 4.8. Ectopic levels of C-terminally tagged eGFP proteins in UvrA$^-$ cells.

UvrA-null cells complemented with ectopically UvrA-eGFP, UvrB-eGFP or UvrA-eGFP. The table shows the relative intensity of each eGFP labelled Uvr protein at 509 nm, the peak emission wavelength.

4.3.5 Cell survival assay of UvrA$^-$ cells complemented with UvrB/C

The observations made in this chapter, and the previous one, suggest that not only can UvrBC complexes find damage, but, independently from UvrA, they are capable of binding to DNA in response to damage. It is still

not clear that damage response pathway is capable of damage processing *in vivo*. To examine this UvrA independent pathway and understand if it is capable of full genome repair, we performed cell survival assays of the cell lines used in the previous section. In the previous section fluorescently labelled UvrB and UvrC bound to the genome in response to UV, in this section we examined if these constructs could increase cell survival. Exposure of $UvrA^-$ cells to 5 J/m^2 UV light (254 nm) greatly impaired survival; however, ectopic expression of UvrA restored viability (figure 4.1, columns 1 and 2) (Section 4.3.1). Next, we complemented $UvrA^-$ with UvrB-eGFP or UvrC-eGFP and found that in both cases there was improved survival (figure 4.9, columns 3 and 4).

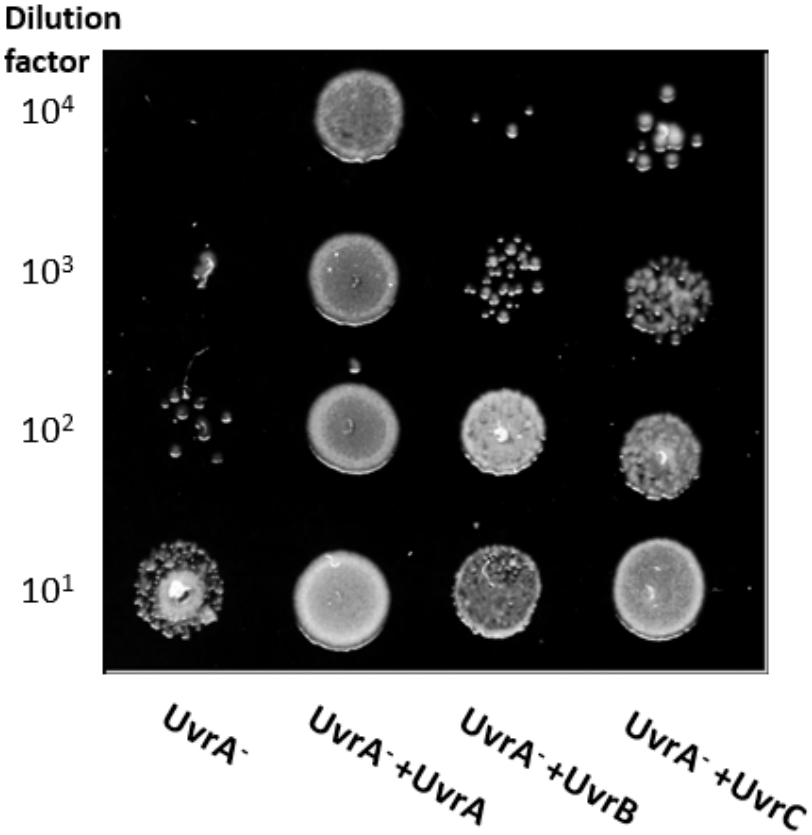

Figure 4.9. Survival of UvrA$^-$ cells exposed to UV damage. Spot plates of decreasing cell titres exposed to 5 J/m^2 Lane 1 UvrA$^-$ cells, lane 2 UvrA$^-$ cells complemented with UvrA-eGFP, lane 3 UvrA$^-$ cells complemented with UvrB-eGFP, lane 4 UvrA$^-$ cells complemented with UvrC-eGFP. UvrA restores full cell viability. Ectopic UvrB or UvrC showed an increase in cell survival compared to UvrA$^-$.

To quantify this effect, we modified the spotting assay into a plating assay. Survival curves were generated by exposing a number of cell dilutions, with varying doses of UV, and counting the colonies that grew following plating (figure 4.10). These values are presented as logarithmic growth relative to cells not exposed to UV, therefore as the magnitude of the negative value increases this indicates more compromised growth. As in

Section 4.3.1, UvrA complementation of UvrA$^-$ showed the greatest level of UV resistance with −1.3 (equivalent to 5%) survival even after 25 J/m^2 UV exposure. In this scenario full NER machinery was not overwhelmed by DNA lesions. Similarly, at 5 J/m^2 UvrA$^-$ cells with UvrB showed small, but significantly higher ($P < 0.05$) log relative cell survival of −5.5 versus non-complemented UvrA$^-$ cells (−6.0; figure 4.10). The improved survival with UvrB was only observed at low doses of UV, at 10 J/m^2 UvrA$^-$ cells complemented with UvrB showed no significantly improved survival. In contrast to UvrB, UvrA$^-$ cells ectopically expressing UvrC showed greater survival than both UvrA$^-$ and UvrA$^-$ complemented UvrB at low and moderate doses of UV. At 5 and 10 J/m^2 UV exposure log relative survival of UvrA$^-$ complemented with UvrC was recorded as −2.4 and −7 respectively; significantly better ($P < 0.05$) than the UvrA$^-$ cells which showed −6.0 and −6.2 log relative survival at the same UV dose. At UV doses above 15 J/m^2, the UvrC complemented cells showed no significant difference in survival from UvrB-complemented cells or UvrA-null cells indicating that UvrA is essential for survival even with additional UvrC present. The improved survivability conferred by UvrC is only significant at low UV doses, indicating the clear importance of UvrA in regular NER.

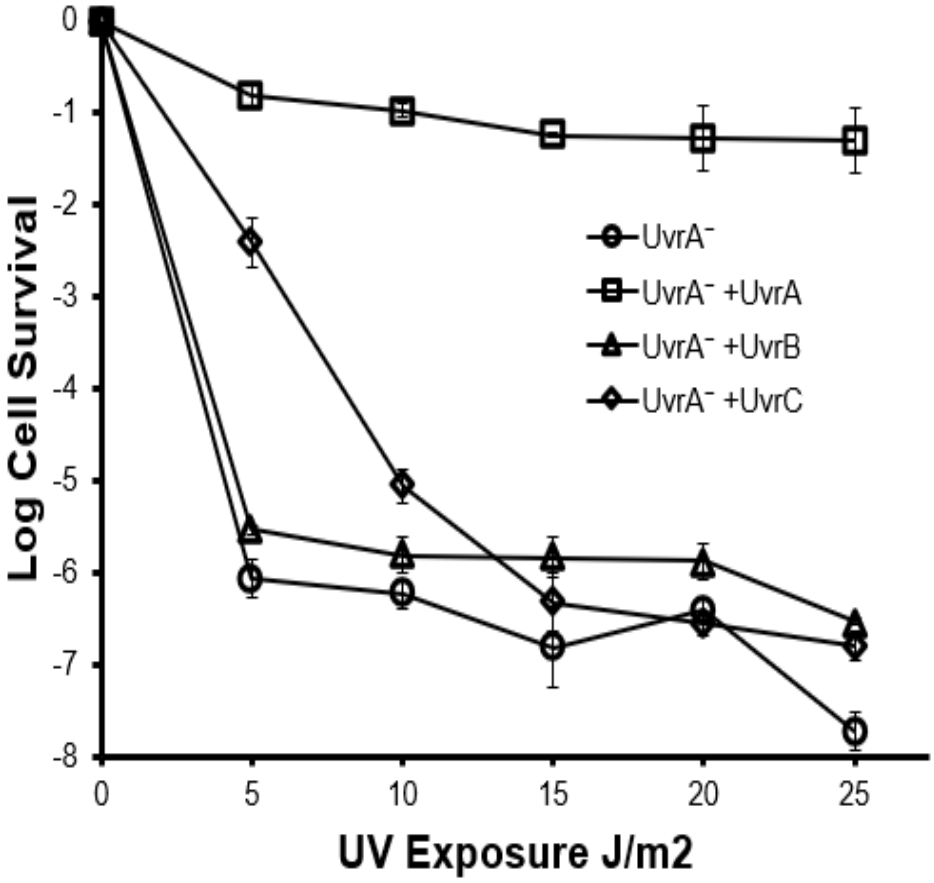

Figure 4.10. Survival of UvrA$^-$ cells exposed to UVC. Quantification of spot plates (figure 4.9) by colony counting. Survival of UvrA$^-$ cells complemented with eGFP tagged NER proteins versus UV dose shows a significant improvement in survival at low UV doses (5-10 J/m^2) for UvrC complemented cells. Cell survival is shown in logarithm units and error bars indicate standard deviation.

4.4 Discussion

To investigate the *in vivo* role of the UvrBC complex we used a UvrA$^-$ cell line and C-terminally e-GFP tagged UvrB and UvrC as these had no effect on cellular NER function. First, we observed the fluorescently tagged proteins in a cellular environment with a full NER background. The genome association of UvrB without damage is low in comparison to UvrC in both UvrA$^+$ and UvrA$^-$, though it is significantly lower in UvrA$^-$. This is likely due to the binding capabilities of UvrB. UvrB is unable to bind DNA without a partner (Kacinski and Rupp, 1981; Kad *et al.*, 2010; Hughes *et al.*, 2013). Under the UvrA$^-$ conditions, UvrB is limited by other *in vivo* binding partners. This observation is supported by other recent *in vivo* imaging which revealed UvrB likely finds UvrA bound to lesions (Stracy *et al.*, 2016). These data also support the catalytic loading of UvrB via UvrA. We observe two significant increases in the number of static molecules when increasing the UV dose suggesting UvrA is able to deposit multiple UvrBs to accommodate a larger number of lesions on DNA (Orren and Sancar, 1989; Stracy *et al.*, 2016). UvrC without UV shows higher genome association than UvrB without UV. This is likely because UvrC can readily bind and scan DNA without a partner, a larger population will be observed as static in our imaging time frame (Hughes *et al.*, 2013).Interestingly at, 25 J/m^2, UvrA$^+$ and UvrA$^-$ with UvrC have the same percentage of cells showing static populations. This data is in agreement with other single molecule studies which show UvrC is likely always in

complex with UvrB. In this model the lack of UvrA would not change the rate at which UvrC is brought to genomic lesions.

4.4.1 UvrA is not necessary for DNA damage binding of UvrB/C

Previous bulk phase studies indicated UvrB and UvrC form a complex in solution and in the previous chapter we demonstrated this complex is able to bind to damage on double stranded DNA (Zou *et al.*, 1997; Moolenaar, Bazuine, *et al.*, 1998; Hughes *et al.*, 2013). The proteins interact via the C-terminal domain of UvrB and homologous region in UvrC, UvrBC is the likely *in vivo* form of UvrC (Hsu *et al.*, 1995; Moolenaar *et al.*, 1995; Sohi *et al.*, 2000; Hughes *et al.*, 2013; Wirth *et al.*, 2016). However, this complex was shown to be incapable of binding damaged duplex DNA unless pre-processed with either a 3′ incision or a bubble around the damage (Zou *et al.*, 1997; Moolenaar, Bazuine, *et al.*, 1998). Consequently, we were surprised to see a slight increase of UvrB-eGFP binding to DNA in response to 5 J/m^2 UV exposure in cells lacking UvrA. With, at the highest estimate, 400 copies of endogenous UvrB per cell increasing to 2000 following SOS response ((Sancar, Clarke, *et al.*, 1981; Crowley and Hanawalt, 1998)) the levels far exceed those of endogenous UvrC (10), which is not SOS induced (Yoakum and Grossman, 1981). Therefore, if the ectopically expressed UvrB-eGFP is loaded by endogenous UvrC in response to UV, this explains the small but significant response. Increasing the UV damage to 25 J/m^2 did not result

in a higher genome association of UvrB-eGFP. These data further suggest, along with the $UvrA^+$ data, that UvrC does not have the capacity to, catalytically, load multiple UvrB molecules at different damage sites, unlike UvrA (Orren and Sancar, 1989; Stracy *et al.*, 2016). It is possible that UvrB is brought to the lesions via UvrD interacting with RNAP via TCR. In this pathway UvrD exposes DNA lesions covered by stalled RNAP, direct interactions between UvrB and the C-terminal domain of UvrD would initiate subsequent DNA unwinding (Ahn, 2000; Manelyte *et al.*, 2009; Epshtein *et al.*, 2014). By measuring their peak fluorescence intensity at 509 nm (figure 4.8) we were able to determine the relative quantities of eGFP. Using UvrC-eGFP as a control the absorption of UvrB was 7.5 times higher equivalent to 1400 molecules of UvrB. At 5 J/m^2 we observe slightly increased survival with the UvrB complemented cells. This is likely due to improved damage detection as there is 1.5 times higher UvrB than post SOS response levels. At 10 J/m^2 we see no improvement compared to the UvrA null cells as the repair mechanism would still be limited by the 10 copies of UvrC.

4.4.2 Ectopic UvrC-eGFP improves cell $UvrA^-$ cell survival

We estimate that 183 molecules of UvrC-eGFP are expressed per cell from our ectopic constructs (figure 4.7 D). It should be noted this is likely an underestimate as not all eGFP will be correctly folded at the time of imaging, as much as 20% of the fluorescent protein may be in a non-fluorescent state (Garcia-Parajo *et al.*, 2001; Ulbrich and Isacoff, 2007; Jain *et al.*, 2011). At 5 J/m^2 we see an increase in cell survival in the $UvrA^-$

complemented with UvrC-eGFP. 5 J/m^2 of UV damage is estimated to generate 120 CPDs per *E. coli* genome (Setlow and Carrier, 1966; Jiang *et al.*, 2007; Kad and Van Houten, 2012). Therefore, the additional 180 UvrC molecules, with the native UvrC, would not be saturated at 5 J/m^2 revealing that the number of UvrBC complexes in our experiments would be able to locate these lesions. This is consistent with the observed severe and UV dose-dependent DNA association of UvrC-eGFP *in vivo*, as UvrB binds UvrC and loads onto the genome. Furthermore, as discussed earlier if Mfd or UvrD was capable of bringing UvrB to lesions independently from UvrA, the UvrC in complex with UvrB would still be overwhelmed by the damage levels and fail to improves cell survival. At 15 J/m^2, and higher, UvrC complemented cells showed no significant difference in survival from UvrB-complemented cells or UvrA-null cells. This clearly demonstrates that UvrA is essential for survival even with additional UvrC present. The improved survivability conferred by UvrC is only significant at low to moderate UV doses. There is no evidence to date that suggests UvrBC alone is capable of excising damage. Therefore, this complex will likely interact with the numerous UvrB-binding proteins *in vivo*. During normal TCR Mfd recruits UvrA to, and displaces, stalled RNAP on DNA lesions, however UvrA is not essential for lesion detection (Selby and Sancar, 1993; Manelyte *et al.*, 2010). UvrD has been conclusively shown to expose DNA lesions covered by stalled RNAP (Epshtein *et al.*, 2014). Mfd (Assenmacher *et al.*, 2006; Deaconescu *et al.*, 2006, 2012) and UvrD (Ahn, 2000; Manelyte *et al.*, 2009) are both capable of interacting with UvrB, the UvrBC complex may directly facilitate

DNA repair via these pathways, in our experiments, independently from UvrA. Recent live cell imaging showed than in UvrA$^-$ cells mfd-RNAP complexes dissociate from each other more slowly than when UvrA is present, providing a route for UvBC interaction in our experiments (Ho, Van Oijen and Ghodke, 2018). Finally UvrBC could interact with photolyase, which is known to stimulate NER in response to pyrimidine dimers, but these early experiments included UvrA (Warm and Hillebrandt, 1962; Sancar, Franklin and Sancar, 1984; Yamamoto, Satake and Shinagawa, 1984). In cells with full NER machinery damage repair is attempted before the energetically expensive SOS response is initiated. Furthermore, in *in vitro* assays, the Uvr proteins have been shown to incise undamaged DNA at surprising high rates (Branum, Reardon and Sancar, 2001). Staggeringly, the rate of nucleotide excision repair on undamaged DNA, measured as nucleotide turnover, was calculated to be comparable to base excision repair acting on spontaneous DNA lesions (Holmquist, 1998; Kunkel and Bebenek, 2000). This unforeseen mechanism could be an important resource for spontaneous mutations (Branum, Reardon and Sancar, 2001). This has been seen before in 'undamaged' DNA substrates but these studies used modified, processed, DNA structures and the oligonucleotides were not released by dual incision in one strand, indicative of NER (Van Houten and Sancar, 1987; Caron and Grossman, 1988; Gordienko and Rupp, 1997; Moolenaar, Bazuine, *et al.*, 1998). However, the Sancar lab showed conclusively that undamaged DNA could be incised by the UvrABC system (Branum, Reardon and Sancar, 2001). UvrBC could help to repair lesions and

inadvertently hold back the SOS response, by clearing low level damage, until the lesions overwhelm this repair response and the risk of deleterious incision and resulting mutagenesis is minimal in comparison to the relative rates of genomic lesions. As such UvrBC could act as an energetically inexpensive, less deleterious route for lesion repair before UvrA, UvrB and UvrD are dramatically upregulated.

4.5 Conclusion

In this chapter we confirm our single molecule data from the previous chapter. We now show UvrBC can bind to *in vitro* fluorescein and *in vivo* cyclobutane pyrimidine dimers. Induction of the SOS response has been shown to have no effect on 6-4 photoproducts in UV irradiated *E. coli*, but does increase the efficiency at which CPDs are removed (Crowley and Hanawalt, 1998). Since CPDs account for 75% of the DNA lesions from UV radiation (Kim, Patel and Choi, 1995; Douki and Cadet, 2001; Sinha and Häder, 2002; Li *et al.*, 2006) and we imaged cells after allowing for SOS response prior to imaging (Crowley and Hanawalt, 1998; Smith, Grossman and Walker, 2002) (**4.2.2**) we can be confident UvrBC has a direct role in CPD processing. We used live cell imaging to show fluorescently tagged UvrB and UvrC could respond to UV damage *in vivo* independently from UvrA. We confirm recent single molecule (Stracy *et al.*, 2016) and pioneering bulk data that UvrA can catalytically load UvrB to DNA lesion (Orren and Sancar, 1989), a function not shared with UvrC. Finally, remarkably, we show that the ectopically expressed UvrC

increases cell survival of the UvrA$^-$ strain. These data suggest UvrBC is likely involved in an unrealised DNA repair pathway, likely via the promiscuous nature of UvrB, that processes low levels of damage pre-SOS response.

Chapter 5: Single molecule analysis of XPD and p44

5.1 Introduction

Initial lesion detection is similar in eukaryotic and prokaryotic NER, XPC manipulates the DNA distorting the double helix, this enables direct lesion interrogation (Bunick *et al.*, 2006; Mocquet *et al.*, 2007; Sugasawa *et al.*, 2009; Clement *et al.*, 2010; Puumalainen *et al.*, 2016). Rad23 can help to stabilize this XPC lesion complex (Araki *et al.*, 2001; Xie *et al.*, 2004). UV-DDB can aid in lesion by promoting ubiquitination of XPC (Keeney, Chang and Linn, 1993; Takao *et al.*, 1993; Fitch *et al.*, 2003; Xie *et al.*, 2004; Fei *et al.*, 2011). This modification help XPC to recruit the rest of TFIIH (Araújo, Nigg and Wood, 2001; Gillette *et al.*, 2006; Bernardes de Jesus *et al.*, 2008).

The TFIIH complex likely forms a ring-like structure with a central space allowing both XPD and XPB to simultaneously interact with DNA (Chang and Kornberg, 2000; Schultz *et al.*, 2000; Greber *et al.*, 2017; Schilbach *et al.*, 2017).

XPD links the TFIIH complex. The core complex, XPB, p62, p52, p44, p34 and p8 have a dynamic interaction with the CAK complex, which is composed of CDK7, cyclin H and MAT1 (Tirode *et al.*, 1999; Chang and Kornberg, 2000; Schultz *et al.*, 2000; Gibbons *et al.*, 2012; Greber *et al.*, 2017; Schilbach *et al.*, 2017). TFIIH binds stably to the damage by the ATPase activity of XPB and its binding partners,p52 and p8 (Compe and

Egly, 2012; Abdulrahman *et al.*, 2013; Luo *et al.*, 2015; Greber *et al.*, 2017). XPD, directed by p44, unwinds the DNA and exposes the DNA lesion (Compe and Egly, 2012; Abdulrahman *et al.*, 2013; Luo *et al.*, 2015; Greber *et al.*, 2017). Unlike bacterial NER, two proteins perform the dual incision of the DNA lesion (Staresincic *et al.*, 2009). XPF makes the 5' incision, DNA polymerase begins resynthesis using the undamaged DNA strand as a template and XPG makes the 3' incision (O'Donovan *et al.*, 1994; Staresincic *et al.*, 2009; Manandhar, Boulware and Wood, 2015). XPD is a single stranded 5' – 3' helicase containing two motor domains (HD1 and HD2) a 4Fe-S cluster, ARCH domain and C-terminal domain which allows for TFIIH incorporation via p44 (Sung *et al.*, 1993; Lehmann, 2001; Abdulrahman *et al.*, 2013). HD1 and HD2 contain the helicase motifs, HD1 also contains the ARCH domain and FeS cluster (Kuper *et al.*, 2014; Greber *et al.*, 2017). Together the FeS cluster and ARCH domains form a deep groove which interacts with single stranded DNA (figure 5.1) and allows for the DNA to thread through and reach the motor domains (Fan *et al.*, 2008; Liu *et al.*, 2008; Abdulrahman *et al.*, 2013; Greber *et al.*, 2017).

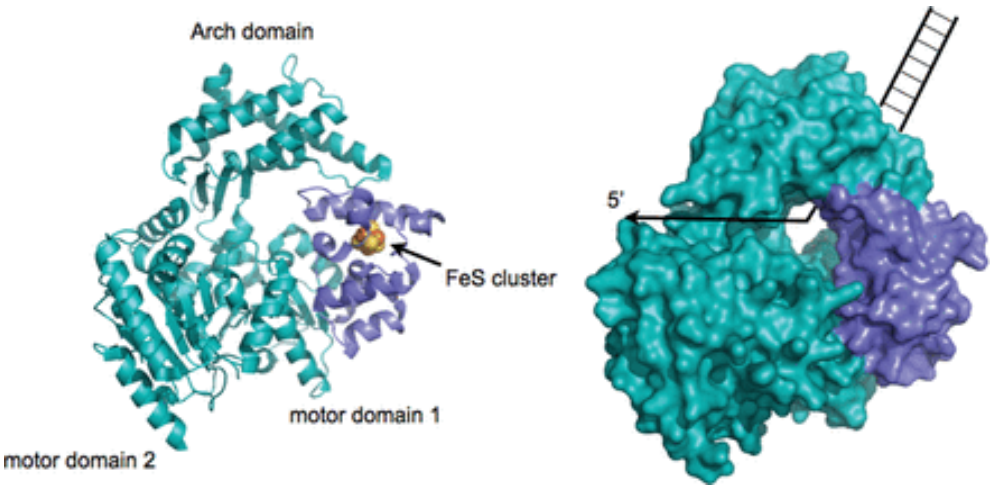

Figure 5.1. Structure of XPD from *Thermoplasma acidophilum*.
Left: cartoon of the XPD structure from *T. acidophilum* with the four major domains labelled. Right: A schematic representation of the likely path of single stranded DNA between a groove created by the Arch domain and FeS cluster.
(Taken from White., 2009)

The helicase motifs are highly conserved the helicase core consisting of two RecA like domains (Singleton, Dillingham and Wigley, 2007), and like other super family 2 helicases, couple ATP hydrolysis to DNA translocation (Dillingham, Wigley and Webb, 2000; Singleton and Wigley, 2002; Liu *et al.*, 2008). Disrupting the FeS cluster in HD1 results in loss of helicase activity but does not affect ATP hydrolysis (Rudolf *et al.*, 2006; Pugh *et al.*, 2008). This FeS mediates single stranded DNA translocation through the coupling of ATP hydrolysis to translocation (Pugh *et al.*, 2008). The C-terminal domain binds directly to the N-terminal domain of p44, XPD (Kim *et al.*, 2015). XPD exhibits low ATPase and helicase

activity without p44, this interaction directly stimulates the both functions of XPD (Schmitt *et al.*, 2014). The binding partner of XPD, p44, is usually considered in partnership with XPD. This subunit of TFIIH has roles in both NER and transcription (Seroz *et al.*, 2000; Dubaele *et al.*, 2003; Kuper *et al.*, 2014). In TFIIH p44 has been shown to bind near HD2 of XPD, cooperating with helicase motifs that couple ATPase and helicase activity (Fairman-Williams, Guenther and Jankowsky, 2010; Kim *et al.*, 2015; Greber *et al.*, 2017).

In this chapter, we examine the proteins' interaction with DNA without its helicase partner, in this state the protein can be transcriptionally active as the helicase activity is not specifically required (Tirode *et al.*, 1999; Coin, Oksenych and Egly, 2007; Kuper *et al.*, 2014). The complex TFIIH structure is stabilized additionally by p44 in tandem with two other poorly understood subunits, p43 and p62 (Tirode *et al.*, 1999; Tremeau-Bravard, Perez and Egly, 2001; Kellenberger *et al.*, 2005; Schmitt *et al.*, 2014; Radu *et al.*, 2017). ATP hydrolysis has been heavily linked to single stranded DNA translocation (Singleton and Wigley, 2002; Liu *et al.*, 2008; Pugh *et al.*, 2008) and other similar XPD family helicases in an analogous way, such as XPDs closest bacterial homologue DinG and PcrA, (Dillingham, Wigley and Webb, 2000; White, 2009; Cheng and Wigley, 2018) but the link with double stranded DNA remains unclear. In this chapter we show a direct link between ATP hydrolysis and double stranded DNA translocation. Using single molecule fluorescence imaging of Qdot labelled XPD and p44 independently on DNA tightropes, we have examined how the proteins interact with double stranded DNA. We find

that both XPD and p44 readily bind and diffuse one-dimensionally along double stranded DNA, though both have a preference for single stranded regions. We have begun to examine the single molecule kinetics of XPD in relationship to ATP. Using a series of XPD mutants and nucleotide conditions we find that ATP hydrolysis rather than ATP binding directs DNA translocation and increasing ATP concentration reduces the lifetime of pauses XPD shows while moving along DNA. As expected, ATP does not affect p44 interaction with DNA. For the first time we show that XPD can recognise damage incorporated into our DNA tightropes.

5.2 Materials and methods

5.2.1 Standard conditions

Unless otherwise stated all experimental procedures in this section were performed at room temperature in XPD buffer (20 mM Tris (pH 8), 10 mM KCl, 5 mM $MgCl_2$ and 1 mM EDTA). 2 mM of ATP or ADP was added as indicated.

5.2.2 DNA tightrope constructs

Damaged tightrope constructs are described in more detail in Chapter 2.3.2 and Chapter3.

5.2.2.1 Single stranded patches

Single stranded patches were created through the ligation of two oligonucleotides to the ends of lambda DNA, and a second ligation to join these constructs. The first ‘long’ primer 5’GGGCGGCGACCT**GCGTGATCTTTGCCTTGCGACAGACTTCCTTGG CT**GGGCGGGCTGGC3’ ligates to one cos end of lambda DNA. We ligated the shorter oligonucleotide, 5’AGGTCGCCGCCCGCCAGCCCGCCC(TEG-bio)3’ to another cos end of lambda. Ligation of these constructs produces a 35 base single stranded region figure 5.3 The addition of streptavidin coated Qdots to the tightropes allows localization of the single stranded region in the same way as the damaged DNA construct.

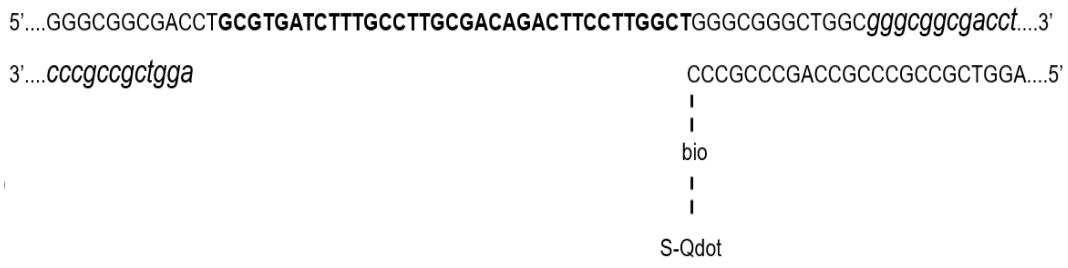

Figure 5.2. Schematic of the construction of a 35 base single stranded patch (bold) using oligonucleotides (capitals) via the cos end of lambda (italics).
Bio represents the biotin conjugated via TEG which can be visualised via streptavidin conjugated Qdots (S-Qdot).

5.2.3 Single Molecule Fluorescence Imaging

XPD and mutant variant were was purified as described previously (Kuper *et al.*, 2014). The proteins were fluorescently labelled as described in Chapter 2.6, labelling has no effect on protein activity (described below). Briefly, XPD-Qdot conjugates were prepared by incubating His tagged XPD (100 nM) Anti-His monoclonal mouse antibody for 20 minutes in XPD buffer. To ensure proteins were labelled with a single Qdot a 4:1 excess of Qdots was used, (Wang *et al.*, 2008). Anti-mouse IgG-conjugated Qdots were incubated for 30 minutes and dilution to 1 nM for imaging.

An NADH-linked ATPase assay was used to examine if labelling affected protein function (Barnett and Kad, 2018). XPD buffer supplemented with 0.5 mM phosphoenol pyruvate solution was stored at 220°C; 1 mM DTT was added upon thawing. Solution was blanked at 340 nm in a spectrophotometer. 10 ml of pyruvate kinase (1000 U/ml) and lactate dehydrogenase 1400 U/ml, premixed stock from MilliporeSigma) per 500 ul reaction were added to a cuvette with 210mM NADH. 50 ng of single stranded DNA (5'GACTACGTACTGTTACGGCTCCATCCTACCGCAATCAGGCCAGATCTGC-3') and 100 nM of protein were used. The change in OD340 was fitted linearly to calculate loss of NADH ($6220 M^{-1} cm^{-1}$ at 340 nm), enabling calculation of kcat. As seen in figure 5.3 labelling has no effect on the ATP activity of XPD or XPD/p44 complexes.

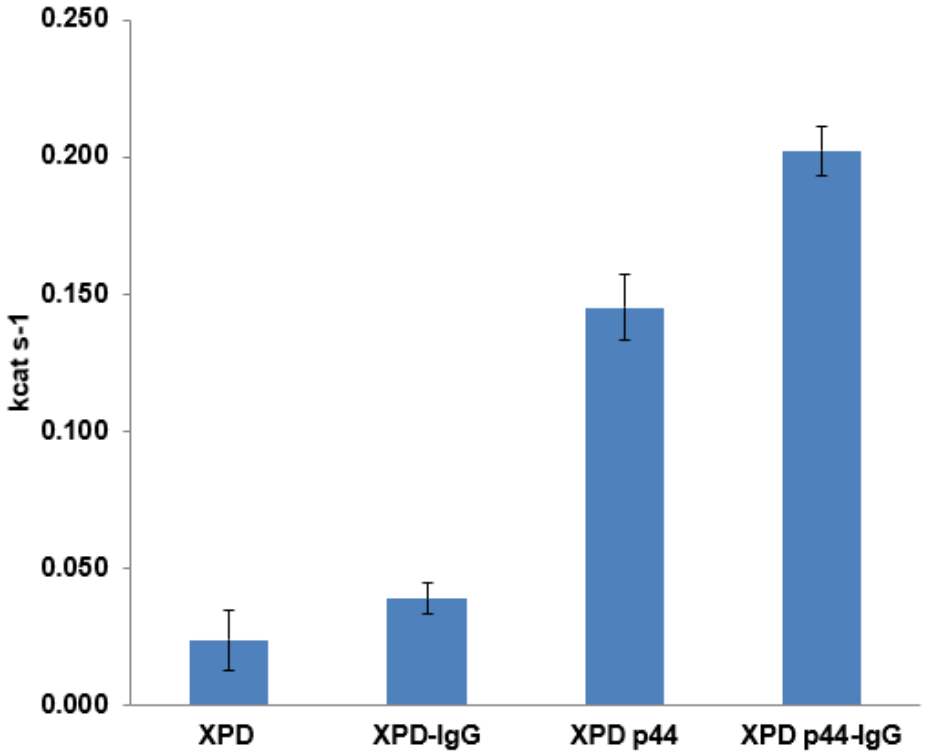

Figure 5.3. XPD ATPase effect of labelling with IgG antibody.
Values for k_{cat} s^{-1} reactions, repeated twice, and the error represents the SD were 0.024 (±0.01), 0.039% (±0.01) and 0.145 (±0.01) 0.202 (±0.01) for XPD, labelled XPD, XPD/p44 and XPD/p44 labelled respectively.

5.2.4 Calculations

The lifetime of attachment of proteins can be gathered from the length of the streak generated from a kymograph, see Chapter 2.12.2 for more detail. Streaks that started and ended in the movie were analyzed only, as streaks that did not start or end during the movie would give inaccurate lifetime values.

These data were plotted as cumulative frequency (CF) histograms and fitted to:

Equation 1: $CF = N(1-e^{(-k.t)})/(1-e^{(-k.t_{max})})$

where N is the number of observed points, t is the bin, t_{max} the maximum bin size and k the reciprocal of the dwell time.

$$\mathrm{MSD}(n\Delta t) = \frac{1}{N-n}\sum_{i=1}^{N-n}\left[(x_{i+n}-x_i)^2+(y_{i+n}-y_i)^2\right]$$

Equation 2 from Chapter 2
N is the total number of fames in the kymograph from the image taken, n the is the frame, x_i and y_i the position of the protein, in one dimension along the tightrope and Δt the time window.

This equation is described in detail in Chapter 2.12.3. Briefly, MSDs were fitted to a straight line when the r^2 value of the fit dropped <0.7, no more data was used. The slope of this linear plot provides the diffusion constant. By replotting the MSD on log-log axis we were able to determine the mechanisms of motion, the slope of this plot defined 'α', the diffusive exponent (Berg, Winter and Von Hippel, 1981; Hughes *et al.*, 2013; Springall, Inchingolo and Kad, 2016).

Unless otherwise stated, 'n' refers to the number of flow chambers or agarose pads used per experiment. Significance was determined using the Student's *t*-test and consequent *P*-values are reported if two values are compared.

If multiple means are compared analysis of variance (ANOVA) was performed with a post hoc test, including a Bonferroni correction to consider multiple comparisons, shdsjd subsequent *p*-values are reported.

5.3 Results

5.3.1 XPD can translocate along dsDNA

To understand how XPD interacts with double stranded DNA we constructed DNA tightropes. This involves suspending single strands of DNA between glass beads inside a manually constructed flow chamber to allow us to control the environmental conditions. These DNA tightropes allow single molecule florescence imaging of the interaction between single proteins and single strands of DNA, in real time, without interference from surface bound protein or DNA. XPD readily bound to DNA tightropes under a variety of nucleotide conditions, though a higher level of tightrope decoration observed was under the 2mM ATP conditions (+ ATP). The interaction between XPD and double stranded DNA is heavily affected by the nucleotide conditions. Protein motility was defined as fluorophore movement of three pixels (figure 5.4) over three frames from the previous position (Kad *et al.*, 2010; Dunn *et al.*, 2011; Hughes *et al.*, 2013; Barnett and Kad, 2018) In the presence of ATP 43% (±5.1% SEM; *n*= 3) of 130 XPD imaged were motile (figure 5.6). Under these conditions motile and static XPD had a lifetime of 20.6 seconds (±4.1, *n* = 3). In the absence of nucleotide XPD behaved very differently. Only 8.2% (±1.1% SEM; *n*= 4) of 102 XPD without nucleotide were motile and had a lifetime on double stranded DNA of 8.32s (±1.1, *n* = 3). XPD in the presence of ADP exhibited similar behaviour. 10.0% (±2.1% SEM; *n*= 4)

of 81 XPD were motile in the presence of 2mM ADP, statistically similar to the no nucleotide condition (p = 0.0.19). Similarly, under these conditions the lifetime on DNA was comparable (figure 5.6) (10s (±2.3, *n* = 3)).

Due to the low motility of XPD without ATP we only examined the diffusion constant of the protein with 2 mM ATP. In the presence of ATP XPD had a diffusion constant of 13.33 x10 $^{-3}$ $\mu m^2 s^{-1}$ and a diffusive exponent of 0.79 suggesting unbiased random diffusion (figure 5.4). These data suggest that ATP is required for translocation of XPD along double stranded DNA. Without ATP the protein binds less to DNA, is less motile and has a reduced lifetime on DNA. We were unable to examine the effect of salt on the diffusive exponent, an indicator of the nature of protein movement, as increasing the salt concentration severely disrupted DNA binding so that the number of XPD interactions with DNA was low so imaging was unsuccessful (Berg, Winter and Von Hippel, 1981; Von Hippel and Berg, 1989; Tafvizi *et al.*, 2008).

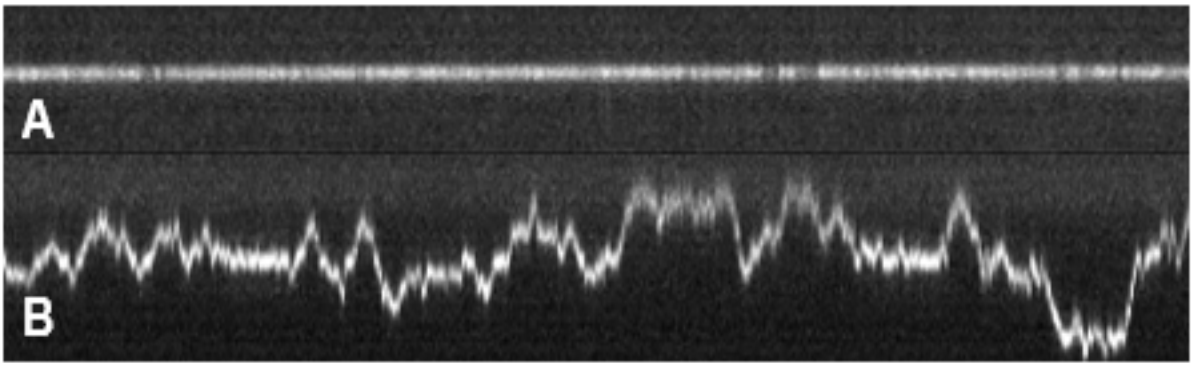

Figure 5.4. Example interaction of XPD and DNA tightropes (A) A static XPD showing no motility on a DNA tightrope **(B)** An example of random unbiased diffusion.

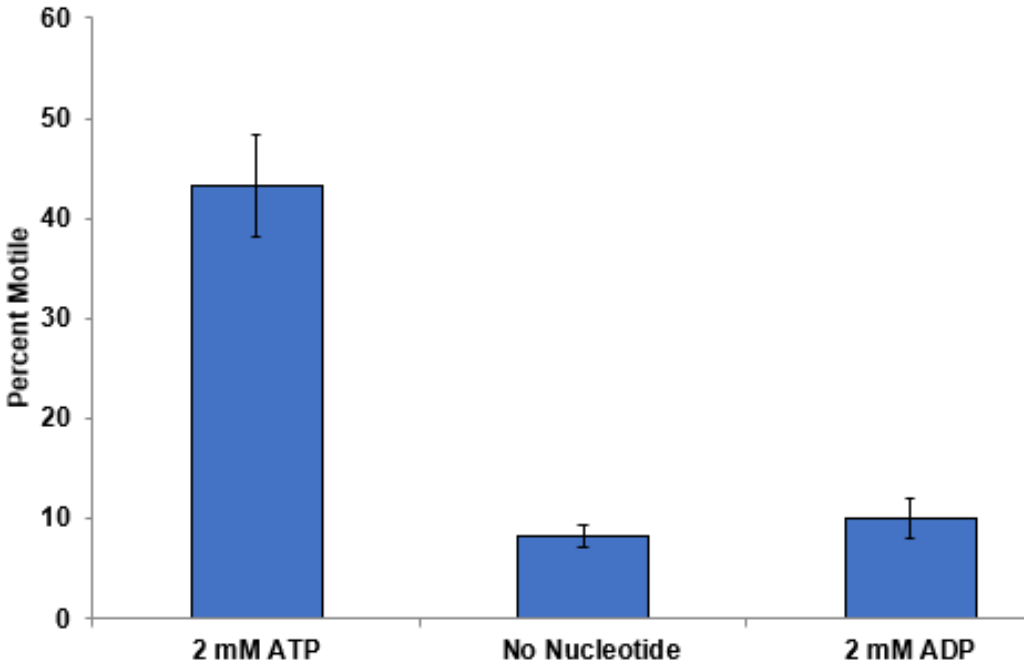

Figure 5.5 Motile properties of XPD at differing nucleotide conditions. Values for mean percentage (±SE, where *n* refers to repeated experiments) motile were 43.3% (±5.1, *n* = 3), 8.2% (±1.1, *n* = 4) and 10.0% (±2.1, *n* = 4) for 2 mM ATP, no nucleotide and 2 mM ADP respectively.

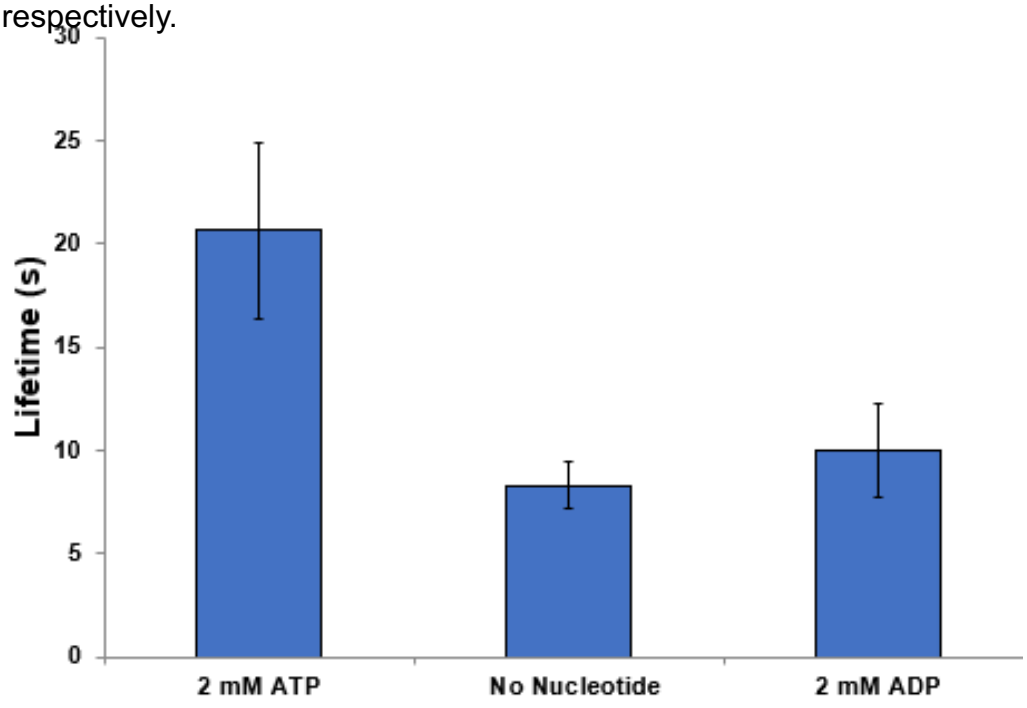

Figure 5.6. Lifetime of XPD on DNA tightropes at differing nucleotide conditions.
Linear streaks were compiled into cumulative frequency histogram, values for lifetime (where *n* refers to repeated experiments)
were 20.64s (±4.1, *n* = 3), 8.32s (±1.1, *n* = 3) and 10.02s (±2.3, *n* = 3) for 2 mM ATP, no nucleotide and 2 mM ADP respectively.

5.3.2 XPD mutants are not motile on DNA

To understand the nature of the interaction between XPD and DNA we used three mutations summarised in Table 5.1**,** all mutants were imaged with 2 mM ATP so as to be comparable to normal XPD function. N-terminal domain mutants were chosen as they are highly important for archaeal XPD function (Sandrock and Egly, 2001; Rudolf *et al.*, 2006; Liu *et al.*, 2008; Kuper *et al.*, 2012, 2014; Pugh, Wu and Spies, 2012). R195E, a helicase domain 1 mutant, had been previously shown to be unable to bind to DNA (data not shown) and was not used further in this study.

Table 5.1. Functional effects of XPD mutations, adapted from (Kuper et al., 2014).

XPD Mutant	Functional Effects						
	ssDNA binding	ATPase	Helicase	Transcription	NER	dsDNA binding	Motile on dsDNA
K719W	+	-	-	-	-	+	-
K48R	+	-	-	+	-	+	-
F129A	-	-	-	+	-	+	-

+ denotes activity, - indicates severely impaired activity. Double stranded DNA data from DNA tightrope assay.

K48R mutant disrupts the Walker A motif, in helicase domain one, and therefore ATP hydrolysis but still allows ATP binding (Kuper *et al.*, 2014). F192A is an iron sulphur cluster mutant which affects ATP hydrolysis-mediated helicase translocation on single stranded DNA, not ATP binding (Rudolf *et al.*, 2006; Singleton, Dillingham and Wigley, 2007; Liu *et al.*, 2008; Kuper *et al.*, 2012, 2014). These two constructs both bind, but are unable to hydrolyse ATP and have similar functional effects but differ in their ability to bind ssDNA (Table 5.1) (Kuper *et al.*, 2014). Therefore, we

sought to examine if they could bind double stranded DNA and examine if the motile state of XPD has ATP bound or ADP.Pi state. The K48R and F192A constructs showed similar motile properties to wild type XPD in the absence of ATP. 6.2% (±1.1% SEM; *n*= 3) of 89 K48R and 8.1% (±1.6% SEM; *n*= 3) of 105 F192A examined were motile in the presence of 2mM ATP (figure 5.7). These mutants suggest, along with the nucleotide data, that ATP binding does not activate motility but the ADP.Pi state is motile state. The final mutant examined, K719W, is unable to bind to p44, abolishing the interaction in helicase domain 2 (Kuper *et al.*, 2014). We were surprised this protein behaved in a similar way to the other mutants. 5.4% (±3.3% SEM; *n*= 3) of 96 K719W molecules were motile, statistically similar to the mutants and the no nucleotide condition of wild type XPD ($p > 0.3$). ATP binding and hydrolysing residues were not directly affected on this construct and we expected the mutant to exhibit similar properties to the wild type on double stranded DNA. All three mutants had lifetimes on double stranded DNA statistically identical to no nucleotide and 2 mM ADP wild type XPD ($p > 0.1$) confirming ATP binding is not the key step in DNA translocation (figure 5.8).

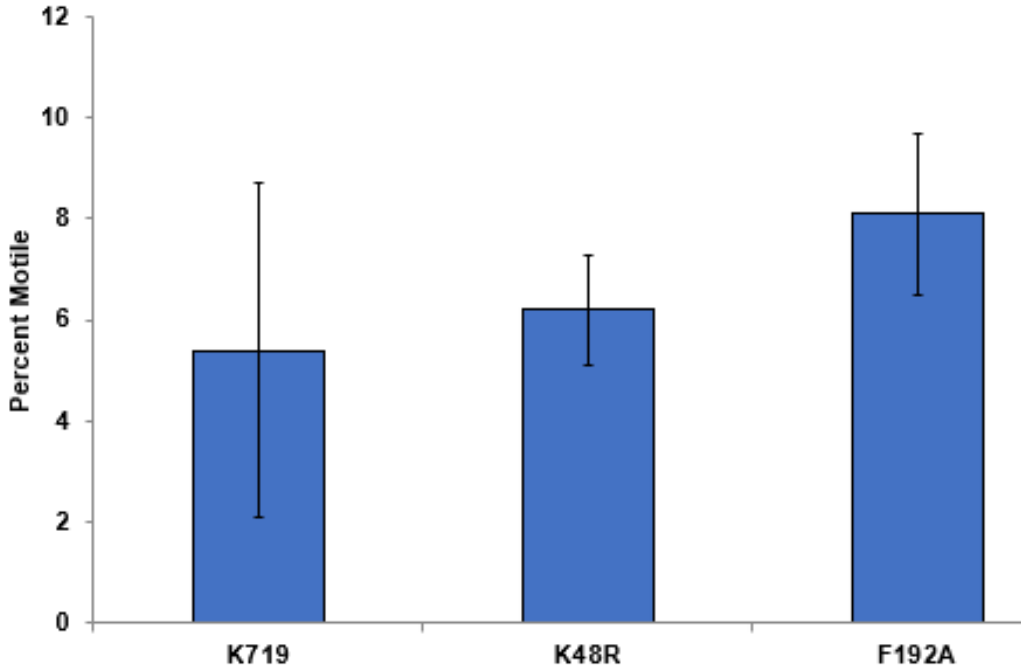

Figure 5.9. Motile properties of XPD mutants.
Values for mean percentage (±SE, where *n* refers to repeated experiments) motile were 5.4% (±3.3, *n* = 3), 6.2% (±1.1, *n* = 3) and 8.1% (±1.6, *n* = 3) for K719W, K48R and F192A respectively. All mutants examined with 2 mM ATP.

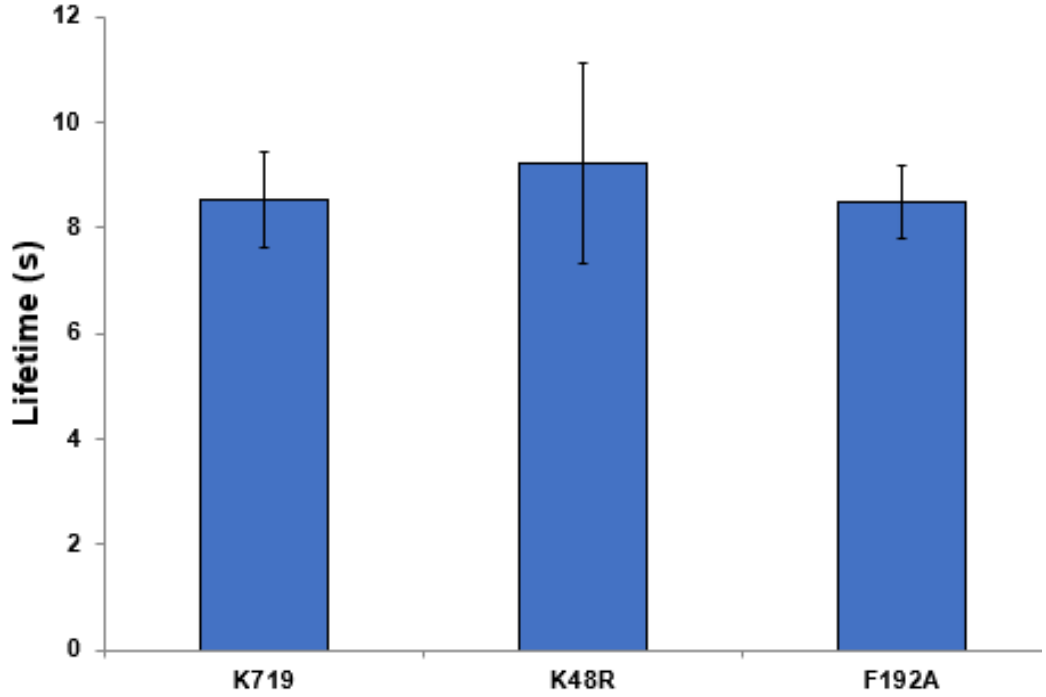

Figure 5.10. Lifetime of XPD on DNA tightropes at differing nucleotide conditions.
Linear streaks were compiled into cumulative frequency histogram, values for lifetime (where *n* refers to repeated experiments)
were 8.54s (±.9, *n* = 3), 9.22s (±1.9, *n* = 4) and 8.50s (±0.7, *n* = 4), for K719W, K48R and F192A respectively. All mutants examined with 2 mM ATP.

To confirm the motile state of XPD was ADP.Pi a pervious student used the transition state analogue, vanadate. Vanadate was used to trap XPD in the post-hydrolysis transition to Pi release. Vanadate traps ADP into nucleotide-binding sites by mimicking the transition state of the γ-phosphate of ATP during ATP hydrolysis (Smith, Zinn and Cantley, 1980; Urbatsch *et al.*, 1995; Kerr, Sauna and Ambudkar, 2001; Loo and Clarke, 2002). ADP-bound XPD were incubated with vanadate and found to have a higher motility on double stranded DNA than 2mM ATP. 73% (±14.0, *n* = 5) of 89 XPD imaged were motile however, when comparing this data with 2 mM ATP, the increase was not statistically different from 2mM ATP (P = 0.1697) (figure 5.9) but does further support the mutant and nucleotide data that show the ADP.PI state is the motile state of XPD.

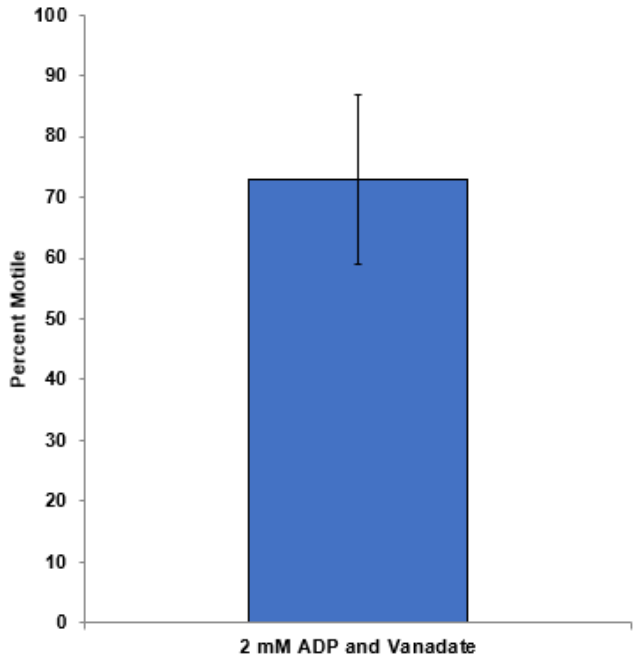

Figure 5.9. Motile properties of XPD with vanadate and ADP.
Values for mean percentage (±SE, where *n* refers to repeated experiments) motile were 73% (±14.0, *n* = 5)

5.3.3 Pause length increases when ATP concentration reduces

Without nucleotide the percentage of motile XPD molecules was drastically reduced from 43% to 8.2%. As we observed this difference in motility, we decided to investigate whether we could image a switch in the states between motile and static XPD. Using five concentrations of ATP we found that decreasing the concentration of ATP resulted in longer pauses during translocation of DNA (figure 5.11). Originally, we tried to extract the lifetime of the pause data using a sliding box method, where an average diffusion constant and diffusive exponent is calculated for a number of molecules and compared with a previous average to detect changes that would be associated with pauses. This method did not extract the pauses that could be seen when examining kymographs. Next, we took the kymograph of a static molecule and used two standard deviations from the middle of the streak as a threshold for whether to mark a molecule as changed from motile state to a paused state. If the value was two standard deviations or more, the protein was considered paused. This method was better but we were still unsatisfied that this number was pulling out all the pauses. As such we used twice the standard deviation as a baseline, from there we referred back to the kymographs generated to extract as many pauses that could be seen by the eye (figure 5.10). The data from the pauses was put into a histogram that resulted in a single distribution that was fitted to a single exponential as the frequency of pause length decreased. The reciprocal of the rate constant is equal to the pause length at each concentration of ATP. At the

lowest concentration of ATP, 0.2 μm, the protein would diffuse along the DNA but with many pauses in its behaviour with an average pause length of 9.1 seconds (figure 5.11). At ATP saturation, 2 mM ATP, the pause length was reduced greatly to 1 second and very few pauses were seen in the kymographs. This data, along with the mutant and nucleotide conditions data, confirm ATP binding is not rate limiting at saturated condition, in XPDs double stranded DNA translocation.

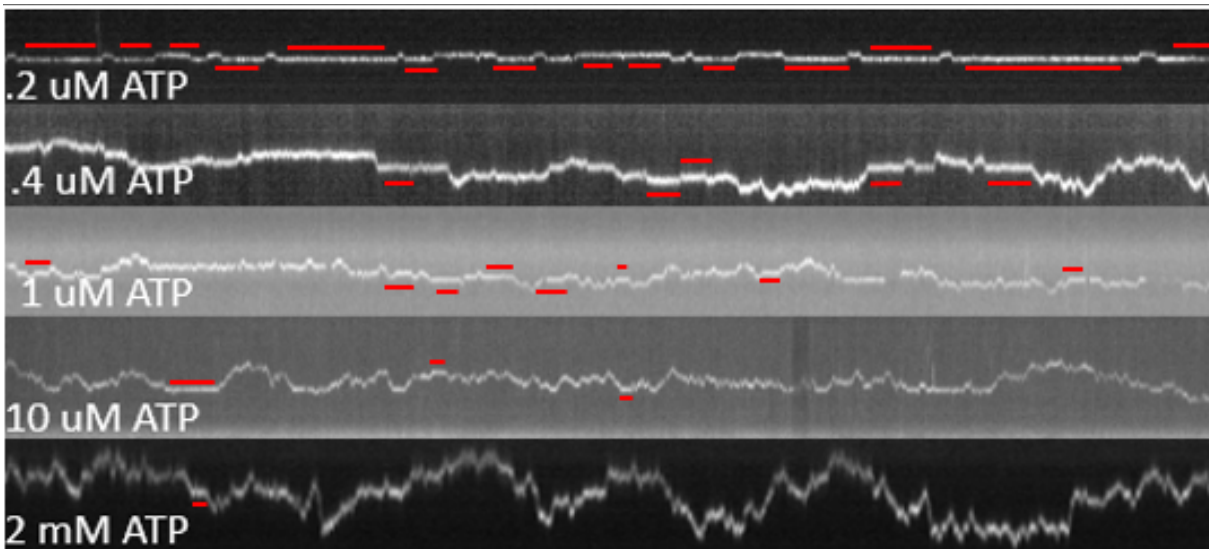

Figure 5.10. Increasing ATP concentration reduces lifetime of pauses during DNA translocation

Representative kymographs at variable ATP concentrations, red lines highlight pauses in translocation.

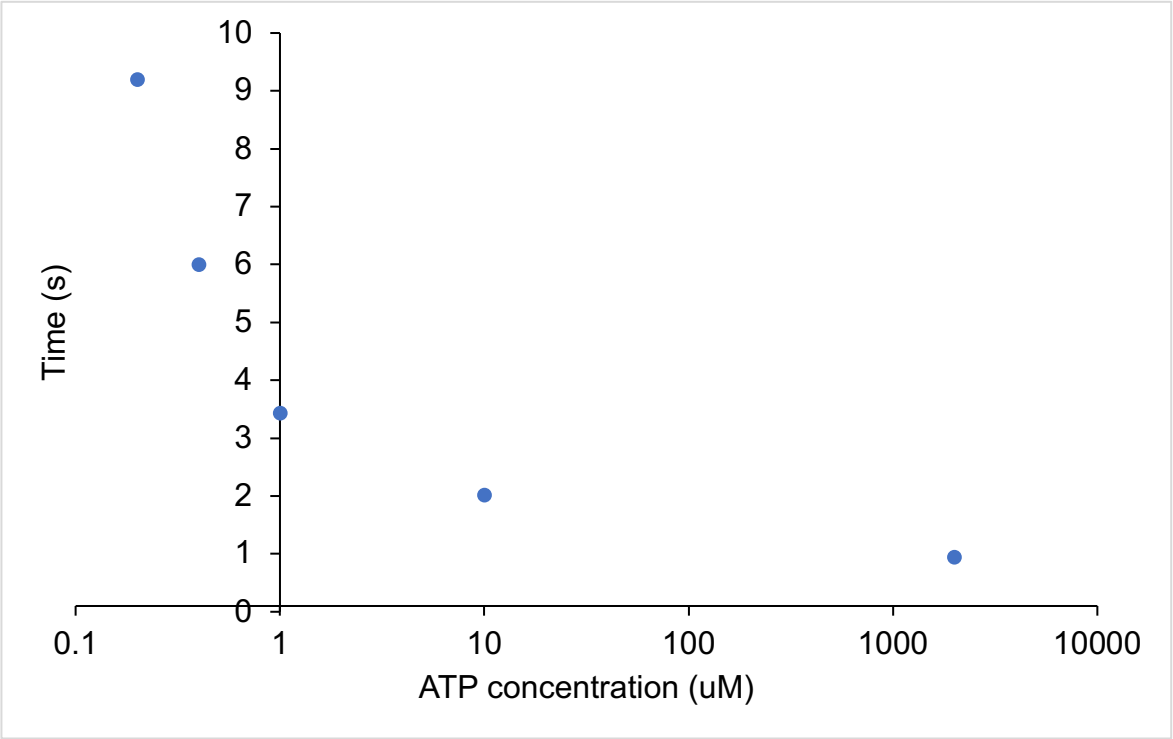

Figure 5.11. Pause length at variable ATP concentrations.
Values for length of pause are 9.2s, 6s, 3.4s, 2s and 0.9s for 0.2 uM, 0.4 uM, 1 uM, 10 uM and 2000 uM ATP respectively.

5.3.4 XPD preferentially binds single stranded regions and damage

XPD has been shown to bind both single and double stranded DNA, but is usually considered a single stranded DNA translocase (Liu *et al.*, 2008; Mui *et al.*, 2011). After showing that XPD readily binds and shows motility on double stranded DNA we sought to examine if the helicase prefers single stranded patches on double stranded DNA. The deep groove that forms between the FeS cluster and ARCH domain (Fan *et al.*, 2008; Liu *et al.*, 2008; Abdulrahman *et al.*, 2013; Greber *et al.*, 2017) has been shown to bind to at least 25 nucleotides of single stranded DNA (Rudolf *et al.*, 2006; Wolski *et al.*, 2008). Therefore, we introduced a 35-nucleotide single stranded patch into our double stranded DNA tightropes. To

visualise the single stranded patch at the single molecule level we labelled the 3' biotin tagged construct with a Qdot figure 5.2 in a similar way the damage construct in Chapter 3.2.2. These single stranded constructs were then introduced and constructed in a flow cell in the same manner as the undamaged DNA tightropes. As seen in figure 5.13 46.25% (±3.5% *n* = 3) of 80 XPD molecules were bound to the single stranded region, significantly higher than the middle of the tightrope (10% discussed in Chapter 3.3.1 ($p < 0.05$). XPD has been shown to have a preference for damage (Rudolf *et al.*, 2010). As such we used our tightrope damage construct to determine if XPD exhibited this bias on double stranded DNA. 29.49% (±1% *n* = 3) of 78 XPD molecules were bound to the damage construct, significantly higher than the middle of the tightrope.

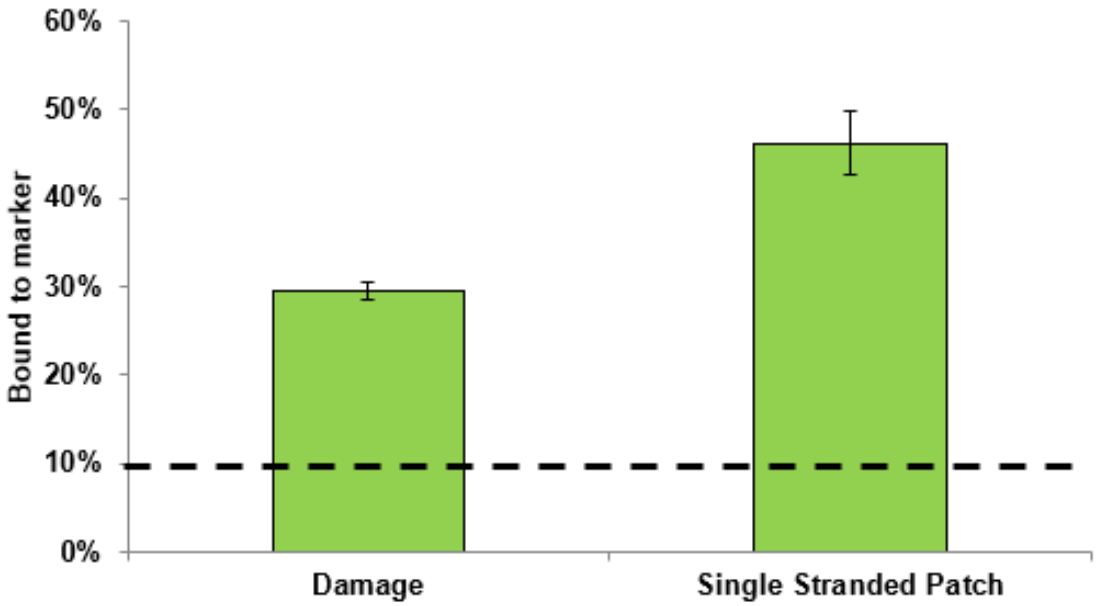

Figure 5.12. Probability of finding XPD colocalized with a construct marker. Values for mean probability percentage (±SEM, where, *n* refers to repeated experiments) bound to damaged DNA were 29.49% (±1.04% *n* = 3) and bound to single stranded patch DNA were 46.25% (±3.54% *n* = 2).
The dashed line represents the probability (10.1%) of random association to damage based upon UvrA-Qdot binding to the mid-point of a DNA tightrope.

5.3.5 Interaction between p44 and dsDNA

As the helicase activity of XPD is heavily regulated by p44 the proteins are often examined together. With this in mind we decided to examine the motile properties of p44 independent of XPD as *in vivo* the NER subunits will not always colocalise and may independently be incorporated into the TFIIH complex. There is evidence that p44, independently from XPD, along with the other TFIIH accessory subunits form a stable core to which the other subunits later bind (Tremeau-Bravard, Perez and Egly, 2001;

Luo *et al.*, 2015; Radu *et al.*, 2017). The p44 used in this study is a construct of residues 1–285, lacking the C-terminal Ring and Zn-finger domains of p44, but is still able to activate the helicase activity of XPD and TFIIH functional (Coin *et al.*, 1998; Compe and Egly, 2012; Kuper *et al.*, 2014). Unsurprisingly ATP had no effect on protein activity, such data from +/- ATP conditions were combined. 56% (±3.4% SEM; *n*= 5) of 110 p44 examined were motile on double stranded DNA, slightly higher than XPD but displayed a lower duration of interaction, both static and motile p44 had a lifetime of 5.66 seconds (±1.1% SEM; *n*= 5) versus 20.6 seconds. These proteins have a diffusion constant of 17.6 x10 $^{-3}$ $\mu m^2 s^{-1}$ and a diffusive exponent of 0.72 indicating unbiased random diffusion (table 5.2**)**.

Table 5.2 Motile properties of p44–Qdot on DNA

d (x10^{-3} um^2 s$^{-1)}$ (±SE)	17.56 (±0.4) *n*= 44
Diffusive exponent (±SE)	0.73 (±0.05) *n* = 44
Lifetime (Seconds)	5.66 *n* = 180

5.3.6 p44 preferentially binds to single stranded regions but not damage

XPD is a single stranded DNA helicase, and with its binding partner, p44, is usually considered in their interaction with single stranded regions of DNA. Since p44 readily translocates along double stranded DNA we examined whether the TFIIH accessory subunit showed the same

preference for single stranded patches. 45.65% (±1% *n* = 2) of 78 p44 molecules were bound to the single stranded region, significantly higher than the middle of the tightrope (10% discussed in Chapter 3 (p = 0.0017) and statistically identical to XPD (p > 0.1). Unsurprisingly p44 showed no preference for damage (figure 5.13), only 13.43% (±1.1% *n* = 3) of 67 p44 molecules were bound to the damage construct, not statistically different to the middle of the tightrope (P=0.1329).

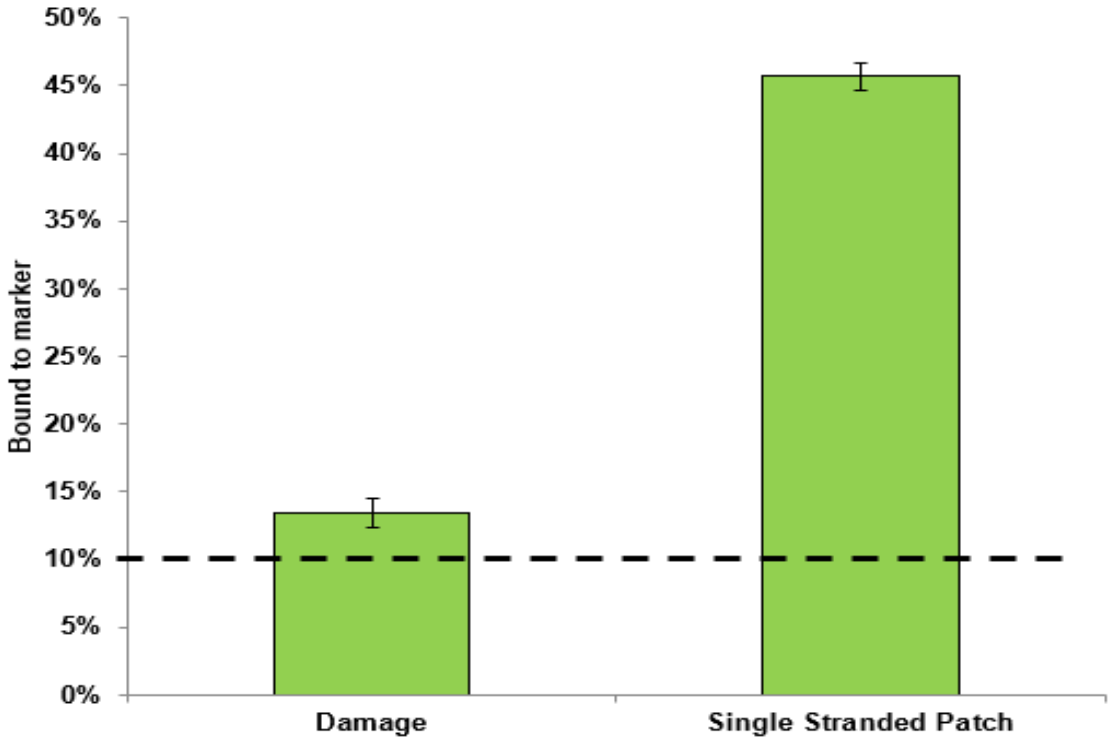

Figure 5.13. Probability of finding p44 colocalized with a construct marker. Values for mean probability percentage (±SEM, where, *n* refers to repeated experiments) bound to damaged DNA were 13.43% (±1.09% *n* = 2) and bound to single stranded patch DNA were 45.65% (±1.03% *n* = 2). The dashed line represents the probability (10.1%) of random association to damage based upon UvrA-Qdot binding to the mid-point of a DNA tightrope.

5.4 Discussion

XPD and p44 together have a crucial role in DNA repair, unwinding the DNA and exposing lesions to the other TFIIH subunits for damage verification and damage removal. In this chapter we investigate the interaction these two TFIIH subunits with double stranded DNA using single molecule fluorescence imaging. Both XPD and p44 bind readily to double stranded DNA, with XPD's interaction heavily regulated by nucleotide. A series of XPD mutant constructs confirms that ATP hydrolysis, not binding, is key to DNA translocation and the motile state is likely ADP.Pi. Varying the concentration of ATP confirmed that ATP binding was not the rate limiting step of DNA translocation and lower concentrations of ATP revealed longer pauses in translocation. Finally, we investigated whether XPD and p44 could locate damage and single stranded patches on double stranded DNA.

5.4.1 XPD is motile on double stranded DNA

The FeS cluster has been shown to link ATP hydrolysis to single stranded DNA translocation (Singleton and Wigley, 2002; Liu *et al.*, 2008; Pugh *et al.*, 2008). DinG, another member of the XPD family, has also recently been shown to require ATP hydrolysis for single stranded translocation (Cheng and Wigley, 2018). PcrA, another DNA helicase, has ATP linked with single stranded DNA translocation, with 50 base pair steps requiring the hydrolysis of 1 ATP molecule (Dillingham, Wigley and Webb, 2000).

The translocation of PcrA has been separated from the helicase activity. The detectable helicase activity of PcrA needs to be activated either by self-assembly or through interactions with other accessory proteins, this could be similar to XPD and p44 (Niedziela-Majka *et al.*, 2007). The link between ATP and double stranded DNA binding and DNA translocation is unclear.

In this chapter using a number of mutants and nucleotide conditions we show ATP hydrolysis is key in double stranded DNA translocation. We had previously shown that the helicase deficient mutant (R195E) affecting helicase domain 1 is unable to bind to double stranded DNA indicating that some degree of helicase activity is needed for DNA loading (Kuper *et al.*, 2014). However, the three mutants we used exhibit comparably lowered helicase activity and were able to bind to our DNA tightropes. We observe high levels of DNA binding in the absence of both ATP and p44, though it should be noted in the absence of ATP DNA binding is decreased. These data suggest the helicase activity is not required for DNA binding and the R195E mutant is unable to bind DNA for a reason unrelated to helicase activity. Previous bulk data showed an ATPase activity, without p44, of 0.12 mol ATP·mol $XPD^{-1}\cdot s^{-1}$ of 1 ATP hydrolysed every 8 seconds (Kuper *et al.*, 2014). Using our DNA tightropes, we observed a lifetime on DNA of 20 seconds. 1/lifetime is equal to 0.5 s^{-1}, these data together suggest with a lifetime on our DNA tightropes of 20seconds, and 1 ATP hydrolysed every 8 seconds (Kuper *et al.*, 2014), 2 ATP molecules are hydrolysed per XPD/DNA interaction. The FeS cluster mediates coupling of ATP hydrolysis to DNA translocation (Rudolf *et al.*,

2006; Pugh *et al.*, 2008). F192A, the FeS mutant, and K48R, the HD1 mutant where the FeS cluster resides, displayed a lower number of proteins motile on DNA tightropes, comparable to no nucleotide conditions of the wild type XPD. This lack of protein motility providing single molecule evidence for the wealth of biochemical data that shows FeS couples ATP hydrolysis to translocation (Dillingham, Wigley and Webb, 2000; Singleton and Wigley, 2002; Liu *et al.*, 2008; Kuper *et al.*, 2014; Greber *et al.*, 2017). The K719W mutant affects residues that direct interaction with p44, abolishing the partnership completely (Kuper *et al.*, 2014; Kim *et al.*, 2015). Consequently, we were surprised this mutant exhibited motility analogous to the other mutants and non-ATP conditions upon DNA tightropes and not the wild type XPD. Essentially the proteins in the absence of p44 are the same and the lack of motility could be due to unforeseen structural changes. The K719W mutant affects residues in HD2 (Kuper *et al.*, 2014). HD1 contains ARCH domain and FeS cluster which form a small groove that interact with DNA (Kuper *et al.*, 2014; Greber *et al.*, 2017). ATP binds and is hydrolyzed between HD1 and HD2, the simultaneous action of these domains is thought to drive DNA translocation (Liu *et al.*, 2008). The lack of motility exhibited by this construct could be due to disrupted ATP hydrolysis between the two motor domains. Both TFIIH subunits readily bound and exhibited one dimensional diffusion along double stranded DNA. ATP mediates XPD binding to DNA, the mutant construct and various nucleotide conditions, specifically the ADP and vanadate conditions, reveal that ATP binding does not activate motility but the ADP.Pi state is motile state. From these

experiments we have constructed a model of interaction (Figure 5.14). Varying the ATP concentration revealed that ATP binding is not the rate limiting step in XPDs double stranded DNA motility and at lower ATP concentrations XPD exhibits increasing longer pauses during translocation.

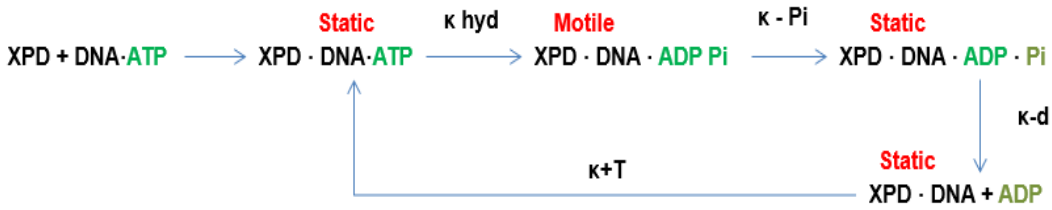

Figure 5.14 Schematic model for the interaction of XPD and double stranded DNA and ATP hydrolysis.

5.4.2 Both TFIIH subunits prefer single stranded DNA

XPD binds to single stranded DNA via a deep groove between the FeS cluster and ARCH domain (Rudolf *et al.*, 2006; Fan *et al.*, 2008; Liu *et al.*, 2008; Wolski *et al.*, 2008; Abdulrahman *et al.*, 2013; Greber *et al.*, 2017). We show the XPD has a clear preference for single stranded regions on double stranded DNA, we did not have the resolution to visualize DNA unwinding but without XPDs binding partner the helicase activity would be limited. The helicase of XPD is only observed in the presence of p44, in our single molecule assay we examined XPD binding to single stranded DNA without its binding partner (Fairman-Williams, Guenther and

Jankowsky, 2010; Kuper *et al.*, 2014; Kim *et al.*, 2015; Greber *et al.*, 2017). Similarly, p44 has a preference to single stranded regions on double stranded DNA. The 35-nucleotide region is vastly outnumbered by double stranded regions of DNA. One molecule of lambda DNA is 48502 base pairs in length, in this study we exploit the cos ends of the DNA to create a single stranded patch (Daniels, Sanger and Coulson, 1983). The vast excess of double stranded DNA (1386:1) highlights the extreme preference for single stranded DNA both of the TFIIH subunits exhibit. We also found that XPD has a preference for our damage tightrope construct confirming earlier studies, using fluorescein for damage as we did, that XPD showed the same bias for lesions (Rudolf *et al.*, 2010). It should be noted that this study used archaeal XPD which does not have a p44 to activate helicase activity and we see damage binding without XPDs TFIIH binding factor (Kelman and White, 2005; Rudolf *et al.*, 2006, 2010; Liu *et al.*, 2008).

5.5 Conclusion

Using single molecule fluorescence imaging of DNA tightropes, we have examined the interaction of fluorescently labelled XPD and p44 independently with double stranded DNA. XPD and p44 can translocate along double stranded DNA tightropes, though both prefer single stranded patches, suggesting they are able to scan DNA searching for other TFIIH factors. We show for the first time at the single molecule level that XPD can recognise DNA lesions incorporated into double stranded DNA. XPD

may scan DNA and assist in initial detection of damage with XPC and this could help initial TFIIH formation around lesions. The binding partner of XPD, p44 has been shown to be key in TFIIH stability (Tirode *et al.*, 1999; Tremeau-Bravard, Perez and Egly, 2001; Kellenberger *et al.*, 2005; Schmitt *et al.*, 2014; Radu *et al.*, 2017). The ability of XPD and p44 to readily translocate along DNA could be an unrealized process in TFIIH formation. Finally, XPD translocation is heavily modulated by ATP hydrolysis, lowering the concentration of this nucleotide results in increasingly longer pauses during DNA scanning. Both XPD and p44 eagerly bind to single stranded patches on double stranded DNA.

Chapter 6 Conclusions

The primary aim of this project was to examine the function of the UvrBC complex. The general role of bacterial NER is well documented, but initial complex formation on DNA lesions has remained unclear, and the UvrBC complex did not have a clearly defined role. UvrBC had previously been shown to form complexes on certain DNA substrates (Zou *et al.*, 1997; Moolenaar, Uiterkamp, *et al.*, 1998; Wirth *et al.*, 2016), and can form a motile complex on double stranded DNA (Hughes *et al.*, 2013). Here, using single molecule fluorescence imaging of DNA tightropes with defined DNA lesions, we found that UvrBC in the absence of UvrA was able to bind to damage at levels consistent with UvrAB, which has clear damage recognition function (Verhoeven, Wyman, *et al.*, 2002; Pakotiprapha *et al.*, 2012; Webster *et al.*, 2012). These results show for the first time, at the single molecule level, a clear damage related role. We also show that UvrA exhibits tension dependence when locating damage when interrogating the DNA preparing for later damage verification by UvrB (Stracy *et al.*, 2016). Next, we examined the *in vivo* role of the UvrBC complex by using live cell fluorescence imaging of eGFP tagged UvrB and UvrC in UvrA knockout cells. To ascertain if UvrB and UvrC could detect damage *in vivo* we imaged the intracellular movement of fluorescent UvrB and UvrC in response to UV damage without interference from UvrA or UvrAB complexes. We demonstrate for the first time UvrB and UvrC, likely in complex, can bind directly to DNA damage *in vivo* independently from UvrA, demonstrating an *in vivo* damage

sensing role for the UvrBC complex. Additionally, we confirm this loading of UvrBC complexes to damaged DNA improves UvrA null cell survival at low levels of UV damage. Taken together, these data indicate UvrBC complexes form *in vivo* and directly contributes to DNA damage processing and repair in a previously unrealised pathway. UvrBC complexes have the capacity to locate genomic lesions independently of UvrA in mechanism of repair exists in cells suffering low levels of damage, likely before the SOS response is initiated.

Finally, we explored the eukaryotic NER proteins, XPD and p44, key subunits in the TFIIH complex that, together, unwind the DNA to expose lesions. XPD and p44 can independently translocate along double stranded DNA tightropes, though both prefer single stranded regions, suggesting they are able to scan DNA searching for other TFIIH factors or DNA structure. Initial TFIIH formation has been heavily linked with p44 and XPD readily forms complexes with its binding partner (Tirode *et al.*, 1999; Tremeau-Bravard, Perez and Egly, 2001; Kellenberger *et al.*, 2005; Schmitt *et al.*, 2014; Radu *et al.*, 2017). These two proteins readily translocate along our double stranded DNA substrates and this could reflect *in vivo* function. XPD has been shown to bypass obstacles on DNA (Honda *et al.*, 2009; Spies, 2014) and together with XPC could assist lesion detection and subsequent TFIIH formation. XPD both show extreme reference for single stranded regions on double stranded DNA. The ability to translocate double stranded DNA and search for these areas is indicative of XPDs defined function. Once bound to single stranded

regions XPD would begin to unwind the DNA, and with arrival of p44, readily exhibit characteristic helicase activity.

Future Work

We show a clear tension DNA dependence of UvrA to detect lesions in agreement with biochemical and structural studies. To investigate the precise mechanism of how UvrA manipulates the DNA, further single molecule analysis with magnetic tweezers should be pursued. Similar recent physical force measurements have interrogated UvrA with undamaged DNA but to understand how the canonical initiator of NER interacts with DNA, further investigation is required. The TFIIH complex interrogates DNA with several of its subunits, force experiments with these complexes will define this exact mechanism. We further show a clear damage detecting role of the UvrBC complex. UvrB has many binding partners *in vivo* and dual fluorescent labelling of these partners, such as Mfd, could reveal close links between global genomic repair and transcription coupled repair. Recent live cell imaging has more clearly defined the interaction between UvrA, Mfd and RNAP and further investigation with UvrB and UvrC could show precise role for the UvrBC complex (Ho, Van Oijen and Ghodke, 2018). Single molecule imaging of these proteins directly on DNA will further clarify the initial damage detection stages of NER and how a small number of NER proteins protect vast amounts of DNA.

We also demonstrate XPD and p44 readily, independently translocate along double stranded DNA. To further understand the role of XPD and p44 on double stranded DNA dual differential imaging of these helicase partners is essential. Other TFIIH subunits such as XPB and XPC should also be investigated in tandem. How these proteins come together to form the multiprotein TFIIH is poorly understood. Our experiments reveal a direct interaction with p44 and DNA independent of XPD. Recent experiments in our lab show p44 and p62 form a motile complex on DNA and this relationship changes in the presence of damaged DNA. These subunits had been forgotten in recent structural investigations and considered only in complex with the helicase subunits of TFIIH. Directly examining single molecules of each subunit, and combinations of subunits, on both single and double stranded DNA to explore currently elusive functions. The initial formation of this complex is heavily debated, single molecule imaging of individual proteins whilst introducing more subunits will provide unparalleled clarity to nucleotide excision repair.

Recent single molecule experiments have shown that UvrA, UvrB and UvrC can form a motile ‘repairosome’ complex on DNA. Further experiments should examine how individual subunits of this complex interact on double stranded DNA. Structural and biochemical data have shown multiple conformations of NER complexes, single molecule imaging could reveal the precise stoichiometry and transitions between states in real time. It would be interesting to examine the interaction of this repairsome with various types of DNA damage and compare this to UvrA and UvrAB, the classic initiator of NER. Single molecule studies would

provide evidence to damage type preference lost in pioneering biochemical studies.

Finally, NER pathways in complex multicellular model organisms, such as *Danio rerio*, and *Xenopus laevis,* should be performed alongside single molecule imaging so as to develop increasing relevant models that directly apply to humans. Currently, defects in UV damage repair pathways, although rare, have devasting phenotypic outcomes with extremely limited therapeutic interventions that result in premature death.

References

Abdulrahman, W. *et al.* (2013) 'ARCH domain of XPD, an anchoring platform for CAK that conditions TFIIH DNA repair and transcription activities', *Proceedings of the National Academy of Sciences*. National Academy of Sciences, 110(8), pp. E633–E642. doi: 10.1073/pnas.1213981110.

Ahmad, S. I. and Hanaoka, F. (2008) 'Molecular mechanisms of xeroderma pigmentosum. Preface.', *Advances in experimental medicine and biology*. Edited by S. I. Ahmad and F. Hanaoka. New York, NY: Springer New York (Advances in Experimental Medicine and Biology), 637, pp. vii–xiv. doi: 10.1007/978-0-387-09599-8.

Ahn, B. (2000) 'A physical interaction of UvrD with nucleotide excision repair protein UvrB', *Molecules and Cells*, 10(5), pp. 592–597. doi: 10.1007/s10059-000-0592-5.

Alexandrovich, A. *et al.* (1999) 'NMR assignments and secondary structure of the UvrC binding domain of UvrB', *FEBS Letters*, 451(2), pp. 181–185. doi: 10.1016/S0014-5793(99)00542-6.

Allers, T. and Lichten, M. (2001) 'Differential timing and control of noncrossover and crossover recombination during meiosis', *Cell*, 106(1), pp. 47–57. doi: 10.1016/S0092-8674(01)00416-0.

Almeida, K. H. and Sobol, R. W. (2007) 'A unified view of base excision repair: Lesion-dependent protein complexes regulated by post-translational modification', *DNA Repair*, 6(6), pp. 695–711. doi: 10.1016/j.dnarep.2007.01.009.

Araki, M. *et al.* (2001) 'Centrosome Protein Centrin 2/Caltractin 1 Is Part of the Xeroderma Pigmentosum Group C Complex That Initiates Global Genome Nucleotide Excision Repair', *Journal of Biological Chemistry*, 276(22), pp. 18665–18672. doi: 10.1074/jbc.M100855200.

Arana, M. E. and Kunkel, T. A. (2010) 'Mutator phenotypes due to DNA replication infidelity', *Seminars in Cancer Biology*, 20(5), pp. 304–311. doi: 10.1016/j.semcancer.2010.10.003.

Araújo, S. J. *et al.* (2000) 'Nucleotide excision repair of DNA with recombinant human proteins: Definition of the minimal set of factors, active forms of TFIIH, and modulation by CAK', *Genes and Development*, 14(3), pp. 349–359. doi: 10.1101/gad.14.3.349.

Araújo, S. J., Nigg, E. A. and Wood, R. D. (2001) 'Strong functional interactions of TFIIH with XPC and XPG in human DNA nucleotide excision repair, without a preassembled repairosome.', *Molecular and cellular biology*, 21(7), pp. 2281–91. doi: 10.1128/MCB.21.7.2281-2291.2001.

Aravind, L., Walker, D. R. and Koonin, E. V (1999) 'Conserved domains in DNA repair proteins and

evolution of repair systems', *Nucleic Acids Research*. Oxford University Press, 27(5), pp. 1223–1242. doi: 10.1093/nar/27.5.1223.

Arthur, H. M. and Eastlake, P. B. (1983) 'Transcriptional control of the uvrD gene of Escherichia coli', *Gene*, 25(2–3), pp. 309–316. doi: 10.1016/0378-1119(83)90235-4.

Ashkin, A. *et al.* (1986) 'Observation of a single-beam gradient force optical trap for dielectric particles', *Optics Letters*. Optical Society of America, 11(5), p. 288. doi: 10.1364/OL.11.000288.

Assenmacher, N. *et al.* (2006) 'Structural basis for transcription-coupled repair: The N terminus of Mfd resembles UvrB with degenerate ATPase motifs', *Journal of Molecular Biology*, 355(4), pp. 675–683. doi: 10.1016/j.jmb.2005.10.033.

Atkinson, J. *et al.* (2009) 'Stimulation of UvrD helicase by UvrAB', *Journal of Biological Chemistry*, 284(14), pp. 9612–9623. doi: 10.1074/jbc.M808030200.

Baba, T. *et al.* (2006) 'Construction of Escherichia coli K-12 in-frame, single-gene knockout mutants: The Keio collection', *Molecular Systems Biology*, 2, p. 2006.0008. doi: 10.1038/msb4100050.

Baharoglu, Z. and Mazel, D. (2014) 'SOS, the formidable strategy of bacteria against aggressions', *FEMS Microbiology Reviews*, 38(6), pp. 1126–1145. doi: 10.1111/1574-6976.12077.

Barnett, J. T. and Kad, N. M. (2018) 'Understanding the coupling between DNA damage detection and UvrA's ATPase using bulk and single molecule kinetics', *The FASEB Journal*, p. fj.201800899R. doi: 10.1096/fj.201800899R.

Batty, D. P. and Wood, R. D. (2000) 'Damage recognition in nucleotide excision repair of DNA.', *Gene*, 241(2), pp. 193–204. Available at: http://www.ncbi.nlm.nih.gov/pubmed/10675030 (Accessed: 24 October 2018).

Bellon, S. F., Coleman, J. H. and Lippard, S. J. (1991) 'DNA Unwinding Produced by Site-Specific Intrastrand Cross-Links of the Antitumor Drug cis-Diamminedichloroplatinum(II)', *Biochemistry*, 30(32), pp. 8026–8035. doi: 10.1021/bi00246a021.

Berg, O. G., Winter, R. B. and Von Hippel, P. H. (1981) 'Diffusion-Driven Mechanisms of Protein Translocation on Nucleic Acids. 1. Models and Theory', *Biochemistry*. American Chemical Society, 20(24), pp. 6929–6948. doi: 10.1021/bi00527a028.

Bernardes de Jesus, B. M. *et al.* (2008) 'Dissection of the Molecular Defects Caused by Pathogenic Mutations in the DNA Repair Factor XPC', *Molecular and Cellular Biology*. American Society for Microbiology Journals, 28(23), pp. 7225–7235. doi: 10.1128/MCB.00781-08.

Bhagwat, A. S. and Roberts, R. J. (1987) 'Genetic analysis of the 5-azacytidine sensitivity of Escherichia coli K-12', *Journal of Bacteriology*. American Society for Microbiology (ASM), 169(4), pp. 1537–1546. doi: 10.1128/jb.169.4.1537-1546.1987.

Bonnet, I. *et al.* (2008) 'Sliding and jumping of single EcoRV restriction enzymes on non-cognate DNA', *Nucleic Acids Research*. Oxford University Press, 36(12), pp. 4118–4127. doi: 10.1093/nar/gkn376.

Boon, E. M. *et al.* (2003) 'DNA-mediated charge transport for DNA repair', *Proceedings of the National Academy of Sciences*, 100(22), pp. 12543–12547. doi: 10.1073/pnas.2035257100.

Branum, M. E., Reardon, J. T. and Sancar, A. (2001) 'DNA repair excision nuclease attacks undamaged DNA: A potential source of spontaneous mutations', *Journal of Biological Chemistry*, 276(27), pp. 25421–25426. doi: 10.1074/jbc.M101032200.

Brem, R., Guven, M. and Karran, P. (2017) 'Oxidatively-generated damage to DNA and proteins mediated by photosensitized UVA', *Free Radical Biology and Medicine*, 107, pp. 101–109. doi: 10.1016/j.freeradbiomed.2016.10.488.

Brewer, L. R. and Bianco, P. R. (2008) 'Laminar flow cells for single-molecule studies of DNA-protein interactions', *Nature Methods*, 5(6), pp. 517–525. doi: 10.1038/nmeth.1217.

van den Broek, B., Noom, M. C. and Wuite, G. J. L. (2005) 'DNA-tension dependence of restriction enzyme activity reveals mechanochemical properties of the reaction pathway', *Nucleic Acids Research*. Oxford University Press, 33(8), pp. 2676–2684. doi: 10.1093/nar/gki565.

Buechner, C. N. *et al.* (2014) 'Strand-specific recognition of DNA damages by XPD provides insights into Nucleotide excision repair substrate versatility', *Journal of Biological Chemistry*, 289(6), pp. 3613–3624. doi: 10.1074/jbc.M113.523001.

Bunick, C. G. *et al.* (2006) 'Biochemical and Structural Domain Analysis of Xeroderma Pigmentosum Complementation Group C Protein †', *Biochemistry*, 45(50), pp. 14965–14979. doi: 10.1021/bi061370o.

Busso, D. *et al.* (2000) 'Distinct regions of MAT1 regulate cdk7 kinase and TFIIH transcription activities', *Journal of Biological Chemistry*, 275(30), pp. 22815–22823. doi: 10.1074/jbc.M002578200.

Camenisch, U. *et al.* (2006) 'Recognition of helical kinks by xeroderma pigmentosum group a protein triggers DNA excision repair', *Nature Structural and Molecular Biology*, 13(3), pp. 278–284. doi: 10.1038/nsmb1061.

Camenisch, U. *et al.* (2007) 'Xeroderma pigmentosum complementation group A protein is driven to nucleotide excision repair sites by the electrostatic potential of distorted DNA', *DNA Repair*, 6(12), pp. 1819–1828. doi: 10.1016/j.dnarep.2007.07.011.

Caron, P. R. and Grossman, L. (1988) 'Involvement of a cryptic ATPase activity of UvrB and its proteolysis product, UvrB in DNA repair', *Nucleic Acids Research*, p. 10952. doi: 10.1093/nar/16.22.10952-b.

Caron, P. R., Kushner, S. R. and Grossman, L. (1985) 'Involvement of helicase II (uvrD gene product) and DNA polymerase I in excision mediated by the uvrABC protein complex.', *Proceedings of the National Academy of Sciences of the United States of America*, 82(15), pp. 4925–4929. doi: 10.1073/pnas.82.15.4925.

Chandrasekhar, D. and Van Houten, B. (1994) 'High resolution mapping of UV-induced photoproducts in the Escherichia coli lacI gene', *Journal of Molecular Biology*, 238(3), pp. 319–332. doi: 10.1006/jmbi.1994.1295.

Chandrasekhar, D. and Van Houten, B. (2000) 'In vivo formation and repair of cyclobutane pyrimidine dimers and 6-4 photoproducts measured at the gene and nucleotide level in Escherichia coli', *Mutation Research - Fundamental and Molecular Mechanisms of Mutagenesis*, 450(1–2), pp. 19–40. doi: 10.1016/S0027-5107(00)00014-2.

Chang, H. H. Y. *et al.* (2017) 'Non-homologous DNA end joining and alternative pathways to double-strand break repair', *Nature Reviews Molecular Cell Biology*, 18(8), pp. 495–506. doi: 10.1038/nrm.2017.48.

Chang, W. H. and Kornberg, R. D. (2000) 'Electron crystal structure of the transcription factor and DNA repair complex, core TFIIH', *Cell*, 102(5), pp. 609–613. doi: 10.1016/S0092-8674(00)00083-0.

Chapman-Smith, A. and Cronan, J. E. (1999) 'The enzymatic biotinylation of proteins: A post-translational modification of exceptional specificity', *Trends in Biochemical Sciences*. Elsevier, pp. 359–363. doi: 10.1016/S0968-0004(99)01438-3.

Chargraff, E. *et al.* (1951) 'Of the desoxyribonucleic salmon sperm*', *J. Biol. Chem.*, 192, pp. 223–230.

Chatterjee N, W. G. (2017) 'Mechanisms of DNA damage, repair and mutagenesis', *Environ Mol Mutagen*, 58(5), pp. 325–263.

Chen, J. *et al.* (2014) 'Single-molecule dynamics of enhanceosome assembly in embryonic stem

cells', *Cell*, 156(6), pp. 1274–1285. doi: 10.1016/j.cell.2014.01.062.

Chen, L. *et al.* (2008) 'Cell cycle-dependent complex formation of BRCA1·CtIP·MRN is important for DNA double-strand break repair', *Journal of Biological Chemistry*, 283(12), pp. 7713–7720. doi: 10.1074/jbc.M710245200.

Cheng, K. and Wigley, D. B. (2018) *DNA translocation mechanism of an XPD family helicase*, *eLife*. eLife Sciences Publications, Ltd. doi: 10.7554/eLife.42400.

Chivers, C. E. *et al.* (2011) 'How the biotin–streptavidin interaction was made even stronger: investigation via crystallography and a chimaeric tetramer', *Biochemical Journal*. Portland Press Ltd, 435(1), pp. 55–63. doi: 10.1042/BJ20101593.

Cinelli, R. A. G. *et al.* (2000) 'The Enhanced Green Fluorescent Protein as a Tool for the Analysis of Protein Dynamics and Localization: Local Fluorescence Study at the Single-molecule Level', *Photochemistry and Photobiology*. Wiley/Blackwell (10.1111), 71(6), pp. 771–776. doi: 10.1562/0031-8655(2000)0710771TEGFPA2.0.CO2.

Claassen, L. A. and Grossman, L. (1991) 'Deletion mutagenesis of the Escherichia coli UvrA protein localizes domains for DNA binding, damage recognition, and protein-protein interactions', *Journal of Biological Chemistry*, 266(17), pp. 11388–11394. Available at: http://www.jbc.org/content/266/17/11388.full.pdf (Accessed: 22 June 2018).

Cleaver, J. E. *et al.* (1999) 'A summary of mutations in the UV-sensitive disorders: Xeroderma pigmentosum, Cockayne syndrome, and trichothiodystrophy', *Human Mutation*, pp. 9–22. doi: 10.1002/(SICI)1098-1004(1999)14:1<9::AID-HUMU2>3.0.CO;2-6.

Clement, F. C. *et al.* (2010) 'Dynamic two-stage mechanism of versatile DNA damage recognition by xeroderma pigmentosum group C protein', *Mutation Research - Fundamental and Molecular Mechanisms of Mutagenesis*, pp. 21–28. doi: 10.1016/j.mrfmmm.2009.08.005.

Cohen, S. E. *et al.* (2010) 'Roles for the transcription elongation factor NusA in both DNA repair and damage tolerance pathways in Escherichia coli', *Proceedings of the National Academy of Sciences*, 107(35), pp. 15517–15522. doi: 10.1073/pnas.1005203107.

Coin, F. *et al.* (1998) 'Mutations in the XPD helicase gene result in XP and TTD phenotypes, preventing interaction between XPD and the p44 subunit of TFIIH', *Nature Genetics*, 20(2), pp. 184–188. doi: 10.1038/2491.

Coin, F. *et al.* (2008) 'Nucleotide Excision Repair Driven by the Dissociation of CAK from TFIIH',

Molecular Cell, 31(1), pp. 9–20. doi: 10.1016/j.molcel.2008.04.024.

Coin, F., Oksenych, V. and Egly, J. M. (2007) 'Distinct Roles for the XPB/p52 and XPD/p44 Subcomplexes of TFIIH in Damaged DNA Opening during Nucleotide Excision Repair', *Molecular Cell*, 26(2), pp. 245–256. doi: 10.1016/j.molcel.2007.03.009.

Compe, E. and Egly, J. M. (2012) 'TFIIH: When transcription met DNA repair', *Nature Reviews Molecular Cell Biology*, pp. 343–354. doi: 10.1038/nrm3350.

Contag, P. R. *et al.* (1998) 'Bioluminescent indicators in living mammals.', *Nature medicine*, 4(2), pp. 245–7. Available at: http://www.ncbi.nlm.nih.gov/pubmed/9461201 (Accessed: 23 November 2018).

Cormack, B. P., Valdivia, R. H. and Falkow, S. (1996) 'FACS-optimized mutants of the green fluorescent protein (GFP)', in *Gene*, pp. 33–38. doi: 10.1016/0378-1119(95)00685-0.

Courcelle, J. *et al.* (2001) 'Comparative gene expression profiles following UV exposure in wild-type and SOS-deficient Escherichia coli.', *Genetics*, 158(1), pp. 41–64. Available at: http://www.ncbi.nlm.nih.gov/pubmed/11333217 (Accessed: 25 October 2018).

Croteau, D. L. *et al.* (2006) 'The C-terminal zinc finger of UvrA does not bind DNA directly but regulates damage-specific DNA binding.', *The Journal of biological chemistry*, 281(36), pp. 26370–81. doi: 10.1074/jbc.M603093200.

Croteau, D. L. *et al.* (2008) 'Cooperative damage recognition by UvrA and UvrB: Identification of UvrA residues that mediate DNA binding', *DNA Repair*, 7(3), pp. 392–404. doi: 10.1016/j.dnarep.2007.11.013.

Crowley, D. J. and Hanawalt, P. C. (1998) 'Induction of the SOS response increases the efficiency of global nucleotide excision repair of cyclobutane pyrimidine dimers, but not 6-4 photoproducts, in UV-irradiated Escherichia coli', *Journal of Bacteriology*, 180(13), pp. 3345–3352. Available at: http://www.ncbi.nlm.nih.gov/pubmed/9642186 (Accessed: 8 November 2018).

Cutchis P. (1974) 'Stratospheric ozone depletion and solar ultraviolet radiation on Earth', *Science*. American Association for the Advancement of Science, 184(4132), pp. 13–19. doi: 10.2307/1737431.

Daniels, D. L., Sanger, F. and Coulson, A. R. (1983) 'Features of bacteriophage lambda: analysis of the complete nucleotide sequence.', *Cold Spring Harbor symposia on quantitative biology*, 47 Pt 2, pp. 1009–24. Available at: http://www.ncbi.nlm.nih.gov/pubmed/6222866 (Accessed: 6 December 2018).

Davenport, R. J. *et al.* (2000) 'Single-molecule study of transcriptional pausing and arrest by E. coli

RNA polymerase', *Science*, 287(5462), pp. 2497–2500. doi: 10.1126/science.287.5462.2497.

Davies, R. (1995) 'Royal Irish Academy Medal Lecture. Ultraviolet radiation damage in DNA', *Biochemical Society Transactions*, 32(2), pp. 407–418.

Deaconescu, A. M. *et al.* (2006) 'Structural Basis for Bacterial Transcription-Coupled DNA Repair', *Cell*, 124(3), pp. 507–520. doi: 10.1016/j.cell.2005.11.045.

Deaconescu, A. M. *et al.* (2012) 'Nucleotide excision repair (NER) machinery recruitment by the transcription-repair coupling factor involves unmasking of a conserved intramolecular interface', *Proceedings of the National Academy of Sciences*, 109(9), pp. 3353–3358. doi: 10.1073/pnas.1115105109.

DellaVecchia, M. J. *et al.* (2004) 'Analyzing the Handoff of DNA from UvrA to UvrB Utilizing DNA-Protein Photoaffinity Labeling', *Journal of Biological Chemistry*, 279(43), pp. 45245–45256. doi: 10.1074/jbc.M408659200.

Derfus, A. M., Chan, W. C. W. and Bhatia, S. N. (2004) 'Probing the Cytotoxicity of Semiconductor Quantum Dots', *Nano Letters*, 4(1), pp. 11–18. doi: 10.1021/nl0347334.

Desai, R., Geeves, M. A. and Kad, N. M. (2015) 'Using fluorescent myosin to directly visualize cooperative activation of thin filaments', *Journal of Biological Chemistry*, 290(4), pp. 1915–1925. doi: 10.1074/jbc.M114.609743.

Dessinges, M.-N. *et al.* (2004) 'Single-molecule assay reveals strand switching and enhanced processivity of UvrD.', *Proc. Natl. Acad. Sci. USA*, 101(17), pp. 6439–6444. doi: 10.1073/pnas.0306713101.

Dianov, G. L. and Hübscher, U. (2013) 'Mammalian base excision repair: The forgotten archangel', *Nucleic Acids Research*, 41(6), pp. 3483–3490. doi: 10.1093/nar/gkt076.

Dillingham, M. S., Wigley, D. B. and Webb, M. R. (2000) 'Demonstration of unidirectional single-stranded DNA translocation by PcrA helicase: Measurement of step size and translocation speed', *Biochemistry*, 39(1), pp. 205–212. doi: 10.1021/bi992105o.

Douki, T. and Cadet, J. (2001) 'Individual determination of the yield of the main UV-induced dimeric pyrimidine photoproducts in DNA suggests a high mutagenicity of CC photolesions', *Biochemistry*, 40(8), pp. 2495–2501. doi: 10.1021/bi0022543.

Doyle, P. S., Ladoux, B. and Viovy, J. L. (2000) 'Dynamics of a tethered polymer in shear flow', *Physical Review Letters*, 84(20), pp. 4769–4772. doi: 10.1103/PhysRevLett.84.4769.

Drew, H. R. *et al.* (1981) 'Structure of a B-DNA dodecamer: conformation and dynamics.', *Proceedings of the National Academy of Sciences of the United States of America*, 78(4), pp. 2179–2183. doi: 10.1073/pnas.78.4.2179.

Drew, H. R. and Travers, A. A. (1984) 'DNA structural variations in the E. coli tyrT promoter', *Cell*, 37(2), pp. 491–502. doi: 10.1016/0092-8674(84)90379-9.

Dubaele, S. *et al.* (2003) 'Basal transcription defect discriminates between xeroderma pigmentosum and trichothiodystrophy in XPD patients', *Molecular Cell*, 11(6), pp. 1635–1646. doi: 10.1016/S1097-2765(03)00182-5.

Dunn, A. R. *et al.* (2011) 'Single Qdot-labeled glycosylase molecules use a wedge amino acid to probe for lesions while scanning along DNA.', *Nucleic acids research*, 39(17), pp. 7487–98. doi: 10.1093/nar/gkr459.

Elf, J., Li, G. W. and Xie, X. S. (2007) 'Probing transcription factor dynamics at the single-molecule level in a living cell', *Science*, 316(5828), pp. 1191–1194. doi: 10.1126/science.1141967.

Epshtein, V. *et al.* (2014) 'UvrD facilitates DNA repair by pulling RNA polymerase backwards', *Nature*, 505(7483), pp. 372–377. doi: 10.1038/nature12928.

Etheridge, T. J. *et al.* (2014) 'Quantification of DNA-associated proteins inside eukaryotic cells using single-molecule localization microscopy', *Nucleic Acids Research*, 42(19), pp. e146–e146. doi: 10.1093/nar/gku726.

Fairman-Williams, M. E., Guenther, U. P. and Jankowsky, E. (2010) 'SF1 and SF2 helicases: Family matters', *Current Opinion in Structural Biology*, pp. 313–324. doi: 10.1016/j.sbi.2010.03.011.

Fan, J. *et al.* (2016) 'Reconstruction of bacterial transcription-coupled repair at single-molecule resolution', *Nature*. Nature Publishing Group, 536(7615), pp. 234–237. doi: 10.1038/nature19080.

Fan, L. *et al.* (2008) 'XPD Helicase Structures and Activities: Insights into the Cancer and Aging Phenotypes from XPD Mutations', *Cell*, 133(5), pp. 789–800. doi: 10.1016/j.cell.2008.04.030.

Fang, T. T. *et al.* (2012) 'Toxicity evaluation of CdTe quantum dots with different size on Escherichia coli', *Toxicology in Vitro*. Pergamon, 26(7), pp. 1233–1239. doi: 10.1016/j.tiv.2012.06.001.

Fei, J. *et al.* (2011) 'Regulation of nucleotide excision repair by UV-DDB: Prioritization of damage recognition to internucleosomal dna', *PLoS Biology*. Public Library of Science, 9(10), p. e1001183. doi: 10.1371/journal.pbio.1001183.

Fekairi, S. *et al.* (2009) 'Human SLX4 Is a Holliday Junction Resolvase Subunit that Binds Multiple

DNA Repair/Recombination Endonucleases', *Cell*, 138(1), pp. 78–89. doi: 10.1016/j.cell.2009.06.029.

Fernández De Henestrosa, A. R. *et al.* (2000) 'Identification of additional genes belonging to the LexA regulon in Escherichia coli', *Molecular Microbiology*, 35(6), pp. 1560–1572. doi: 10.1046/j.1365-2958.2000.01826.x.

Filippova, E. M. *et al.* (2003) 'Quantifying double-strand breaks and clustered damages in DNA by single-molecule laser fluorescence sizing', *Biophysical Journal*. The Biophysical Society, 84(2 I), pp. 1281–1290. doi: 10.1016/S0006-3495(03)74943-1.

Fitch, M. E. *et al.* (2003) 'The DDB2 nucleotide excision repair gene product p48 enhances global genomic repair in p53 deficient human fibroblasts', *DNA Repair*, 2(7), pp. 819–826. doi: 10.1016/S1568-7864(03)00066-1.

Fribourg, S. *et al.* (2000) 'Structural characterization of the cysteine-rich domain of TFIIH p44 subunit', *Journal of Biological Chemistry*, 275(41), pp. 31963–31971. doi: 10.1074/jbc.M004960200.

Gambotto, A. *et al.* (2000) 'Immunogenicity of enhanced green fluorescent protein (EGFP) in BALB/c mice: identification of an H2-K^d-restricted CTL epitope', *Gene Therapy 2000 7:23*. Nature Publishing Group, 7(23), p. 2036. doi: 10.1038/sj.gt.3301335.

Gantchev, T. G. and Hunting, D. J. (2010) 'Modeling the Interactions of the Nucleotide Excision Repair UvrA $_2$ Dimer with DNA', *Biochemistry*, 49(51), pp. 10912–10924. doi: 10.1021/bi1012035.

Gao, X. *et al.* (2005) 'In vivo molecular and cellular imaging with quantum dots', *Current Opinion in Biotechnology*. Elsevier Current Trends, pp. 63–72. doi: 10.1016/j.copbio.2004.11.003.

Garcia-Parajo, M. F. *et al.* (2001) 'The nature of fluorescence emission in the red fluorescent protein DsRed, revealed by single-molecule detection', *Proceedings of the National Academy of Sciences*, 98(25), pp. 14392–14397. doi: 10.1073/pnas.251525598.

Gascón, J. *et al.* (1995) 'Sensitivity of selected bacterial species to UV radiation', *Current Microbiology*, 30(3), pp. 177–182. doi: 10.1007/BF00296205.

Geourjon, C. and Deléage, G. (1994) 'SOPM: a self-optimized method for protein secondary structure prediction', *Protein Engineering*, 7(2), pp. 157–64. doi: 10.1093/protein/7.2.157.

Gibbons, B. J. *et al.* (2012) 'Subunit architecture of general transcription factor TFIIH', *Proceedings of the National Academy of Sciences*. National Academy of Sciences, 109(6), pp. 1949–1954. doi: 10.1073/pnas.1105266109.

Gillette, T. G. *et al.* (2006) 'Distinct functions of the ubiquitin-proteasome pathway influence nucleotide

excision repair', *EMBO Journal*. European Molecular Biology Organization, 25(11), pp. 2529–2538. doi: 10.1038/sj.emboj.7601120.

Gogoi, S. K. *et al.* (2006) 'Green fluorescent protein-expressing Escherichia coli as a model system for investigating the antimicrobial activities of silver nanoparticles', *Langmuir*. American Chemical Society, 22(22), pp. 9322–9328. doi: 10.1021/la060661v.

Goosen, N. and Moolenaar, G. F. (2008) 'Repair of UV damage in bacteria', *DNA Repair*, 7(3), pp. 353–379. doi: 10.1016/j.dnarep.2007.09.002.

Gordienko, I. and Rupp, W. D. (1997) 'The limited strand-separating activity of the UvrAB protein complex and its role in the recognition of DNA damage', *EMBO Journal*, 16(4), pp. 889–895. doi: 10.1093/emboj/16.4.889.

Gorman, J. *et al.* (2012) 'Single-molecule imaging reveals target-search mechanisms during DNA mismatch repair', *Proceedings of the National Academy of Sciences*, 109(45), pp. E3074–E3083. doi: 10.1073/pnas.1211364109.

Graneli, A. *et al.* (2006) 'Long-distance lateral diffusion of human Rad51 on double-stranded DNA', *Proceedings of the National Academy of Sciences*, 103(5), pp. 1221–1226. doi: 10.1073/pnas.0508366103.

Greber, B. J. *et al.* (2017) 'The cryo-electron microscopy structure of human transcription factor IIH', *Nature*, 549(7672), pp. 414–417. doi: 10.1038/nature23903.

Grilley, M. *et al.* (1989) 'Isolation and characterization of the Escherichia coli mutL gene product', *Journal of Biological Chemistry*, 264(2), pp. 1000–1004.

De Gruijl, F. R. and Van der Leun, J. C. (2000) 'Environment and health: 3. Ozone depletion and ultraviolet radiation', *Cmaj*, 163(7), pp. 851–855.

Grünberg, S. and Hahn, S. (2013) 'Structural insights into transcription initiation by RNA polymerase II', *Trends in Biochemical Sciences*, pp. 603–611. doi: 10.1016/j.tibs.2013.09.002.

Gruskin, E. A. and Lloyd, R. S. (1988) 'Molecular analysis of plasmid DNA repair within ultraviolet-irradiated Escherichia coli. II. UvrABC-initiated excision repair and photolyase-catalyzed dimer monomerization', *Journal of Biological Chemistry*, 263(25), pp. 12738–12743. Available at: http://www.ncbi.nlm.nih.gov/pubmed/3045128 (Accessed: 15 January 2019).

Habraken, Y. *et al.* (1998) 'ATP-dependent assembly of a ternary complex consisting of a DNA mismatch and the yeast MSH2-MSH6 and MLH1-PMS1 protein complexes', *Journal of Biological*

Chemistry, 273(16), pp. 9837–9841. doi: 10.1074/jbc.273.16.9837.

Haines, N. M. *et al.* (2014) 'Stalled transcription complexes promote DNA repair at a distance', *Proceedings of the National Academy of Sciences*. National Academy of Sciences, 111(11), pp. 4037–4042. doi: 10.1073/pnas.1322350111.

Hanawalt, P. C. *et al.* (1979) *DNA repair in bacteria and mammalian cells.*, *Annual review of biochemistry*. doi: 10.1146/annurev.bi.48.070179.004031.

Hanawalt, P. C. and Haynes, R. H. (1965) 'Repair replication of DNA in bacteria: Irrelevance of chemical nature of base defect', *Biochemical and Biophysical Research Communications*. Academic Press, 19(4), pp. 462–467. doi: 10.1016/0006-291X(65)90147-6.

Hellman, L. M. and Fried, M. G. (2007) 'Electrophoretic mobility shift assay (EMSA) for detecting protein-nucleic acid interactions', *Nature Protocols*, 2(8), pp. 1849–1861. doi: 10.1038/nprot.2007.249.

Herbert, A. and Rich, A. (1999) 'Left-handed Z-DNA: structure and function', *Genetica*, 106(1), pp. 37–47. doi: 10.1023/A:1003768526018.

von Hippel, P. H. and Berg, O. G. (1986) 'On the specificity of DNA-protein interactions.', *Proceedings of the National Academy of Sciences of the United States of America*, 83(6), pp. 1608–12. Available at: http://www.ncbi.nlm.nih.gov/pubmed/3456604 (Accessed: 13 January 2019).

Von Hippel, P. H. and Berg, O. G. (1989) 'Facilitated target location in biological systems', *Journal of Biological Chemistry*, pp. 675–678. doi: 10.1074/jbc.RA117.000130.

Ho, H. N., Van Oijen, A. M. and Ghodke, H. (2018) 'The transcription-repair coupling factor Mfd associates with RNA polymerase in the absence of exogenous damage', *Nature Communications*. Nature Publishing Group, 9(1), p. 1570. doi: 10.1038/s41467-018-03790-z.

Holmquist, G. P. (1998) 'Endogenous lesions, S-phase-independent spontaneous mutations, and evolutionary strategies for base excision repair', *Mutation Research - Fundamental and Molecular Mechanisms of Mutagenesis*. Elsevier, 400(1–2), pp. 59–68. doi: 10.1016/S0027-5107(98)00051-7.

Honda, M. *et al.* (2009) 'Single-Molecule Analysis Reveals Differential Effect of ssDNA-Binding Proteins on DNA Translocation by XPD Helicase', *Molecular Cell*, 35(5), pp. 694–703. doi: 10.1016/j.molcel.2009.07.003.

Van Houten, B. *et al.* (1987) 'DNase I footprint of ABC excinuclease.', *The Journal of biological chemistry*, 262(27), pp. 13180–7. Available at: http://www.ncbi.nlm.nih.gov/pubmed/3308871

(Accessed: 18 May 2016).

Houten, B. Van (1990) 'Nucleotide Excision Repair in Escherichia coli', 54(1), pp. 18–51.

Van Houten, B. *et al.* (2005) '"Close-fitting sleeves": DNA damage recognition by the UvrABC nuclease system', *Mutation Research - Fundamental and Molecular Mechanisms of Mutagenesis*, 577(1-2 SPEC. ISS.), pp. 92–117. doi: 10.1016/j.mrfmmm.2005.03.013.

Van Houten, B., Eisen, J. A. and Hanawalt, P. C. (2002) 'A cut above: Discovery of an alternative excision repair pathway in bacteria', *Proceedings of the National Academy of Sciences*. National Academy of Sciences, 99(5), pp. 2581–2583. doi: 10.1016/j.chroma.2012.12.023.

Van Houten, B. and Sancar, A. (1987) 'Repair of N-methyl-N'-nitro-N-nitrosoguanidine-induced DNA damage by ABC excinuclease', *Journal of Bacteriology*. American Society for Microbiology Journals, 169(2), pp. 540–545. doi: 10.1128/jb.169.2.540-545.1987.

Van Houten, B. and Snowden, A. (1993) 'Mechanism of action of the Escherichia coli UvrABC nuclease: Clues to the damage recognition problem', *BioEssays*, pp. 51–59. doi: 10.1002/bies.950150108.

Hsu, D. S. *et al.* (1995) 'Structure and function of the UvrB protein', *Journal of Biological Chemistry*. American Society for Biochemistry and Molecular Biology, 270(14), pp. 8319–8327. doi: 10.1074/jbc.270.14.8319.

Hughes, C. D. *et al.* (2013) 'Real-time single-molecule imaging reveals a direct interaction between UvrC and UvrB on DNA tightropes', *Nucleic Acids Research*, 41(9), pp. 4901–4912. doi: 10.1093/nar/gkt177.

Huisman, O., D'Ari, R. and Gottesman, S. (1984) 'Cell-division control in Escherichia coli: specific induction of the SOS function SfiA protein is sufficient to block septation.', *Proceedings of the National Academy of Sciences of the United States of America*. National Academy of Sciences, 81(14), pp. 4490–4494. doi: 10.1073/pnas.81.14.4490.

Husain, I. *et al.* (1985) 'Effect of DNA polymerase I and DNA helicase II on the turnover rate of UvrABC excision nuclease.', *Proceedings of the National Academy of Sciences of the United States of America*, 82(20), pp. 6774–8. doi: 10.1073/pnas.82.20.6774.

Ikawa, M. *et al.* (1995) 'Green fluorescent protein as a marker in transgenic mice', *Development, Growth and Differentiation*. Wiley/Blackwell (10.1111), 37(4), pp. 455–459. doi: 10.1046/j.1440-169X.1995.t01-2-00012.x.

Ira, G. *et al.* (2003) 'Srs2 and Sgs1-Top3 Suppress Crossovers during Double-Strand Break Repair in Yeast', *Cell*, 115(4), pp. 401–411. doi: 10.1016/S0092-8674(03)00886-9.

Jaciuk, M. *et al.* (2011) 'Structure of UvrA nucleotide excision repair protein in complex with modified DNA.', *Nature structural & molecular biology*, 18(2), pp. 191–7. doi: 10.1038/nsmb.1973.

Jain, A. *et al.* (2011) 'Probing cellular protein complexes using single-molecule pull-down', *Nature*, 473(7348), pp. 484–488. doi: 10.1038/nature10016.

Jiang, Y. *et al.* (2007) 'Detecting ultraviolet damage in single DNA molecules by atomic force microscopy', *Biophysical Journal*. The Biophysical Society, 93(5), pp. 1758–1767. doi: 10.1529/biophysj.107.108209.

Joyce, C. M. and Grindley, N. D. F. (1984) 'Method for determining whether a gene of Escherichia coli is essential: Application to the polA gene', *Journal of Bacteriology*, 158(2), pp. 636–643. Available at: http://www.ncbi.nlm.nih.gov/pubmed/6233260 (Accessed: 19 October 2018).

Kabata, H. *et al.* (1993) 'Visualization of single molecules of RNA polymerase sliding along DNA', *Science*, 262(5139), pp. 1561–1563. doi: 10.1126/science.8248804.

Kacinski, B. M. and Rupp, W. D. (1981) 'E. coli uvrB protein binds to DNA in the presence of uvrA protein', *Nature*. Nature Publishing Group, 294(5840), pp. 480–481. doi: 10.1038/294480a0.

Kacinski, B. M., Sancar, A. and Rupp, W. D. (1981) 'A general approach for purifying proteins encoded by cloned genes without using a functional assay: Isolation of the uvrA gene product from radiolabeled maxicells', *Nucleic Acids Research*, 9(18), pp. 4495–4508. doi: 10.1093/nar/9.18.4495.

Kad, N. M. *et al.* (2010) 'Collaborative Dynamic DNA Scanning by Nucleotide Excision Repair Proteins Investigated by Single- Molecule Imaging of Quantum-Dot-Labeled Proteins', *Molecular Cell*. Elsevier Ltd, 37(5), pp. 702–713. doi: 10.1016/j.molcel.2010.02.003.

Kad, N. M. and Van Houten, B. (2012) 'Dynamics of lesion processing by bacterial nucleotide excision repair proteins.', *Progress in molecular biology and translational science*. NIH Public Access, 110, pp. 1–24. doi: 10.1016/B978-0-12-387665-2.00001-8.

Kainov, D. E. *et al.* (2008) 'Structural basis for group A trichothiodystrophy', *Nature Structural and Molecular Biology*, 15(9), pp. 980–984. doi: 10.1038/nsmb.1478.

Karakas, E. *et al.* (2007) 'Structure of the C-terminal half of UvrC reveals an RNase H endonuclease domain with an Argonaute-like catalytic triad', *The EMBO Journal*. John Wiley & Sons, Ltd, 26(2), pp. 613–622. doi: 10.1038/sj.emboj.7601497.

Keeney, S., Chang, G. J. and Linn, S. (1993) 'Characterization of a human DNA damage binding protein implicated in xeroderma pigmentosum E.', *The Journal of biological chemistry*, 268(28), pp. 21293–300. Available at: http://www.ncbi.nlm.nih.gov/pubmed/8407967 (Accessed: 14 January 2019).

Kellenberger, E. *et al.* (2005) 'Solution structure of the C-terminal domain of TFIIH P44 subunit reveals a novel type of C4C4 ring domain involved in protein-protein interactions', *Journal of Biological Chemistry*, 280(21), pp. 20785–20792. doi: 10.1074/jbc.M412999200.

Kelman, Z. and White, M. F. (2005) 'Archaeal DNA replication and repair', *Current Opinion in Microbiology*, pp. 669–676. doi: 10.1016/j.mib.2005.10.001.

Keriel, A. *et al.* (2002) 'XPD mutations prevent TFIIH-dependent transactivation by nuclear receptors and phosphorylation of RARα', *Cell*, 109(1), pp. 125–135. doi: 10.1016/S0092-8674(02)00692-X.

Kerr, K. M., Sauna, Z. E. and Ambudkar, S. V (2001) 'Correlation between steady-state ATP hydrolysis and Vanadate-induced ADP trapping in human P-glycoprotein: Evidence for ADP release as the rate-limiting step in the catalytic cycle and its modulation by substrates', *Journal of Biological Chemistry*. American Society for Biochemistry and Molecular Biology, 276(12), pp. 8657–8664. doi: 10.1074/jbc.M010044200.

Kiefer, J. (2007) 'Effects of Ultraviolet Radiation on DNA', in Obe, G. and Vijayalaxmi (eds) *Chromosomal Alterations: Methods, Results and Importance in Human Health*. Berlin, Heidelberg: Springer Berlin Heidelberg, pp. 39–53. doi: 10.1007/978-3-540-71414-9_3.

Kim, J. K., Patel, D. and Choi, B. S. (1995) 'CONTRASTING STRUCTURAL IMPACTS INDUCED BY cis-syn CYCLOBUTANE DIMER AND (6–4) ADDUCT IN DNA DUPLEX DECAMERS: IMPLICATION IN MUTAGENESIS AND REPAIR ACTIVITY', *Photochemistry and Photobiology*, 62(1), pp. 44–50. doi: 10.1111/j.1751-1097.1995.tb05236.x.

Kim, J. S. *et al.* (2015) 'Crystal structure of the Rad3/XPD regulatory domain of Ssl1/p44', *Journal of Biological Chemistry*. American Society for Biochemistry and Molecular Biology, 290(13), pp. 8321–8330. doi: 10.1074/jbc.M115.636514.

Kim, S. W., Kwak, J. Il and An, Y. J. (2016) 'Fluorescent approach for visually observing quantum dot uptake in living organisms', *Chemosphere*. Pergamon, 144, pp. 1763–1770. doi: 10.1016/j.chemosphere.2015.10.065.

Kisker, C., Kuper, J. and Van Houten, B. (2013) 'Prokaryotic nucleotide excision repair', *Cold Spring Harbor Perspectives in Biology*, 5(3). doi: 10.1101/cshperspect.a012591.

Kitagawa, M. *et al.* (2005) 'Complete set of ORF clones of Escherichia coli ASKA library (A complete set of E. coli K-12 ORF archive): unique resources for biological research', *DNA Research*, 12(5), pp. 291–299. doi: 10.1093/dnares/dsi012.

Kochaniak, A. B. *et al.* (2009) 'Proliferating cell nuclear antigen uses two distinct modes to move along DNA', *Journal of Biological Chemistry*, 284(26), pp. 17700–17710. doi: 10.1074/jbc.M109.008706.

Kong, M. *et al.* (2017) 'Single-Molecule Methods for Nucleotide Excision Repair: Building a System to Watch Repair in Real Time', in *Methods in Enzymology*, pp. 213–257. doi: 10.1016/bs.mie.2017.03.027.

Kuhlman, T. E. and Cox, E. C. (2012) 'Gene location and DNA density determine transcription factor distributions in Escherichia coli', *Molecular Systems Biology*, 8, p. 610. doi: 10.1038/msb.2012.42.

Kuhn, H. and Frank-Kamenetskii, M. D. (2008) 'Labeling of unique sequences in double-stranded DNA at sites of vicinal nicks generated by nicking endonucleases', *Nucleic Acids Research*, 36(7), p. e40. doi: 10.1093/nar/gkn107.

Kunkel, T. A. (2009) 'Evolving views of DNA replication (in)fidelity', *Cold Spring Harbor Symposia on Quantitative Biology*, 74, pp. 91–101. doi: 10.1101/sqb.2009.74.027.

Kunkel, T. A. and Bebenek, K. (2000) 'DNA Replication Fidelity', *Annual Review of Biochemistry*, 69(1), pp. 497–529. doi: 10.1146/annurev.biochem.69.1.497.

Kuper, J. *et al.* (2012) 'Functional and structural studies of the nucleotide excision repair helicase XPD suggest a polarity for DNA translocation', *EMBO Journal*, 31(2), pp. 494–502. doi: 10.1038/emboj.2011.374.

Kuper, J. *et al.* (2014) 'In TFIIH, XPD Helicase Is Exclusively Devoted to DNA Repair', *PLoS Biology*. Edited by J. T. Kadonaga, 12(9), p. e1001954. doi: 10.1371/journal.pbio.1001954.

Larochelle, S. *et al.* (2012) 'Cyclin-dependent kinase control of the initiation-to-elongation switch of RNA polymerase II', *Nature Structural and Molecular Biology*, 19(11), pp. 1108–1115. doi: 10.1038/nsmb.2399.

Leake, M. C. (2014) 'Analytical tools for single-molecule fluorescence imaging in cellulo', *Physical Chemistry Chemical Physics*, pp. 12635–12647. doi: 10.1039/c4cp00219a.

Lehmann, A. R. (2001) 'The xeroderma pigmentosum group D (XPD) gene: one gene, two functions, three diseases', *Genes & Development*, 15(1), pp. 15–23. doi: 10.1101/gad.859501.

Lerman, L. S. (1961) ‘Structural considerations in the interaction of DNA and acridines’, *Journal of Molecular Biology*, 3(1), pp. IN13–IN14. doi: 10.1016/S0022-2836(61)80004-1.

Lewis, L. K. *et al.* (1994) ‘Identification of high affinity binding sites for LexA which define new DNA damage-inducible genes in Escherichia coli’, *Journal of Molecular Biology*, 241(4), pp. 507–523. doi: 10.1006/jmbi.1994.1528.

Li, J. *et al.* (2006) ‘Similarities and differences between cyclobutane pyrimidine dimer photolyase and (6-4) photolyase as revealed by resonance raman spectroscopy: Electron transfer from the FAD cofactor to ultraviolet-damaged DNA’, *Journal of Biological Chemistry*, 281(35), pp. 25551–25559. doi: 10.1074/jbc.M604483200.

Li, X. and Heyer, W. D. (2008) ‘Homologous recombination in DNA repair and DNA damage tolerance’, *Cell Research*, 18(1), pp. 99–113. doi: 10.1038/cr.2008.1.

Lin, J. J. and Sancar, A. (1992) ‘Active site of (A)BC excinuclease. I. Evidence for 5’ incision by UvrC through a catalytic site involving Asp399, Asp438, Asp466, and His538 residues’, *Journal of Biological Chemistry*, 267(25), pp. 17688–17692. Available at: http://www.ncbi.nlm.nih.gov/pubmed/1387639 (Accessed: 1 August 2018).

Little, J. W. (1991) ‘Mechanism of specific LexA cleavage: Autodigestion and the role of RecA coprotease’, *Biochimie*, 73(4), pp. 411–421. doi: 10.1016/0300-9084(91)90108-D.

Little, J. W. and Mount, D. W. (1982) ‘The SOS regulatory system of Escherichia coli’, *Cell*, 29(1), pp. 11–22. doi: 10.1016/0092-8674(82)90085-X.

Liu, H. *et al.* (2008) ‘Structure of the DNA Repair Helicase XPD’, *Cell*, 133(5), pp. 801–812. doi: 10.1016/j.cell.2008.04.029.

Liu, Y. *et al.* (2004) ‘RAD51C Is Required for Holliday Junction Processing in Mammalian Cells’, *Science*, 303(5655), pp. 243–246. doi: 10.1126/science.1093037.

Loo, T. W. and Clarke, D. M. (2002) ‘Vanadate trapping of nucleotide at the ATP-binding sites of human multidrug resistance P-glycoprotein exposes different residues to the drug-binding site’, *Proceedings of the National Academy of Sciences*. National Academy of Sciences, 99(6), pp. 3511–3516. doi: 10.1073/pnas.022049799.

Luo, J. *et al.* (2015) ‘Architecture of the Human and Yeast General Transcription and DNA Repair Factor TFIIH’, *Molecular Cell*, 59(5), pp. 794–806. doi: 10.1016/j.molcel.2015.07.016.

Machius, M. *et al.* (1999) ‘Crystal structure of the DNA nucleotide excision repair enzyme UvrB from

Thermus thermophilus.', *Proceedings of the National Academy of Sciences of the United States of America*, 96(21), pp. 11717–22. Available at: http://www.ncbi.nlm.nih.gov/pubmed/10518516 (Accessed: 28 April 2016).

Malinina, L. *et al.* (1999) 'Structure of the d(CGCCCGCGGGCG) dodecamer: A kinked A-DNA molecule showing some B-DNA features', *Journal of Molecular Biology*, 285(4), pp. 1679–1690. doi: 10.1006/jmbi.1998.2424.

Malta, E. *et al.* (2008) 'Functions of base flipping in E. coli nucleotide excision repair', *DNA Repair*, 7(10), pp. 1647–1658. doi: 10.1016/j.dnarep.2008.06.011.

Malta, E., Moolenaar, G. F. and Goosen, N. (2007) 'Dynamics of the UvrABC nucleotide excision repair proteins analyzed by fluorescence resonance energy transfer', *Biochemistry*, 46(31), pp. 9080–9088. doi: 10.1021/bi7002235.

Manandhar, M., Boulware, K. S. and Wood, R. D. (2015) 'The ERCC1 and ERCC4 (XPF) genes and gene products', *Gene*. NIH Public Access, pp. 153–161. doi: 10.1016/j.gene.2015.06.026.

Manelyte, L. *et al.* (2009) 'The unstructured C-terminal extension of UvrD interacts with UvrB, but is dispensable for nucleotide excision repair', *DNA Repair*, 8(11), pp. 1300–1310. doi: 10.1016/j.dnarep.2009.08.005.

Manelyte, L. *et al.* (2010) 'Regulation and Rate Enhancement during Transcription-Coupled DNA Repair', *Molecular Cell*, 40(5), pp. 714–724. doi: 10.1016/j.molcel.2010.11.012.

Maragò, O. M. *et al.* (2013) 'Optical trapping and manipulation of nanostructures', *Nature Nanotechnology*, pp. 807–819. doi: 10.1038/nnano.2013.208.

Maslowska, K. H., Makiela-Dzbenska, K. and Fijalkowska, I. J. (2019) 'The SOS system: A complex and tightly regulated response to DNA damage', *Environmental and Molecular Mutagenesis*, 60(4), pp. 368–384. doi: 10.1002/em.22267.

Mathieu, N., Kaczmarek, N. and Naegeli, H. (2010) 'Strand- and site-specific DNA lesion demarcation by the xeroderma pigmentosum group D helicase', *Proceedings of the National Academy of Sciences*, 107(41), pp. 17545–17550. doi: 10.1073/pnas.1004339107.

Matson, S. W. and Robertson, A. B. (2006) 'The UvrD helicase and its modulation by the mismatch repair protein MutL', *Nucleic Acids Research*, pp. 4089–4097. doi: 10.1093/nar/gkl450.

Mellon, I. and Hanawalt, P. C. (1989) 'Induction of the Escherichia coli lactose operon selectively increases repair of its transcribed DNA strand', *Nature*, 342(6245), pp. 95–98. doi:

10.1038/342095a0.

Miller, R. V and Kokjohn, T. A. (1990) 'General Microbiology of recA : Environmental and Evolutionary Significance', *Annual Review of Microbiology*, 44(1), pp. 365–394. doi: 10.1146/annurev.mi.44.100190.002053.

Mocquet, V. *et al.* (2007) 'The human DNA repair factor XPC-HR23B distinguishes stereoisomeric benzo[a]pyrenyl-DNA lesions', *EMBO Journal*. European Molecular Biology Organization, 26(12), pp. 2923–2932. doi: 10.1038/sj.emboj.7601730.

Moolenaar, G. F. *et al.* (1995) 'The C-terminal region of the UvrB protein of Escherichia coli contains an important determinant for UvrC binding to the preincision complex but not the catalytic site for 3′-incision', *Journal of Biological Chemistry*, 270(51), pp. 30508–30515. doi: 10.1074/jbc.270.51.30508.

Moolenaar, G. F., Bazuine, M., *et al.* (1998) 'Characterization of the Escherichia coli Damage-independent UvrBC Endonuclease Activity', *Journal of Biological Chemistry*, 273(52), pp. 34896–34903. doi: 10.1074/jbc.273.52.34896.

Moolenaar, G. F., Uiterkamp, R. S., *et al.* (1998) 'The C-terminal region of the Escherichia coli UvrC protein, which is homologous to the C-terminal region of the human ERCC1 protein, is involved in DNA binding and 5'-incision.', *Nucleic acids research*, 26(2), pp. 462–8. doi: 10.1093/nar/26.2.462.

Moolenaar, G. F. *et al.* (2000) 'The role of ATP binding and hydrolysis by UvrB during nucleotide excision repair', *Journal of Biological Chemistry*, 275(11), pp. 8044–8050. doi: 10.1074/jbc.275.11.8044.

Moolenaar, G. F. *et al.* (2002) 'Cho, a second endonuclease involved in Escherichia coli nucleotide excision repair.', *Proceedings of the National Academy of Sciences of the United States of America*. National Academy of Sciences, 99(3), pp. 1467–1472. doi: 10.1073/pnas.032584099.

Moolenaar, G. F., Höglund, L. and Goosen, N. (2001) 'Clue to damage recognition by UvrB: Residues in the β-hairpin structure prevent binding to non-damaged DNA', *EMBO Journal*, 20(21), pp. 6140–6149. doi: 10.1093/emboj/20.21.6140.

Moolenaar, G. F., Moorman, C. and Goosen, N. (2000) 'Role of the Escherichia coli Nucleotide Excision Repair Proteins in DNA Replication', *Journal of Bacteriology*. American Society for Microbiology, 182(20), pp. 5706–5714. doi: 10.1128/JB.182.20.5706-5714.2000.Updated.

Moolenaar, G. F., Schut, M. and Goosen, N. (2005) 'Binding of the UvrB dimer to non-damaged and damaged DNA: Residues Y92 and Y93 influence the stability of both subunits', *DNA Repair*. Elsevier,

4(6), pp. 699–713. doi: 10.1016/j.dnarep.2005.03.001.

Moreland, R. J. *et al.* (1999) 'A role for the TFIIH XPB DNA helicase in promoter escape by RNA polymerase II', *Journal of Biological Chemistry*. American Society for Biochemistry and Molecular Biology, 274(32), pp. 22127–22130. doi: 10.1074/jbc.274.32.22127.

Mu, D. and Sancar, A. (1997) 'Model for XPC-independent transcription-coupled repair of pyrimidine dimers in humans', *Journal of Biological Chemistry*, 272(12), pp. 7570–7573. doi: 10.1074/jbc.272.12.7570.

Mui, T. P. *et al.* (2011) 'ATP-stimulated, DNA-mediated redox signaling by XPD, a DNA repair and transcription helicase', *Journal of the American Chemical Society*, 133(41), pp. 16378–16381. doi: 10.1021/ja207222t.

Mullenders, L. H. F. (2018) 'Solar UV damage to cellular DNA: From mechanisms to biological effects', *Photochemical and Photobiological Sciences*, 17(12), pp. 1842–1852. doi: 10.1039/c8pp00182k.

Mullineaux, C. W. *et al.* (2006) 'Diffusion of green fluorescent protein in three cell environments in Escherichia coli', *Journal of Bacteriology*. American Society for Microbiology Journals, 188(10), pp. 3442–3448. doi: 10.1128/JB.188.10.3442-3448.2006.

Murade, C. U. *et al.* (2009) 'Interaction of oxazole yellow dyes with DNA studied with hybrid optical tweezers and fluorescence microscopy', *Biophysical Journal*, 97(3), pp. 835–843. doi: 10.1016/j.bpj.2009.05.024.

Myles, G. M., Hearst, J. E. and Sancar, A. (1991) 'Site-Specific Mutagenesis of Conserved Residues within Walker A and B Sequences of Escherichia coli UvrA Protein', *Biochemistry*. Wiley, 30(16), pp. 3824–3834. doi: 10.1021/bi00230a004.

Neher, E. and Sakmann, B. (1976) 'Single-channel currents recorded from membrane of denervated frog muscle fibres', *Nature*. Nature Publishing Group, 260(5554), pp. 799–802. doi: 10.1038/260799a0.

Ng, H. L., Kopka, M. L. and Dickerson, R. E. (2000) 'The structure of a stable intermediate in the a ↔ B DNA helix transition', *Proceedings of the National Academy of Sciences of the United States of America*, 97(5), pp. 2035–2039. doi: 10.1073/pnas.040571197.

Niedziela-Majka, A. *et al.* (2007) 'Bacillus stearothermophilus PcrA monomer is a single-stranded DNA translocase but not a processive helicase in vitro', *Journal of Biological Chemistry*. American

Society for Biochemistry and Molecular Biology, 282(37), pp. 27076–27085. doi: 10.1074/jbc.M704399200.

Nimonkar, A. V. *et al.* (2011) 'BLM-DNA2-RPA-MRN and EXO1-BLM-RPA-MRN constitute two DNA end resection machineries for human DNA break repair', *Genes and Development*, 25(4), pp. 350–362. doi: 10.1101/gad.2003811.

O'Donovan, A. *et al.* (1994) 'XPG endonuclease makes the 3′ Incision in human DNA nucleotide excision repair', *Nature*, 371(6496), pp. 432–435. doi: 10.1038/371432a0.

Odell, I. D., Wallace, S. S. and Pederson, D. S. (2013) 'Rules of engagement for base excision repair in chromatin', *Journal of Cellular Physiology*, 228(2), pp. 258–266. doi: 10.1002/jcp.24134.

Oksenych, V. *et al.* (2009) 'Molecular insights into the recruitment of TFIIH to sites of DNA damage', *EMBO Journal*, 28(19), pp. 2971–2980. doi: 10.1038/emboj.2009.230.

Olivera, B. M. and Bonhoeffer, F. (1974) 'Replication of Escherichia coli requires DNA polymerase I', *Nature*, 250(5466), pp. 513–514. doi: 10.1038/250513a0.

Ordabayev, Y. A. *et al.* (2018) 'Regulation of UvrD Helicase Activity by MutL', *Journal of Molecular Biology*, 430(21), pp. 4260–4274. doi: 10.1016/j.jmb.2018.08.022.

Orren, D. K. *et al.* (1992) 'Post-incision steps of nucleotide excision repair in Escherichia coli', *Journal of Biological Chemistry*, 267(2), pp. 780–788.

Orren, D. K. and Sancar, A. (1989) 'The (A)BC excinuclease of Escherichia coli has only the UvrB and UvrC subunits in the incision complex (damage recognition)', *Biochemistry*, 86, pp. 5237–5241. Available at: https://www.ncbi.nlm.nih.gov/pmc/articles/PMC297596/pdf/pnas00281-0030.pdf (Accessed: 20 June 2018).

Orren, D. K. and Sancar, A. (1990) 'Formation and enzymatic properties of the UvrB DNA complex', *J. Biol. Chem.*, 265(26), pp. 15796–15803. Available at: http://www.ncbi.nlm.nih.gov/entrez/query.fcgi?cmd=Retrieve&db=pubmed&dopt=Citation&list_uids=2168423.

Pakotiprapha, D. *et al.* (2008) 'Crystal Structure of Bacillus stearothermophilus UvrA Provides Insight into ATP-Modulated Dimerization, UvrB Interaction, and DNA Binding', *Molecular Cell*, 29(1), pp. 122–133. doi: 10.1016/j.molcel.2007.10.026.

Pakotiprapha, D. *et al.* (2009) 'A Structural Model for the Damage-sensing Complex in Bacterial Nucleotide Excision Repair *'. doi: 10.1074/jbc.M900571200.

Pakotiprapha, D. *et al.* (2012) 'Structure and mechanism of the UvrA-UvrB DNA damage sensor', *Nat Struct Mol Biol*. 2012/02/07, 19(3), pp. 291–298. doi: 10.1038/nsmb.2240nsmb.2240 [pii].

Perera, A. V. *et al.* (2016) 'Cho endonuclease functions during DNA interstrand cross-link repair in Escherichia coli', *Journal of Bacteriology*. American Society for Microbiology (ASM), 198(22), pp. 3099–3108. doi: 10.1128/JB.00509-16.

Petalcorin, M. I. R. *et al.* (2006) 'CeBRC-2 Stimulates D-loop Formation by RAD-51 and Promotes DNA Single-strand Annealing', *Journal of Molecular Biology*, 361(2), pp. 231–242. doi: 10.1016/j.jmb.2006.06.020.

Phillips, D. B. *et al.* (2012) 'An optically actuated surface scanning probe', *Optics Express*, 20(28), p. 29679. doi: 10.1364/OE.20.029679.

Pollard, E. C. (1974) 'Cellular and molecular effects of solar ultraviolet radiation', in *Photochemistry and Photobiology*. Springer US, pp. 301–308. doi: 10.1111/j.1751-1097.1974.tb06580.x.

Prasher, D. C. *et al.* (1992) 'Primary structure of the Aequorea victoria green-fluorescent protein', *Gene*, 111(2), pp. 229–233. doi: 10.1016/0378-1119(92)90691-H.

Pugh, R. A. *et al.* (2008) 'The iron-containing domain is essential in Rad3 helicases for coupling of ATP hydrolysis to DNA translocation and for targeting the helicase to the single-stranded DNA-double-stranded DNA junction', *Journal of Biological Chemistry*, 283(3), pp. 1732–1743. doi: 10.1074/jbc.M707064200.

Pugh, R. A., Wu, C. G. and Spies, M. (2012) 'Regulation of translocation polarity by helicase domain 1 in SF2B helicases', *EMBO Journal*. European Molecular Biology Organization, 31(2), pp. 503–514. doi: 10.1038/emboj.2011.412.

Puumalainen, M. R. *et al.* (2016) 'Xeroderma pigmentosum group C sensor: Unprecedented recognition strategy and tight spatiotemporal regulation', *Cellular and Molecular Life Sciences*. Springer, pp. 547–566. doi: 10.1007/s00018-015-2075-z.

Qiu, R. *et al.* (2015) 'MutL traps MutS at a DNA mismatch', *Proceedings of the National Academy of Sciences of the United States of America*, 112(35), pp. 10914–10919. doi: 10.1073/pnas.1505655112.

Radu, L. *et al.* (2017) 'The intricate network between the p34 and p44 subunits is central to the activity of the transcription/DNA repair factor TFIIH', *Nucleic Acids Research*, 45(18), pp. 10872–10883. doi: 10.1093/nar/gkx743.

Reardon, J. T. *et al.* (1993) 'THE JOURNAL of BIOLWICAL CHEMISTRY', 268(28), pp. 21301–21308. Available at: http://www.jbc.org/content/268/28/21301.full.pdf (Accessed: 4 July 2018).

Riedinger, C. *et al.* (2010) 'Structure of Rpn10 and its interactions with polyubiquitin chains and the proteasome subunit Rpn12', *Journal of Biological Chemistry*, 285(44), pp. 33992–34003. doi: 10.1074/jbc.M110.134510.

Rubenstein, D. A., Yin, W. and Frame, M. D. (2012) 'Fundamentals of Fluid Mechanics', in *Biofluid Mechanics*, pp. 11–48. doi: 10.1016/B978-0-12-381383-1.00002-3.

Rudolf, J. *et al.* (2006) 'The DNA Repair Helicases XPD and FancJ Have Essential Iron-Sulfur Domains', *Molecular Cell*, 23(6), pp. 801–808. doi: 10.1016/j.molcel.2006.07.019.

Rudolf, J. *et al.* (2010) 'The helicase XPD unwinds bubble structures and is not stalled by DNA lesions removed by the nucleotide excision repair pathway', *Nucleic Acids Research*. Oxford University Press, 38(3), pp. 931–941. doi: 10.1093/nar/gkp1058.

Runyon, G. T. and Lohman, T. M. (1993) 'Kinetics of Escherichia coli Helicase II-Catalyzed Unwinding of Fully Duplex and Nicked Circular DNA', *Biochemistry*, 32(15), pp. 4128–4138. doi: 10.1021/bi00066a039.

Sancar, A., Wharton, R. P., *et al.* (1981) 'Identification of the uvrA gene product', *Journal of Molecular Biology*. Academic Press, 148(1), pp. 45–62. doi: 10.1016/0022-2836(81)90234-5.

Sancar, A., Clarke, N. D., *et al.* (1981) 'Identification of the uvrB gene product', *Journal of Molecular Biology*. Academic Press, 148(1), pp. 63–76. doi: 10.1016/0022-2836(81)90235-7.

Sancar, A., Kacinski, B. M., *et al.* (1981) 'Identification of the uvrC gene product', *Proc Natl Acad Sci U S A*, 78(9), pp. 5450–5454. Available at: http://www.ncbi.nlm.nih.gov/pubmed/7029536 (Accessed: 22 June 2018).

Sancar, A., Franklin, K. A. and Sancar, G. B. (1984) 'Escherichia coli DNA photolyase stimulates uvrABC excision nuclease in vitro.', *Proceedings of the National Academy of Sciences of the United States of America*, 81(23), pp. 7397–7401. doi: 10.1073/pnas.81.23.7397.

Sancar, A. and Rupp, W. D. (1983) 'A novel repair enzyme: UVRABC excision nuclease of Escherichia coli cuts a DNA strand on both sides of the damaged region', *Cell*. Cell Press, 33(1), pp. 249–260. doi: 10.1016/0092-8674(83)90354-9.

Sancar, A. and Sancar, G. B. (1988) 'DNA Repair Enzymes', *Ann. Rev. Biochem.*, 57, pp. 29–67. Available at: https://www.annualreviews.org/doi/pdf/10.1146/annurev.bi.57.070188.000333

(Accessed: 4 July 2018).

Sandrock, B. and Egly, J. M. (2001) 'A Yeast Four-hybrid System Identifies Cdk-activating Kinase as a Regulator of the XPD Helicase, a Subunit of Transcription Factor IIH', *Journal of Biological Chemistry*, 276(38), pp. 35328–35333. doi: 10.1074/jbc.M105570200.

Sano, T., Vajda, S. and Cantor, C. R. (1998) 'Genetic engineering of streptavidin, a versatile affinity tag', *Journal of Chromatography B: Biomedical Applications*, pp. 85–91. doi: 10.1016/S0378-4347(98)00316-8.

Sassanfar, M. and Roberts, J. W. (1990) 'Nature of the SOS-inducing signal in Escherichia coli. The involvement of DNA replication', *Journal of Molecular Biology*, 212(1), pp. 79–96. doi: 10.1016/0022-2836(90)90306-7.

Saxton, M. J. (2001) 'Anomalous subdiffusion in fluorescence photobleaching recovery: A Monte Carlo study', *Biophysical Journal*, 81(4), pp. 2226–2240. doi: 10.1016/S0006-3495(01)75870-5.

Schägger, H., Cramer, W. A. and von Jagow, G. (1994) 'Analysis of molecular masses and oligomeric states of protein complexes by blue native electrophoresis and isolation of membrane protein complexes by two-dimensional native electrophoresis.', *Analytical biochemistry*, 217(2), pp. 220–30. Available at: http://www.ncbi.nlm.nih.gov/pubmed/8203750 (Accessed: 2 August 2018).

Schilbach, S. *et al.* (2017) 'Structures of transcription pre-initiation complex with TFIIH and Mediator', *Nature*. Europe PMC Funders, 551(7679), pp. 204–209. doi: 10.1038/nature24282.

Schmitt, D. R. *et al.* (2014) 'The structure of the TFIIH p34 subunit reveals a Von Willebrand Factor a like fold', *PLoS ONE*. Edited by T. Miyata, 9(7), p. e102389. doi: 10.1371/journal.pone.0102389.

Schultz, P. *et al.* (2000) 'Molecular structure of human TFIIH', *Cell*, 102(5), pp. 599–607. doi: 10.1016/S0092-8674(00)00082-9.

Seeberg, E. (1978) 'Reconstitution of an Escherichia coli repair endonuclease activity from the separated uvrA+ and uvrB+/uvrC+ gene products.', *Proceedings of the National Academy of Sciences*, 75(6), pp. 2569–2573. doi: 10.1073/pnas.75.6.2569.

Seidel, R. *et al.* (2004) 'Real-time observation of DNA translocation by the type I restriction modification enzyme EcoR124I', *Nature Structural and Molecular Biology*, 11(9), pp. 838–843. doi: 10.1038/nsmb816.

Selby, C. P. and Sancar, A. (1993) 'Molecular mechanism of transcription-repair coupling.', *Science*, 260(5104), pp. 53–8. Available at: http://www.ncbi.nlm.nih.gov/pubmed/8465200 (Accessed: 24

October 2018).

Selby, C. P. and Sancar, A. (1997) ‘Cockayne syndrome group B protein enhances elongation by RNA polymerase II.’, *Proceedings of the National Academy of Sciences of the United States of America*. National Academy of Sciences, 94(21), pp. 11205–9. doi: 10.1073/pnas.94.21.11205.

Seroz, T. *et al.* (2000) ‘p44/SSL1, the regulatory subunit of the XPD/RAD3 helicase, plays a crucial role in the transcriptional activity of TFIIH’, *Journal of Biological Chemistry*. American Society for Biochemistry and Molecular Biology, 275(43), pp. 33260–33266. doi: 10.1074/jbc.M004764200.

Setlow, R. B. and Carrier, W. L. (1966) ‘Pyrimidine dimers in ultraviolet-irradiated DNA’s’, *Journal of Molecular Biology*, 17(1), pp. 237–254. doi: 10.1016/S0022-2836(66)80105-5.

Shao, X. and Grishin, N. V (2000) ‘Common fold in helix-hairpin-helix proteins.’, *Nucleic acids research*. Oxford University Press, 28(14), pp. 2643–50. doi: 10.1093/nar/28.14.2643.

Shashkova, S. and Leake, M. C. (2017) ‘Single-molecule fluorescence microscopy review: shedding new light on old problems’, *Bioscience Reports*, 37(4), p. BSR20170031. doi: 10.1042/BSR20170031.

Shimomura, O., Johnson, F. H. and Saida, Y. (1962) ‘Extraction, purification and properties of aequorin, a bioluminescent’, *Journal of cellular and comparative physiology*. Wiley-Blackwell, 59(3), pp. 223–239. doi: 10.1002/jcp.1030590302.

Sibghat-Ullah, Sancar, A. and Hearst, J. E. (1990) ‘The repair patch of E.coli (A)BC excinuclease’, *Nucleic Acids Research*. Oxford University Press, 18(17), pp. 5051–5053. doi: 10.1093/nar/18.17.5051.

Simons, M. *et al.* (2015) ‘Directly interrogating single quantum dot labelled UvrA 2 molecules on DNA tightropes using an optically trapped nanoprobe’, *Scientific reports*, 5, p. 18486. doi: 10.1038/srep18486.

Singh, S. *et al.* (2002) ‘Solution structure and DNA-binding properties of the C-terminal domain of UvrC from E. Coli’, *EMBO Journal*. European Molecular Biology Organization, 21(22), pp. 6257–6266. doi: 10.1093/emboj/cdf627.

Singleton, M. R., Dillingham, M. S. and Wigley, D. B. (2007) ‘Structure and mechanism of helicases and nucleic acid translocases.’, *Annual Review of Biochemistry*. Annual Reviews, 76(1), pp. 23–50. doi: 10.1146/annurev.biochem.76.052305.115300.

Singleton, M. R. and Wigley, D. B. (2002) ‘Modularity and specialization in superfamily 1 and 2 helicases’, *Journal of Bacteriology*. American Society for Microbiology (ASM), pp. 1819–1826. doi:

10.1128/JB.184.7.1819-1826.2002.

Sinha, R. P. and Häder, D.-P. P. (2002) 'UV-induced DNA damage and repair: a review.', *Photochemical & photobiological sciences : Official journal of the European Photochemistry Association and the European Society for Photobiology*, 1(4), pp. 225–36. doi: 10.1039/b201230h.

Sischka, A. *et al.* (2005) 'Molecular mechanisms and kinetics between DNA and DNA binding ligands', *Biophysical Journal*. The Biophysical Society, 88(1), pp. 404–411. doi: 10.1529/biophysj.103.036293.

Skorvaga, M. *et al.* (2002) 'The -Hairpin Motif of UvrB Is Essential for DNA Binding, Damage Processing, and UvrC-mediated Incisions', *Journal of Biological Chemistry*, 277(2), pp. 1553–1559. doi: 10.1074/jbc.M108847200.

Skorvaga, M. *et al.* (2004) 'Identification of residues within UvrB that are important for efficient DNA binding and damage processing', *Journal of Biological Chemistry*, 279(49), pp. 51574–51580. doi: 10.1074/jbc.M409266200.

Sliney, D. H. (2007) 'Radiometric Quantities and Units Used in Photobiology and Photochemistry: Recommendations of the Commission Internationale de l'Eclairage (International Commission on Illumination)', *Photochemistry and Photobiology*, 83(2), pp. 425–432. doi: 10.1562/2006-11-14-ra-1081.

Smith, B. T., Grossman, A. D. and Walker, G. C. (2002) 'Localization of UvrA and Effect of DNA Damage on the Chromosome of Bacillus subtilis Localization of UvrA and Effect of DNA Damage on the Chromosome of Bacillus subtilis', 184(2), pp. 488–493. doi: 10.1128/JB.184.2.488.

Smith, R. L., Zinn, K. and Cantley, L. C. (1980) *A Study of the Vanadate-trapped State of the (Na,K)-ATPase EVIDENCE AGAINST INTERACTING NUCLEOTIDE SITE MODELS**, *THE JOURNAL OF BIOLOGICAL CHEMIETRY Printedin U.S.A*. Available at: http://www.jbc.org/content/255/20/9852.full.pdf (Accessed: 16 January 2019).

Sohi, M. *et al.* (2000) 'Crystal structure of Escherichia coli UvrB C-terminal domain, and a model for UvrB-uvrC interaction.', *FEBS letters*, 465(2–3), pp. 161–164. doi: 10.1016/S0014-5793(99)01690-7.

Spies, M. (2014) 'Two steps forward, one step back: Determining XPD helicase mechanism by single-molecule fluorescence and high-resolution optical tweezers', *DNA Repair*. NIH Public Access, 20, pp. 58–70. doi: 10.1016/j.dnarep.2014.01.013.

Springall, L. *et al.* (2017) 'Recruitment of UvrBC complexes to UV-induced damage in the absence of

UvrA increases cell survival', *Nucleic Acids Research*, 46(3), pp. 1256–1265. doi: 10.1093/nar/gkx1244.

Springall, L., Inchingolo, A. V. and Kad, N. M. (2016) 'DNA-protein interactions studied directly using single molecule fluorescence imaging of quantum dot tagged proteins moving on DNA tightropes', in *Methods in Molecular Biology*, pp. 141–150. doi: 10.1007/978-1-4939-3631-1_11.

Staresincic, L. *et al.* (2009) 'Coordination of dual incision and repair synthesis in human nucleotide excision repair', *EMBO Journal*, 28(8), pp. 1111–1120. doi: 10.1038/emboj.2009.49.

Starr, M. P. (1981) *The Prokaryotes : a handbook on habitats, isolation, and identification of bacteria*. Springer-Verlag. Available at: https://books.google.co.uk/books?id=RpPuCAAAQBAJ&pg=PA79&lpg=PA79&dq=Nasim+A,+James+AP+(1978)+Life+under+conditions+of+high+irradiation.+In:+Kushner+DJ+(ed)+Microbial+life+in+extreme+environments.+New+York:+Academic+Press,+pp+409–439&source=bl&ots=F7uPrOg (Accessed: 15 January 2019).

Stayton, P. S. *et al.* (1999) 'Streptavidin-biotin binding energetics', *Biomolecular Engineering*, pp. 39–44. doi: 10.1016/S1050-3862(99)00042-X.

Stracy, M. *et al.* (2016) 'Single-molecule imaging of UvrA and UvrB recruitment to DNA lesions in living Escherichia coli', *Nature Communications*. Nature Publishing Group, 7, p. 12568. doi: 10.1038/ncomms12568.

Strick, T. R., Croquette, V. and Bensimon, D. (2000) 'Single-molecule analysis of DNA uncoiling by a type II topoisomerase', *Nature*, 404(6780), pp. 901–904. doi: 10.1038/35009144.

Sugasawa, K. *et al.* (2009) 'Two-Step Recognition of DNA Damage for Mammalian Nucleotide Excision Repair: Directional Binding of the XPC Complex and DNA Strand Scanning', *Molecular Cell*, 36(4), pp. 642–653. doi: 10.1016/j.molcel.2009.09.035.

Sugiyama, T. *et al.* (2006) 'Rad52-mediated DNA annealing after Rad51-mediated DNA strand exchange promotes second ssDNA capture', *EMBO Journal*, 25(23), pp. 5539–5548. doi: 10.1038/sj.emboj.7601412.

Sugiyama, T., New, J. H. and Kowalczykowski, S. C. (1998) 'DNA annealing by Rad52 protein is stimulated by specific interaction with the complex of replication protein A and single-stranded DNA', *Proceedings of the National Academy of Sciences of the United States of America*, 95(11), pp. 6049–6054. doi: 10.1073/pnas.95.11.6049.

Sung, P. *et al.* (1993) 'Human xeroderma pigmentosum group D gene encodes a DMA helicase', *Nature*, 365(6449), pp. 852–855. doi: 10.1038/365852a0.

Sung, P. and Klein, H. (2006) 'Mechanism of homologous recombination: Mediators and helicases take on regulatory functions', *Nature Reviews Molecular Cell Biology*, 7(10), pp. 739–750. doi: 10.1038/nrm2008.

Tafvizi, A. *et al.* (2008) 'Tumor suppressor p53 slides on DNA with low friction and high stability', *Biophysical Journal*, 95(1). doi: 10.1529/biophysj.108.134122.

Tafvizi, A. *et al.* (2011) 'A single-molecule characterization of p53 search on DNA', *Proceedings of the National Academy of Sciences*. National Academy of Sciences, 108(2), pp. 563–568. doi: 10.1073/pnas.1016020107.

Takao, M. *et al.* (1993) 'A 127 kDa component of a UV-damaged DNA-binding complex, which is defective in some xeroderma pigmentosum group E patients, is homologous to a slime mold protein', *Nucleic Acids Research*. Oxford University Press, 21(17), pp. 4111–4118. doi: 10.1093/nar/21.17.4111.

Tang, C., Iwahara, J. and Clore, G. M. (2006) 'Visualization of transient encounter complexes in protein-protein association', *Nature*. Nature Publishing Group, 444(7117), pp. 383–386. doi: 10.1038/nature05201.

Tapias, A. *et al.* (2004) 'Ordered Conformational Changes in Damaged DNA Induced by Nucleotide Excision Repair Factors', *Journal of Biological Chemistry*, 279(18), pp. 19074–19083. doi: 10.1074/jbc.M312611200.

Taylor, E. M. *et al.* (1997) 'Xeroderma pigmentosum and trichothiodystrophy are associated with different mutations in the XPD (ERCC2) repair/transcription gene', *Proceedings of the National Academy of Sciences of the United States of America*, 94(16), pp. 8658–63. doi: 10.1073/pnas.94.16.8658.

Theis, K. *et al.* (1999) 'Crystal structure of UvrB, a DNA helicase adapted for nucleotide excision repair.', *The EMBO journal*, 18(24), pp. 6899–6907. doi: 10.1093/emboj/18.24.6899.

Thiagalingam, S. and Grossman, L. (1991) 'THE JOURNAL OF BIOLOGICAL CHEMISTRY Both ATPase Sites of Escherichia coli UvrA Have Functional Roles in Nucleotide Excision Repair*', 266(17), pp. 11395–11403. Available at: http://www.jbc.org/content/266/17/11395.full.pdf (Accessed: 21 June 2018).

Thiagalingams, S. and Grossman, L. (1993) ‘The Multiple Roles for ATP in the Escherichia coli UvrABC Endonuclease-catalyzed Incision Reaction*’, *THE JOURNAL Q*, 268(24), pp. 18382–18389. Available at: http://www.jbc.org/content/268/24/18382.full.pdf (Accessed: 20 June 2018).

Thomas, M. C. and Chiang, C. M. (2006) ‘The general transcription machinery and general cofactors.’, *Critical reviews in biochemistry and molecular biology*, pp. 105–178. doi: 10.1080/10409230600648736.

Thompson, R. E., Larson, D. R. and Webb, W. W. (2002) ‘Precise nanometer localization analysis for individual fluorescent probes’, *Biophysical Journal*. The Biophysical Society, 82(5), pp. 2775–2783. doi: 10.1016/S0006-3495(02)75618-X.

Timmins, J. *et al.* (2009) ‘Structural and Mutational Analyses of Deinococcus radiodurans UvrA2 Provide Insight into DNA Binding and Damage Recognition by UvrAs’, *Structure*. Elsevier, 17(4), pp. 547–558. doi: 10.1016/j.str.2009.02.008.

Tirode, F. *et al.* (1999) ‘Reconstitution of the transcription factor TFIIH: Assignment of functions for the three enzymatic subunits, XPB, XPD, and cdk7’, *Molecular Cell*. Elsevier, 3(1), pp. 87–95. doi: 10.1016/S1097-2765(00)80177-X.

Travers, A. and Muskhelishvili, G. (2015) ‘DNA structure and function’, *FEBS Journal*, 282(12), pp. 2279–2295. doi: 10.1111/febs.13307.

Tremeau-Bravard, A., Perez, C. and Egly, J. M. (2001) ‘A Role of the C-terminal Part of p44 in the Promoter Escape Activity of Transcription Factor IIH’, *Journal of Biological Chemistry*, 276(29), pp. 27693–27697. doi: 10.1074/jbc.M102457200.

Troelstra, C. *et al.* (1992) ‘ERCC6, a member of a subfamily of putative helicases, is involved in Cockayne’s syndrome and preferential repair of active genes.’, *Cell*, 71(6), pp. 939–53. Available at: http://www.ncbi.nlm.nih.gov/pubmed/1339317 (Accessed: 14 January 2019).

Truglio, J. J. *et al.* (2004) ‘Interactions between UvrA and UvrB: the role of UvrB’s domain 2 in nucleotide excision repair’, *The EMBO Journal*, 237600263, pp. 2498–2509. Available at: https://www.ncbi.nlm.nih.gov/pmc/articles/PMC449773/pdf/7600263a.pdf (Accessed: 20 June 2018).

Truglio, J. J. *et al.* (2005) ‘Structural insights into the first incision reaction during nucleotide excision repair’, *EMBO Journal*. European Molecular Biology Organization, 24(5), pp. 885–894. doi: 10.1038/sj.emboj.7600568.

Truglio, J. J., Croteau, D. L., *et al.* (2006) ‘Prokaryotic nucleotide excision repair: The UvrABC

system', *Chemical Reviews*, 106(2), pp. 233–252. doi: 10.1021/cr040471u.

Truglio, J. J., Karakas, E., *et al.* (2006) 'Structural basis for DNA recognition and processing by UvrB.', *Nature structural & molecular biology*, 13(4), pp. 360–364. doi: 10.1038/nsmb1072.

Tsien, R. Y. (1998) 'THE GREEN FLUORESCENT PROTEIN', *Annual Review of Biochemistry*, 67(1), pp. 509–544. doi: 10.1146/annurev.biochem.67.1.509.

Ulbrich, M. H. and Isacoff, E. Y. (2007) 'Subunit counting in membrane-bound proteins', *Nature Methods*, 4(4), pp. 319–321. doi: 10.1038/nmeth1024.

Uphoff, S. *et al.* (2013) 'Single-molecule DNA repair in live bacteria.', *Proceedings of the National Academy of Sciences of the United States of America*, 110(20), pp. 8063–8068. doi: 10.1073/pnas.1301804110.

Urbatsch, I. L. *et al.* (1995) 'P-glycoprotein is stably inhibited by vanadate-induced trapping of nucleotide at a single catalytic site', *Journal of Biological Chemistry*, 270(33), pp. 19383–19390. doi: 10.1074/jbc.270.33.19383.

Verhoeven, E. E. *et al.* (2000) 'Catalytic sites for 3' and 5' incision of Escherichia coli nucleotide excision repair are both located in UvrC', *Journal of Biological Chemistry*. American Society for Biochemistry and Molecular Biology, 275(7), pp. 5120–5123. doi: 10.1074/jbc.275.7.5120.

Verhoeven, E. E. *et al.* (2001) 'Architecture of nucleotide excision repair complexes: DNA is wrapped by UvrB before and after damage recognition.', *The EMBO journal*, 20(3), pp. 601–11. doi: 10.1093/emboj/20.3.601.

Verhoeven, E. E., van Kesteren, M., *et al.* (2002) 'The C-terminal region of Escherichia coli UvrC contributes to the flexibility of the UvrABC nucleotide excision repair system.', *Nucleic acids research*, 30(11), pp. 2492–500. Available at: http://www.pubmedcentral.nih.gov/articlerender.fcgi?artid=117173&tool=pmcentrez&rendertype=abstract.

Verhoeven, E. E., Wyman, C., *et al.* (2002) 'The presence of two UvrB subunits in the UvrAB complex ensures damage detection in both DNA strands', *EMBO Journal*, 21(15), pp. 4196–4205. doi: 10.1093/emboj/cdf396.

Visse, R. *et al.* (1993) 'The first zinc-binding domain of UvrA is not essential for UvrABC-mediated DNA excision repair', *Mutation Research-DNA Repair*. Elsevier, 294(3), pp. 263–274. doi: 10.1016/0921-8777(93)90009-6.

Wacker, M. and Holick, M. F. (2013) 'Sunlight and Vitamin D: A global perspective for health', *Dermato-Endocrinology*, 5(1), pp. 51–108. doi: 10.4161/derm.24494.

Wagner, K. *et al.* (2009) 'Single-molecule analysis reveals two separate DNA-binding domains in the Escherichia coli UvrA dimer', *Nucleic Acids Research*, 37(6), pp. 1962–1972. doi: 10.1093/nar/gkp071.

Wagner, K., Moolenaar, G. F. and Goosen, N. (2010) 'Role of the two ATPase domains of Escherichia coli UvrA in binding non-bulky DNA lesions and interaction with UvrB', *DNA Repair*, 9(11), pp. 1176–1186. doi: 10.1016/j.dnarep.2010.08.008.

Wagner, K., Moolenaar, G. F. and Goosen, N. (2011) 'Role of the insertion domain and the zinc-finger motif of Escherichia coli UvrA in damage recognition and ATP hydrolysis', *DNA Repair*. Elsevier B.V., 10(5), pp. 483–496. doi: 10.1016/j.dnarep.2011.02.002.

Walker, G. C. (1984) 'Mutagenesis and inducible responses to deoxyribonucleic acid damage in Escherichia coli', *Microbiological Reviews*, 48(1), pp. 60–93. doi: 10.1128/mmbr.48.1.60-93.1984.

Walling, M. A., Novak, J. A. and Shepard, J. R. E. (2009) 'Quantum dots for live cell and in vivo imaging', *International Journal of Molecular Sciences*. Multidisciplinary Digital Publishing Institute (MDPI), pp. 441–491. doi: 10.3390/ijms10020441.

Wang, H. *et al.* (2006) 'UvrB domain 4, an autoinhibitory gate for regulation of DNA binding and ATPase activity', *Journal of Biological Chemistry*. American Society for Biochemistry and Molecular Biology, 281(22), pp. 15227–15237. doi: 10.1074/jbc.M601476200.

Wang, H. *et al.* (2008) 'Functional characterization and atomic force microscopy of a DNA repair protein conjugated to a quantum dot', *Nano Letters*. NIH Public Access, 8(6), pp. 1631–1637. doi: 10.1021/nl080316l.

Wang, H. *et al.* (2009) 'DNA wrapping is required for DNA damage recognition in the Escherichia coli DNA nucleotide excision repair pathway.', *Proceedings of the National Academy of Sciences of the United States of America*, 106(31), pp. 12849–12854. doi: 10.1073/pnas.0902281106.

Wang, J. C. (1979) 'Helical repeat of DNA in solution.', *Proceedings of the National Academy of Sciences of the United States of America*, 76(1), pp. 200–203. doi: 10.1073/pnas.76.1.200.

Wang, J., Mueller, K. L. and Grossman, L. (1994) 'A mutational study of the C-terminal zinc-finger motif of the Escherichia coli UvrA protein', *Journal of Biological Chemistry*, 269(14), pp. 10771–10775. Available at: http://www.jbc.org/content/269/14/10771.full.pdf (Accessed: 21 June 2018).

Warm, W. and Hillebrandt, B. (1962) ‘A NON-PHQTQREACTIVABLE MUTANT OF E. COLI B.’, *Photochemistry and Photobiology*. Wiley/Blackwell (10.1111), 1(3), pp. 271–272. doi: 10.1111/j.1751-1097.1962.tb08100.x.

Watson, J. D. and Crick, F. H. C. (1953) ‘Molecular structure of nucleic acids: A structure for deoxyribose nucleic acid’, *Nature*, 171(4356), pp. 737–738. doi: 10.1038/171737a0.

Webster, M. P. J. *et al.* (2012) ‘Crystal structure of the UvrB dimer: Insights into the nature and functioning of the UvrAB damage engagement and UvrB-DNA complexes’, *Nucleic Acids Research*, 40(17), pp. 8743–8758. doi: 10.1093/nar/gks633.

Weems, J. C. *et al.* (2017) ‘Cockayne syndrome B protein regulates recruitment of the Elongin A ubiquitin ligase to sites of DNA damage’, *Journal of Biological Chemistry*, 292(16), pp. 6431–6437. doi: 10.1074/jbc.C117.777946.

Wessels, J. T. *et al.* (2007) ‘In vivo imaging in experimental preclinical tumor research - A review’, *Cytometry Part A*, pp. 542–549. doi: 10.1002/cyto.a.20419.

White, M. F. (2009) ‘Structure, function and evolution of the XPD family of iron–sulfur-containing 5′→3′ DNA helicases’, *Biochemical Society Transactions*. Portland Press Limited, 37(3), pp. 547–551. doi: 10.1042/BST0370547.

Willson, R. C. *et al.* (1981) ‘Observations of solar irradiance variability’, *Sciences*, 211(4483), pp. 700–702. doi: 10.1126/science.211.4483.700.

Wilson, T. E., Grawunder, U. and Lieber, M. R. (1997) ‘Yeast DNA ligase IV mediates non-homologous DNA end joining’, *Nature*, 388(6641), pp. 495–498. doi: 10.1038/41365.

Wing, R. *et al.* (1980) ‘Crystal structure analysis of a complete turn of B-DNA’, *Nature*, 287(5784), pp. 755–758. doi: 10.1038/287755a0.

Wirth, N. *et al.* (2016) ‘Conservation and divergence in nucleotide excision repair lesion recognition’, *Journal of Biological Chemistry*, 291(36), pp. 18932–18946. doi: 10.1074/jbc.M116.739425.

Wolski, S. C. *et al.* (2008) ‘Crystal structure of the FeS cluster-containing nucleotide excision repair helicase XPD’, *PLoS Biology*. Edited by G. Petsko, 6(6), pp. 1332–1342. doi: 10.1371/journal.pbio.0060149.

Wongsrikeao, P. *et al.* (2011) ‘Antiviral restriction factor transgenesis in the domestic cat’, *Nature Methods*. NIH Public Access, 8(10), pp. 853–859. doi: 10.1038/nmeth.1703.

Wuite, G. J. L. *et al.* (2000) ‘An integrated laser trap/flow control video microscope for the study of

single biomolecules', *Biophysical Journal*, 79(2), pp. 1155–1167. doi: 10.1016/S0006-3495(00)76369-7.

Xie, Z. *et al.* (2004) 'Roles of Rad23 protein in yeast nucleotide excision repair', *Nucleic Acids Research*. Oxford University Press, 32(20), pp. 5981–5990. doi: 10.1093/nar/gkh934.

Yamamoto, K., Satake, M. and Shinagawa, H. (1984) 'A multicopy phr-plasmid increases the ultraviolet resistance of a recA strain of Escherichia coli.', *Mutation research*, 131(1), pp. 11–8. Available at: http://www.ncbi.nlm.nih.gov/pubmed/6229697 (Accessed: 29 October 2018).

Yamamoto, N. *et al.* (2009) 'Update on the Keio collection of Escherichia coli single-gene deletion mutants', *Molecular Systems Biology*, 5, p. 335. doi: 10.1038/msb.2009.92.

Yoakum, G. H. and Grossman, L. (1981) 'Identification of E. coli uvrC protein', *Nature*. Nature Publishing Group, 292(5819), pp. 171–173. doi: 10.1038/292171a0.

Yoon, H. *et al.* (1992) 'SSL1, a suppressor of a HIS4 5'-UTR stem-loop mutation, is essential for translation initiation and affects UV resistance in yeast.', *Genes & development*, 6(12B), pp. 2463–77. Available at: http://www.ncbi.nlm.nih.gov/pubmed/1340463 (Accessed: 8 August 2018).

Zhu, Q. *et al.* (2012) 'Lack of CAK complex accumulation at DNA damage sites in XP-B and XP-B/CS fibroblasts reveals differential regulation of CAK anchoring to core TFIIH by XPB and XPD helicases during nucleotide excision repair', *DNA Repair*. NIH Public Access, 11(12), pp. 942–950. doi: 10.1016/j.dnarep.2012.09.003.

Zlatanova, J. and van Holde, K. (2006) 'Single-Molecule Biology: What Is It and How Does It Work?', *Molecular Cell*, 24(3), pp. 317–329. doi: 10.1016/j.molcel.2006.10.017.

Zou, Y. *et al.* (1997) 'Formation of DNA repair intermediates and incision by the ATP-dependent UvrB-UvrC endonuclease', *Journal of Biological Chemistry*, 272(8), pp. 4820–4827. doi: 10.1074/jbc.272.8.4820.

Zou, Y. and Houten, B. Van (1999) 'Strand opening by the UvrA 2 B complex allows dynamic recognition of DNA damage', 18(17), pp. 4889–4901.